ENGINEERING AN AORTIC VALVE WITH CELLULAR AND MECHANICAL FUNCTIONALITY

A Dissertation

Presented to

The Academic Faculty

by

Aline Louise Yonezawa Nachlas

In Partial Fulfillment

of the Requirements for the Degree

Biomedical Engineering in the

Wallace H. Coulter Department of Biomedical Engineering

Georgia Institute of Technology and Emory University

December 2019

COPYRIGHT © 2019 BY ALINE LY NACHLAS

ENGINEERING AN AORTIC VALVE WITH CELLULAR AND MECHANICAL FUNCTIONALITY

Approved by:

Dr. [Michael E. Davis], Advisor
School of [Biomedical Engineering]
Georgia Institute of Technology

Dr. [Wei Sun]
School of [Biomedical Engineering]
Georgia Institute of Technology

Dr. [K. Jane Grande-Allen]
School of [Bioengineering]
Rice University

Dr. [Johnna S. Temenoff]
[Biomedical Engineering]
Georgia Institute of Technology

Dr. [Wilbur Lam]
School of [Biomedical Engineering]
Georgia Institute of Technology

Dr. [Chunhui Xu]
[School of Medicine]
Emory University

Date Approved: May 20, 2019

I dedicate this thesis to my family, loving husband, and to those who are no longer with us, Francisco Sassi, Hidenori Yonezawa, Rosalie and Edward Nachlas, and Rita Reynolds.

ACKNOWLEDGEMENTS

I would like to thank my advisor, Dr. Michael E. Davis, for giving me the opportunity to conduct this thesis project and for the immense support throughout my PhD. I also cannot thank him enough for believing in me and giving me the opportunity to work on my own project idea. I complete my PhD studies with a completely new way of thinking and problem solving because Dr. Davis gave me the opportunity to think independently and figure things out on my own. Thank you for being the best advisor I could have asked for!

To my thesis committee members, Drs. K. Jane Grande-Allen, Wilbur Lam, Wei Sun, Johnna Temenoff and Chunhui Xu, thank you for supporting this work and providing constructive and valuable feedback. I also want to thank our collaborators Dr. Ajit Yoganathan and Dr. Wei Sun and their graduate students who worked alongside me throughout this thesis. I am also grateful for all the help Dr. Joan Fernandez provided with the shear stress bioreactor.

Additionally, I want to especially thank Sophie Li for her incredible intelligence, hard work, and support during this work. Without Sophie's support, we would have not made this much progress. I would also like to thank all the Davis Lab members who have helped me these past five years with the science and also provided immense support throughout this journey. To my lunch buddies from HSRB, thank you for always being supportive and companions during my time here.

Most of all, I would like to thank my parents, my brother, Mickey, and my husband, Debora, Fabio, Fred, Nick, and Alex for supporting me during this incredible journey!

TABLE OF CONTENTS

LIST OF TABLES

LIST OF FIGURES

LIST OF SYMBOLS AND ABBREVIATIONS

αSMA	alpha-smooth Muscle Actin
3D	Three-dimensional
ANOVA	Analysis of variance
CD	Cluster of differentiation
DMAB	para-Dimethylaminobenzaldehyde
ECM	Extracellular matrix
F-actin	Filamentous actin
GAGs	Glycosaminoglycan
GelMA	Gelatin methacrylate
hADSC	Human adipose derived stromal cells
HDFs	Human dermal fibroblasts
hESCs	Human embryonic stem cells
hVIC	Human VICs
iVIC(s)	Induced valvular interstitial cell(s)
MALDI-TOF	Matrix-assisted laser desorption/ionization Time of Flight
MPa	Mega Pascals
MSCs	Mesenchymal stem cells
MWCO	Molecular weight cut-off
NMR	Nuclear magnetic resonance
NVP	1-vinyl-2-pyrrolidinone
PBS	Phosphate buffered saline
PCL	Poly-ε-caprolactone
PEGDA	Polyethylene (glycol) diacrylate
PGA	Poly(glycolic acid)

PGS	Poly(glycerol sebacate)
PLLA	Poly-l-lactic acid
PU	Polyurethanes
RGDS	Arg-Gly-Asp-Ser
SMC(s)	Smooth muscle cell(s)
SVA	Succinimidyl valerate
TEHV(s)	Tissue engineered heart valve(s)
TEOA	Triethanolamine
VEC(s)	Valvular endothelial cell(s)
VIC(s)	Valvular interstitial cell(s)

SUMMARY

Heart valve disease is an increasing clinical burden associated with high morbidity and mortality. Current, valve replacements have a number of risks, such as thrombogenicity and calcification. For pediatric patients, a significant issue is the lack of small implants capable of growing, resulting in several surgical interventions for valve refitting. Patient-specific, tissue engineered heart valves (TEHVs) have the potential to address these issues through their self-repairing and remodeling capacity. The overall objective of this thesis was to develop a TEHV that functions under physiological aortic valve conditions and has the potential to repair and remodel over time. The central hypothesis is a TEHV can be created by mimicking the structural components of the valve leaflet layers using 3D bioprinting and incorporating valvular interstitial cell (VIC)-like cells to actively regenerate and remodel. First, we generated a potential suitable cell source of human iPSC-derived mesenchymal stem cells (iMSCs) that mature into VIC-like cells. Next, we used 3D printing and a combination of poly-ε-caprolactone (PCL) and gelatin methacrylate - polyethylene (glycol) diacrylate (GelMA/PEGDA) hydrogel to create a cell-laden multilayered leaflet that recapitulates the layers of the valve leaflet. Lastly, the PCL-component of the valve leaflet was mounted onto a valve stent and feasibility studies were conducted using a left-ventricle flow simulator to evaluate the hemodynamic performance of the PCL-TEHV under aortic valve conditions. We demonstrated a cell source can be derived from autologous iPSCs, generated a multilayered leaflet scaffold using a combination of natural and synthetic biomaterials, and verified the feasibility of the leaflet under aortic flow conditions. These promising findings are the first steps to a pre-clinical TEHV with the ability to regenerate and remodel with the patient.

CHAPTER 1 INTRODUCTION

1.1 Motivation

An estimated two to three million children live with heart disease, about 5% of whom have heart valve disease [4-6]. This is mainly due to congenital heart defects in industrialized countries and the persistence of rheumatic fever in underdeveloped regions [7-9]. Valve disease is treated by replacement or valve repair. In most cases valve repair is not possible, and valve implants have a number of risks, such as thrombogenicity and calcification. A significant issue for pediatric patients is the lack of small implants capable of growing, often requiring several surgical interventions for valve refitting [4, 10]. Tissue engineered heart valves (TEHVs) have the potential to address limitations with current implants through their self-repairing and remodeling capacity.

Despite advances in TEHVs, the challenge to develop a mechanically functional TEHV for long-term implantation remains. The mechanical strength of valves is attributed to the microstructure of the leaflet layers, valvular interstitial cells (VICs), and overall macrostructure of the valve design. Thus far, we have shown that we can generate a suitable cell source of human iPSC-derived mesenchymal stem cells (iMSCs) that mature into VIC-like cells [11]. To develop a mechanically functional TEHV, we have recapitulated features of the valve leaflet layers using 3D bioprinting and conducted feasibility studies using a left-ventricle flow simulator. The overall goal is to develop a TEHV that functions under physiological aortic valve conditions and has the potential to repair and remodel over time. We hypothesize we can create a TEHV by mimicking the structural components of the valve leaflet layers using 3D bioprinting and incorporating VIC-like cells to actively regenerate and remodel its surrounding matrix under physiological flow conditions.

CHAPTER 2 SPECIFIC AIMS

Aim 1: To differentiate iPSCs into iVICs using both biochemical and mechanical cues.

iPSCs will be differentiated into iMSCs using a modified (feeder-free) protocol [2] and then encapsulated in polyethylene (glycol) diacrylate (PEGDA) hydrogels of varying stiffness, grafted with adhesion and degradation peptides. We will determine the efficiency of the differentiation protocol using flow cytometry to stain for MSC surface markers CD90, CD44, CD105, CD29, CD73, αSMA, and CD45. VIC phenotype will be characterized by the expression of αSMA, vimentin, F-actin, and ECM production after 1,7, 14, and 28 days and compared to native VICs.

Aim 2: To develop a multilayered leaflet with remodeling potential that mimics the structural and mechanical properties of native heart valve leaflets.

Two types of biomaterials, biodegradable poly-ε-caprolactone (PCL) and a formulation of gelatin methacrylate (GelMA) and polyethylene diacrylate (PEGDA) will be used to generate a multilayered leaflet scaffold. These two biomaterials are hypothesized to enable us to incorporate cells into the leaflet scaffold in addition to replicating the leaflet layers because these biomaterials are compatible with 3D printing. Furthermore, since the geometry and design are key components for a functional TEHV, 3D bioprinting and molding will be the primary approach used. To generate a load-bearing layer mimicking the fibrosa, PCL scaffolds will be 3D printed with three different strand orientations to assess which scaffold can recapitulate the anisotropy and alignment of the collagen fibers found in native leaflets. The overall material properties of the scaffold and its ability to degrade over time will be assessed with uniaxial testing. The interaction of iMSCs with the PCL scaffold will be characterized by alamarBlue and immunostaining for αSMA and vimentin. To develop cell-laden ventricularis and spongiosa layers, a blend of GelMA and

PEGDA will be used, and the mechanical properties as well as the cell viability will be characterized. Both PCL and the GelMA/PEGDA hydrogel will be combined to generate a multilayered scaffold for testing under pulsatile shear stress conditions, and the VIC-like phenotype and collagen type I production will be assessed via immunostaining.

Aim 3: To generate a TEHV prototype and evaluate the hemodynamic profile using a pulsatile flow loop.

The leaflet, composed of the PCL layer only, will be assembled onto a 3D printed valve ring of 19 mm outer diameter and inner diameter of 17 mm for initial prototyping. The assembled TEHV will be tested to assess the hemodynamics and performance of the valve using a pulsatile left-ventricular flow loop. Valve kinematics will be evaluated by the effective orifice area, mean and max transvalvular pressure gradient, regurgitation volume, and the leakage and closing volume. These parameters will be compared to commercially available valve protheses of similar size.

CHAPTER 3 LITERATURE REVIEW [i]

3.1 Prevalence of Heart Valve Disease

Heart valve disease is a worldwide clinical burden resulting in high morbidity and mortality [13-15]. With a prevalence of 2.5%, heart valve disease can range from degeneration of valves, to congenital defects, to rheumatic fever depending on social and geographical location [16]. As life-expectancy increases in industrialized countries, age-dependent degeneration is expected to triple the prevalence of heart valve disease by 2050 [7]. Meanwhile, structural malformation of heart valves, known as congenital heart valve disease, occurs in 1 to 2% of live births worldwide [17]. In socioeconomically vulnerable populations, rheumatic fever is a source for heart valve disease in children and adults who develop streptococcal throat infection that is left untreated [8, 18]. Rheumatic heart valve disease results in valve damage and progression of heart failure.

3.2 Heart Valve Physiology

The main function of heart valves is to maintain unidirectional flow of blood throughout the heart, and it does so by passively opening and closing over 100,000 times per day [19]. In the heart, there are four valves: tricuspid, pulmonary, mitral, and aortic. Diseased valves can result in the back flow of blood and abnormal pressure gradients in heart chambers. The valves most prone to disease are the mitral and aortic valve in the left ventricle [20]. When these valves become diseased, there can be regurgitation or stenosis of the valve leaflets. Regurgitation or valve insufficiency is described as the leakage of a valve during diastole. This can be caused by abnormalities in the aortic root geometry or rupture of the papillary muscles in the aortic or mitral valve, respectively [20]. Valve stenosis is the narrowing or obstruction of the valve opening, often caused by degenerative remodeling or congenital malformation [18]. The most common form of valve disease is

aortic valve stenosis [16]. Thus, most of the biomaterial applications for heart valve tissue engineering in this literature review will focus on aortic valve tissue engineering.

Currently, there are limited therapeutics to prevent valve degeneration. Thus, heart valve disease is treated through either valve repair or valve replacement, with the latter being the most common treatment. This is because diagnosis of valve disease occurs when the disease has progressed to a point where repair is not feasible. Valves can be replaced with mechanical or biological prostheses through invasive open-heart surgery or transcatheter delivery. While valve prostheses have increased patient lifespan, there are numerous limitations. Some of those include the inability to remodel and maintain the structure similar to native valves. This is especially a drawback for pediatric patients due to the valve's incapacity to grow and remodel with somatic growth. As a result, a child in need of a valve replacement will likely undergo several resizing surgeries, underscoring the need for a "living valve" that can actively regenerate and remodel to minimize the need for multiple surgeries in pediatric patients and reduce the limitations of current implants for adults [21].

In this literature review, the current approaches for treating heart valve disease will be discussed, followed by the design considerations for heart valve tissue engineering, a summary of biomaterials, fabrication techniques, and emerging technologies used to meet TEHV design criteria. Evaluations of TEHVs in *in vivo* and in physiological conditions are important to determine whether design considerations have been met. Thus, a summary of *in vivo* models and bioreactors are also discussed.

3.3 Current Approaches for Treating Heart Valve Disease

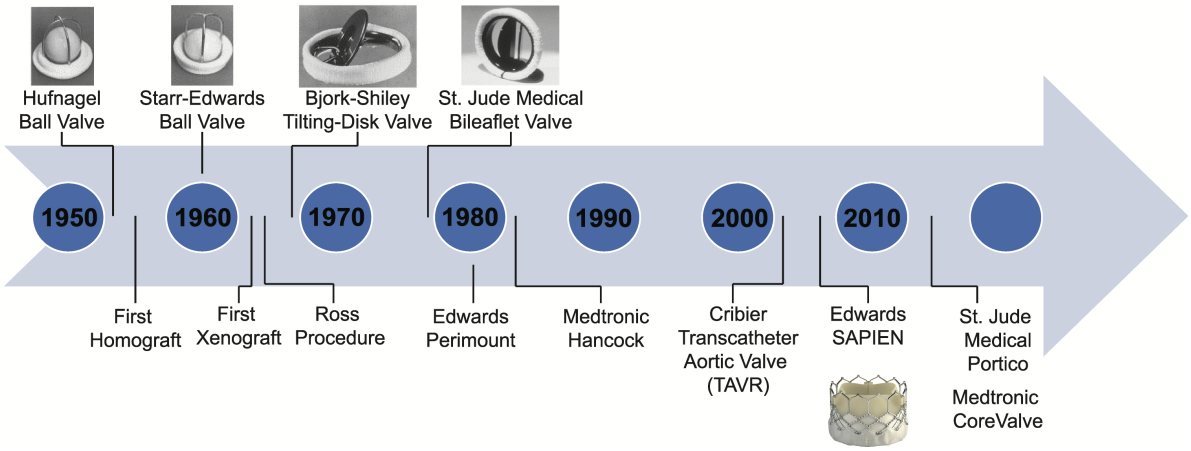

Figure 1. The evolution of valve prostheses. The rapid development of heart valve prostheses began with the first implantation of Hufnagel's mechanical ball valve in the 1950s. Since then, the field has expanded to include a variation of different mechanical valve designs, as well as biological valve implants. Today, different technologies exist to treat a wider variety of people previously unsuitable for valve replacement, such as transcatheter valve implantation. Valve images adapted with permission [2]. Copyright 2003, Elsevier. Edwards SAPIEN valve adapted with permission [3]. Copyright 2016, the authors, published under the terms of CC-BY 4.0 license.

The invention and implantation of prosthetic heart valves to treat patients with dysfunctional, diseased valves came about in the 1950s. This followed the development of several surgical techniques in the years prior, including cardiac catheterization, the cardiopulmonary bypass pump, and the discovery of heparin and dicumarol as anticoagulants [22]. Since then, a wide variety of valve prostheses have been developed throughout the years (Figure 1) and can be divided into three main categories: mechanical, biological, and transcatheter. The advantages and disadvantages for each type of valve prostheses are summarized in Table 1.

Table 1. Advantages and Disadvantages of Valve Prostheses.

Prosthesis	Advantages	Disadvantages	Ref.
Mechanical	– Durable (20-30 years) – Lower reoperation rates	– Requires life-long anticoagulation – Higher risk of hemorrhages and thromboembolism – Risk of infection	[23] [24] [25] [26] [27]
Biological	– Physiological hemodynamics – Does not require anticoagulants – Low risk for major bleeding, stroke, and valve thrombosis	– Less durable (10-15 years) – Risk of structural valve deterioration – Higher reoperation rates	
Transcatheter Biological	– Treatment option for intermediate- to high-risk patients – Reduced invasiveness and faster recovery	– Early development stages – Long-term follow up is scarce – Prosthesis-patient mismatch – High risk for stroke – Similar disadvantages as bioprosthesis	[26] [28]

3.3.1 *Mechanical*

Charles Hufnagel created the first heart valve prosthesis, a mechanical prosthesis consisting of a polymethyl methacrylate acrylic ball valve implanted into the descending aorta. This approach was far from ideal, as a common complaint was the noise from the valve opening and closing, which resembled the noise of a ticking time bomb. Albert Starr and Dwight Harken built upon Hufnagel's idea to create a caged ball valve. Following the successful implantation of these valves into the mitral and aortic valve positions in 1960, several designs for the ball valve prosthesis were developed by Starr and M. Lowell Edwards in order to reduce their thrombogenicity [22]. The Starr-Edwards ball valve consisted of a silicone ball that moved forward into a cage to open and fell back into the

sewer ring to close. Since their creation, over 200,000 ball valves have been implanted [29].

In order to address problems associated with the Starr-Edwards ball valves, including turbulence and shear stress, Viking Bjork and Donald Shiley created the tilting disk valve in the late 1960s [22]. The Bjork-Shiley valve consisted of a single graphite tilting disk coated in pyrolite carbon, which was held in place by two metal struts. In the 1970s, the original design was modified to a convexo-concave shape, but the new design was prone to fracture, often resulting in patient death [29]. Today, Bjork-Shiley valves are no longer manufactured, but other manufacturers, such as Medtronic-Hall and Aortech Ultracor, still produce tilting disk valves [29].

The most common mechanical valve design today is the bileaflet valve, created in 1977 by St. Jude Medical [29]. Bileaflet valves consist of two pivoting semicircular leaflets that open completely, making them popular because of all mechanical valve designs available, they offer the least impedance to blood flow. Today, several manufacturers produce bileaflet valves, including St. Jude Medical, OnX, and Sorin, that differ in composition and design [30].

According to two large randomized studies, mechanical valve prostheses are recommended for more active patients under the age of 60, as these prostheses are durable with the potential to last over 20 years, and often do not require replacement surgeries [23-25]. However, recipients of mechanical heart valves are at a higher risk for thromboembolism, and so they must remain on lifelong anticoagulation therapy, exposing them to higher risks of bleeding and hemorrhages associated with this therapy [25, 27]. The thrombogenicity of materials used in mechanical valves, high shear stress profile, and backflow of blood are reasons why patients with mechanical valves require lifelong anticoagulation therapy [26]. The high shear stress can cause damage to blood cells and

activate the blood clotting-pathways, resulting in thrombosis and potential risk of stroke. Mechanical valves are more susceptible to infections that are difficult to treat and oftentimes require replacement of the prosthesis [27]. For infants born with congenital valve defects, mechanical valves are not ideal, as they do not come in sizes small enough (16 mm to 29 mm in diameter) for newborns, and they fail to grow [31].

3.3.2 *Biological*

To eliminate the need for anticoagulation treatment in patients who have undergone valve surgeries, biological materials were sought after to replace diseased valves. Since the late 1950s, many different types of biological valves have been created, ranging from valves coming from the patient's own body (autografts and autologous valves), to valves from human donors (homografts), to valves from other animal species (xenografts).

Valve prostheses fashioned from the patient's own tissue arose shortly after the development of mechanical valves. In 1967, Donald Ross described a procedure in which a patient's healthy pulmonary valve was excised and used to replace the diseased aortic valve [30]. Meanwhile, a valve prosthesis was placed in the pulmonary position. While technically complex, patients who have undergone the Ross procedure have better long-term survival compared to alternatives [30]. This is due to its excellent hemodynamic profile, lack of anticoagulation therapy, and ability to grow and integrate with patient [31]. Around the same time, valve prostheses constructed by the surgeon's hands using the patient's own tissue were implanted, but due to the technically demanding nature of this procedure, it was eventually abandoned [29].

Homografts are valve prostheses donated from human cadavers, organ donors, or heart transplant patients, and are sterilized and preserved in preparation for implantation [29]. Similarly, xenografts are valve prostheses typically from porcine aortic valves or bovine pericardium, and these are often preserved with glutaraldehyde to stabilize collagen

structure and reduce antigenicity [32]. Since their production in 1965, xenografts have become the most frequently implanted biological valve [20]. Two common classes of xenografts include porcine aortic valves, such as the St. Jude Medical Epic and Medtronic Hancock, and bovine pericardial valves, such as the Edwards Perimount and Sorin Mitroflow [22].A xenograft currently coming into the market is the Edwards Inspiris Resilia, a bovine pericardial valve designed to better resist calcification.

While biological heart valves eliminate the need for anticoagulation therapy, they are not as durable as mechanical heart valves. Patients must often undergo valve replacement surgery within 10 to 15 years, as biological valves degrade over time [33]. Thus, biological heart valves are often recommended for patients above 60 to 70 years of age [26]. For pediatric patients who desire to avoid anticoagulation therapy, biological heart valves are available, but they are not ideal, as younger patients have a higher rate of degradation and thus require biological valves to be replaced more often [32, 34].

3.3.3 *Transcatheter*

In the past decade, a new category of heart valve prostheses has emerged. Transcatheter valve prostheses consist of tissue mounted on an expandable stent, and they are introduced into the body in a variety of ways, such as via the femoral artery, the aorta, or the subclavian artery. Today, many variations of transcatheter valves exist, including the Edwards SAPIEN, Medtronic CoreValve, and the St. Jude Medical Portico [30]. Currently, all transcatheter valves are composed of biological tissue as this is necessary for the leaflets to be crimped into a catheter. However, there are concerns that the crimping may cause damage to the tissue and possibly affect long-term durability [35, 36].

As a less invasive alternative to heart valve replacement surgery, transcatheter valve replacement allows patients who pose a high surgical risk to receive valve replacements they would otherwise not receive. While promising, studies have shown that some patients

undergoing transcatheter valve replacement have died soon after the procedure, and others show no improvement in valve functionality or quality of life [37]. Despite advances in the transcatheter delivery mechanism, stroke remains the major complication for transcatheter valve replacement [28]. While over 50,000 adult patients have received transcatheter valve implants since 2002, transcatheter technologies for pediatric patients with congenital heart disease are severely lacking [38]. Recently a study for by Driessen-Mol et al. investigated the long-term functionality of a tissue engineered transcatheter valve, which could overcome the limitations of current transcatheter valves that do not have the capacity to self-repair [39]. Although the results from this study demonstrated promising tissue and self-repair remodeling, there was evidence of paravalvular leakage and regurgitation which would need to be investigated [39]. The minimal invasiveness and fast recovery time of transcatheter valve replacement can be advantageous for younger patients, especially since valve-in-valve procedures are now an option to replace damaged or degraded valve prostheses [28, 40].

3.4 Tissue engineered heart valves

Tissue engineered heart valves (TEHVs) can potentially address the shortcomings of current implants by incorporating biomaterials with autologous cells that enable growth and biological integration. The ideal heart valve prosthesis is anti-thrombogenic, biocompatible, durable, resistant to calcification, and exhibits a physiological hemodynamic profile [41]. In addition, the valve's capability to integrate and grow with somatic growth would eliminate the need for multiple surgeries children must undergo. The overall TEHV should demonstrate excellent hemodynamics and match patient anatomy. At a cellular level, the biomaterials used for the TEHV construct should promote cellular integration by enabling cell adhesion, proliferation, ECM production, and remodeling. Most importantly, the scaffold must promote physiological cell phenotype and

degrade at a rate that matches ECM production. Despite advances, there are no commercially available valves that meet all these requirements.

Biomaterials suitable for TEHVs fall under several classes: decellularized extracellular matrix (ECM; xenografts or homografts), natural polymers, and synthetic polymers. The different classes of biomaterials are discussed in detail in Section 3.10 and 3.11. In addition, the fabrication process for each biomaterial type is taken into consideration, as it can influence cellular behavior, cell viability, mechanical properties, and long-term durability of the scaffold. Thus, when designing a TEHV, there are three main design considerations for choosing a biomaterial: 1) cellular interaction and response to scaffold; 2) fabrication process and its impact on the microarchitecture of scaffold; 3) long-term mechanical properties and function in a physiological setting. These three main design criteria will be further discussed in the next section.

3.4.1 *Design considerations for heart valve tissue engineering*

There are several design criteria for tissue engineering heart valve scaffolds. A TEHV must be non-immunogenic, non-thrombogenic, biodegradable, must promote cellular proliferation and viability, and must be functional in physiological conditions. In this section, an overview of cells, structure, and function of native valves are discussed. Subsequently, a detailed summary of the design considerations for TEHVs and an overview of the current state of the field is provided.

3.5 Native cells

Heart valves are populated with cells that maintain the strength and durability required for repetitive stress and strain over a lifetime. This is accomplished by cells that actively produce and remodel the extracellular matrix (ECM) of the leaflets to repair damages sustained from constant flexion and extension of the leaflets [42-44]. The two

major cell types important for tissue homeostasis are valvular interstitial cells (VICs) and valvular endothelial cells (VECs) (Table 2). Apart from those two cell types, there is also evidence of smooth muscle cells (SMCs) and nerve cells [19, 45]. Thus, the cell source used in TEHVs is an important component for long-term durability, as the lack of cells in valve prostheses have been shown to be the main source of failure for mechanical and biological implants [10].

Table 2. Properties of Valvular Interstitial Cells and Valvular Endothelial Cells.

Reproduced with permission.[44] Copyright 2016, Wiley.

Characteristic	**Valvular interstitial cells**	**Ref.**	**Valvular endothelial cells**	**Ref.**
Cell of origin	Blastocytes → embryonic stem cells → endocardial epithelial cells → mesenchymal cells → VICs	[46]	Blastocytes → embryonic stem cells → endocardial endothelial cells →VECs	[47]
Morphology	Round, rhomboid, tail and spindle-shaped	[48]	Cobblestone, elongated, marginal folds and surface micro-appendage shape	[49]
Metabolic activities	Lysyl oxidase and prolyl 4-hydroxylase production, matrix metalloproteinases and tissue inhibitors of metalloproteinase expression, p38 mitogen-activated protein kinase synthesis	[50-52]	von Willebrand factor production, angiotensin-converting enzyme activity, prostacyclin biosynthesis, endothelial nitric oxide synthase production	[49]
Major phenotypes	Fibroblasts (vimentin), smooth muscle cells (actin), osteoblasts	[48] [53, 54]	Smooth muscle cells (actin, myosin), fibroblasts (vimentin), endothelial cells	[55]
Communication	Adherens junctions, gap junctions	[56]	Gap junctions, tight junctions	[57]
Contractility	Epinephrine or angiotensin II stimulation	[58]	Vasoactive agents	[59]
Immunogenicity	Induce donor-specific T cells	[60]	Induce $CD4^+$ T cells	[61]
Matrix synthesis	Collagens, elastin, proteoglycans, fibronectin	[53] [62]	Collagens, matrix metalloproteinases	[59]
Role in valve disease	Adverse environment causes them to remodel the ECM by secreting growth factors and excessive ECM, leading to different diseases	[63] [64]	Adverse environment causes ECM deposition, oxidized lipoprotein accumulation leading to different diseases	[65]
Response to disease	Both repairing and damaging roles related to calcification	[66]	Expression of calcification-inhibitory proteins (osteoprotegerin), angiogenesis and excessive vascularization	[67] [68]

3.5.1 *VICs*

Valvular interstitial cells make up a heterogeneous cell population found throughout the leaflet. These cells can have a spectrum of sub-phenotypes resembling mesenchymal stem cells, fibroblasts, and smooth muscle cells [19]. VICs behave similarly to mesenchymal stems cells as they are able to differentiate into osteoblasts, adipocytes, and chondrocytes [19, 69, 70]. They also exhibit fibroblast-like properties through their ability to synthesize extracellular matrix proteins such as collagen, glycosaminoglycan, and elastin; however, VICs are distinct from other fibroblasts such as pericardial or dermal fibroblasts [48, 71]. Previous studies have also identified VICs to have positive expression of alpha smooth muscle actin (αSMA) and expression of contractile proteins, a characteristic of SMCs and "activated" fibroblasts [72].

Although not fully understood, VICs have dynamic phenotypes which are categorized under five sub-phenotypes: embryonic progenitor endothelial/mesenchymal cells, quiescent VICs, activated VICs, progenitor VICs, and osteoblast VICs [48]. The cell plasticity of VICs is necessary for the development and maturation of valves but can also play a role in pathological progression. In developing valves, VICs are in an activated state with expression of αSMA and vimentin [48]. Meanwhile, healthy valve cells only express vimentin, suggesting cells are quiescent and fibroblast-like. In the diseased state, VICs are contractile due to higher expression of αSMA. They also have higher levels of ECM production and secretion of cytokines, proteases, and growth factors [48, 73]. If activation persists, VICs can transdifferentiate into osteoblast-like cells, which have been associated with calcific nodule formation and heart valve calcification [73].

The activation of VICs, production of ECM, and secretion of matrix remodeling enzymes can be regulated by the presence of different bioactive molecules as well as mechanical stretch [74-77]. VICs have the capacity to respond to local cellular,

microstructural, and hemodynamic environments through cell-cell and cell-matrix interactions. Cell-cell interaction occurs through cadherins, desmosomes, and gap junctions [78]. However, cellular communication can also occur through paracrine signaling. For instance, when VICs were co-cultured with valvular endothelial cells (VECs) there was a reduction of VIC activation due to VEC nitric oxide production [79]. VICs are also responsive to changes in substrate mechanics. When VICs were cultured on higher modulus (15 kPa) scaffolds, more activation was observed compared to substrates of 3 kPa [80]. Lastly, the hemodynamic environment VICs are exposed to can influence their properties. In a study by Merryman et al., VICs isolated from the left side of the heart were stiffer due to a difference in cytoskeletal composition and collagen biosynthesis compared to cells from the right side of the heart [81].

3.5.2 *VECs*

Valvular endothelial cells (VECs) form a cell layer that lines the blood-contacting surfaces of the valve leaflets. The monolayer of cells is responsible for rendering the leaflet non-thrombogenic. Apart from this, VECs also regulate the immune and inflammatory responses and play a role in regulating VIC phenotype through paracrine signaling [41]. VECs were traditionally assumed to behave similarly to vascular endothelial cells. While there are some similarities such as the expression of Von Willebrand factor, release of nitric oxide and endothelin-1, and presence of prostacyclin and gap junctions, there are also distinct differences between the two cell types [79, 82-85]. The major difference between valvular and vascular endothelial cells is that VECs align circumferentially or perpendicular to the direction of blood flow, while vascular endothelial cells align parallel to the direction of flow [86-88]. VECs have also been shown to have a higher proliferation rate compared to vascular endothelial cells [89].

VECs respond to changes in mechanical environment through the activation of mechanotransduction pathways, which are detected in the blood flow through glycoproteins on the surface of endothelial cells [90]. As a result, flow-mediated mechanotransduction can result in the activation of protective or pathological signaling pathways [91]. For instance, a study demonstrated that changes in shear stress led to morphological changes in VECs, which can result in cell dysfunction and pathogenesis [59]. VECs are also important for modulating VIC function through paracrine signaling. As mentioned before, NO production of VECs is protective in that it maintains VICs in a quiescent phenotype [92]. Meanwhile, when VECs become dysfunctional, VICs have been shown to exhibit a more activated phenotype with elevated expression of αSMA [93]. Furthermore, VECs appear to have different phenotypes and genetic profiles depending on their location on the aortic valve leaflets. This may be because the aortic side of the leaflets experience disturbed flow when the valve closes during diastole, while the ventricular side experiences steady pulsatile flow, promoting a more protective phenotype [59].

3.5.3 *Design criteria*

The cell source selected for tissue engineering heart valves will greatly impact the likelihood of their success. Thus, there are several considerations for selecting a cell source. First, the type of cell is important to consider as there are three main options: xenogeneic, allogenic, and autologous. While xenogenic sources may be readily available, long-term they are not a viable clinical translational option. Allogenic cells are also not ideal as they can invoke an immune response and would require long-term immunosuppressive therapy. Thus, autologous human cells would be optimal for creating a TEHV.

The characteristics of the cell source are significant considerations for TEHVs. The ideal cell source for seeding TEHVs would be one that can be expanded sufficiently and has the potential to be differentiated into the two main cell types found in heart valves, both

VECs and VICs. If these cells are to be differentiated, it is important to characterize their phenotype and biological function. From our review of VECs and VICs, we understand that the phenotype of valve cells is very dynamic and easily impacted by extrinsic factors. The reason for these changes in phenotype is not yet fully understood. Thus, there is no direct metric to determine if differentiated cells from other sources are "truly" valve cells. The only method to characterize these cells is to identify similarity in their function, surface markers, and genetic profile. VICs are known to have expression of αSMA during an activated state. Another phenotype characteristic is the expression of prolyl 4-hydroxylase, which indicates collagen synthesis [72].

However, the cellular function may be the most important factor to consider. For instance, VECs regulate permeability, both immune and inflammatory responses, and VIC phenotype through paracrine signaling [44]. Meanwhile, VICs maintain tissue homeostasis by high proliferation activity and ECM repair and remodeling. The activation of VICs should be managed, as the persistence of a myofibroblast phenotype can result in upregulation of cell proliferation and ECM production, which has been associated with VIC transdifferentiation into osteoblast-like cells and ultimately, valve calcification. The cell source is an important component of the TEHV, with its success being dependent on the effects of the scaffold's micro- and macro-structure and bioactivity.

3.5.4 *Cell source for TEHVs*

A number of cell sources have been applied to tissue engineering heart valves, with most of them coming from animal sources such as porcine, bovine and ovine. (Table 3) [44]. These cell types are frequently used because they are easily accessible and economical. Previous studies have used mesenchymal stem cells (MSCs), VICs, VECs, endothelial progenitor cells, bone marrow progenitor cells, autologous amniotic fluid cells, myofibroblasts, and smooth muscle cells [44]. Similar cell types were also investigated

using human cell sources. The important take away from past studies is that each cell type has advantages and disadvantages. For instance, MSCs collected from bone marrow resembled fibroblasts and had multi-lineage differentiation potential. When MSCs were cultured on different scaffolds such as polyglycolic acid (PGA) with poly-l-lactic acid (PLLA), cells under mechanical stimulation demonstrated collagen deposition similar to VICs [94]. In another case, autologous amniotic fluid cells were used to seed a trileaflet valve composed of polyglycolic acid and poly-4-hydroxybutyrate (PGA-P4HB). After 1 week of implantation *in utero*, scaffolds demonstrated cellular integration characterized by increased cellularity and GAG content [95]. Furthermore, human fibroblasts and endothelial cells isolated from saphenous veins were used to seed a polyurethane nanofibrous scaffold [96]. The fibroblasts were able to spread on the fibrous scaffold, while the endothelial cells formed a monolayer over the fibroblasts. The cells responded better to a dynamic culture setting, showing more proliferation and ECM production [96]. Although these studies are promising, the direct application of primary cells for TEHVs may not be suitable for clinical translation, as allogenic cells can induce an immune response in the recipient of the TEHV [44]. Also, primary cells have limited proliferation capabilities, while stem cells can result in uncontrollable proliferation [44]. These are some limitations that need to be considered when selecting a cell source for TEHVs. While we do not report extensively on cell types for TEHVs, more information can be obtained by Jana et al [44].

Table 3. Cell types used for tissue engineering heart valves.

Reproduced with permission.[44] Copyright 2016, Wiley.

Cell type	Organ source (tissue/animal)	Ref.
Animal sources		
Mesenchymal stem cell	Bone marrow/ovine	[97]
Valvular interstitial cell	Aortic valve/porcine	[98, 99]
Valvular endothelial cell	Aortic valve/bovine	[100, 101]
Endothelial progenitor cell	Peripheral blood/sheep	[102]
Endothelial cell	Carotid artery/lamb	[103]
Bone marrow progenitor cell	Bone marrow/lamb	[104]
Autologous amniotic fluid cell	Amniotic fluid/sheep	[95]
Smooth muscle cell	Aortic root sinus/porcine	[105, 106]
Myofibroblast	Aortic wall/porcine	[107]
Human sources		
Mesenchymal stem cell	Bone marrow	[108, 109]
	Adipose tissue	[110, 111]
	Umbilical cord matrix	[112]
	Umbilical cord blood	[113]
	Amniotic fluid	[114]
	Chorionic villi	[115]
Endothelial progenitor cell	Amniotic fluid	[116]
	Peripheral blood	[117]
	Umbilical cord blood	[112]
Valvular interstitial cell	Aortic valve	[118]
Induced pluripotent stem cell	Skin (fibroblasts)	[119]

3.6 Structure

In the heart, there are four valves: the tricuspid and mitral valves control blood flowing from the atrium to the ventricles, while the pulmonary and aortic valves regulate blood from the ventricles to the pulmonary artery and the aorta, respectively. The tricuspid, pulmonary, and aortic valves are composed of three leaflets. Meanwhile, the mitral valve has two cusps that have chordae tendineae attached to the posterior surface of the valve to prevent the cusps from prolapsing.

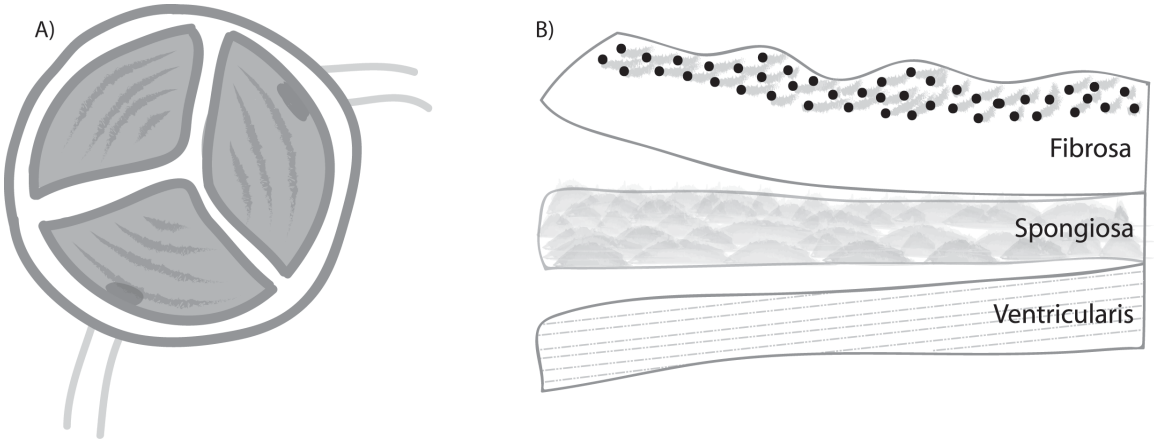

Figure 2. Anatomical structure of aortic valve and a cross-sectional view of the three layers of the valve leaflet. A) There are three leaflets in the aortic valve, which open and close to allow for unidirectional blood flow. Each leaflet is composed of three layers known as the fibrosa, spongiosa, and ventricularis. The fibrosa layer has collagen fibers aligned in the circumferential direction, while the ventricularis is composed of elastin fibers aligned in the radial direction. Valvular endothelial cells line the outer layers of the fibrosa and the ventricularis, and within the valve leaflet, there are valvular interstitial cells.

The mechanical strength of valves is attributed to the structure of the layers in the leaflet, and more specifically, the arrangement and orientation of the ECM. The thickness of valve leaflet ranges between 300 to 700 μm and is composed of collagen type I/III, proteoglycans, glycosaminoglycans (GAGs), and elastin [72]. The leaflet is comprised of three layers known as the fibrosa, spongiosa, and ventricularis (Figure 2) [10, 41, 120]. An important feature of the valve leaflets is the microstructure in each of the three layers of the leaflet. The fibrosa layer makes up almost half of the leaflet thickness, where dense collagen type-I fibers are aligned in a circumferential direction [19, 121]. The highly organized structure of the collagen fibers enables the fibrosa to be the load-bearing layer during diastole [85, 122]. The spongiosa is the middle layer rich in glycosaminoglycans,

known to act as a lubricant between the two leaflet layers [123]. Furthermore, the ventricularis layer has elastin fibers radially aligned, providing the leaflets with elastic properties [85, 121].

In a study to characterize the mechanical properties of the valve leaflets using uniaxial tensile testing, it was observed that the leaflets experience about 1-2 MPa in the radial direction and 8-12 MPa during the nonlinear transition [85, 123, 124]. However, at physiological stress and strain, the leaflets can experience about 200 - 400kPa in stress, and about 0.1 and 0.4 in strain in the circumferential and radial directions, respectively [85]. At a cellular level, one study showed that the modulus of each individual layer of the leaflet varied. For instance, in porcine valves, the ventricularis ranged between 8 to 17 kPa, the spongiosa ranged between 5 to 7 kPa, and fibrosa ranged between 8 to 19 kPa [125]. The stiffness of each layer of the leaflet was determined via atomic force microscopy (AFM), which has inherent limitations. These ranges should be used as a guide as there is evidence from finite element (FE) analysis that despite each layer having unique features they function as a homogenous structure during deformation rather than a heterogenous structure [126]. The properties of the ECM should be carefully designed to mimic the macro function of the leaflets.

3.6.1 *Design criteria*

Despite efforts in the field of TEHVs, the ability to successfully replicate the trilayer leaflet structure remains a challenge. The structure of the valve leaflets significantly impacts its ability to mechanically function in physiological conditions. The most important design criterion for developing functional leaflets is the anisotropic properties observed in native valves. Anisotropy is achieved by the different orientations of collagen and elastin fibers. To replicate this property, a fabrication process that can reproduce these unique orientations will need to be identified and implemented. Furthermore, the overall

mechanical properties need to be within the 200 - 400 kPa range for proper function in physiological conditions, as stated previously [85]. At a cellular level, cells experience a modulus that is magnitudes lower. This is an important consideration as previous studies have demonstrated that VICs transition to a myofibroblast phenotype when cultured on stiffer surfaces [127, 128]. In summary, the anisotropic properties, overall modulus of 200-400 kPa, and ability to sustain a healthy cell phenotype are all properties that should be considered in the design of TEHVs.

3.6.2 *Recapitulating Microstructure in TEHVs*

In an attempt to recapitulate the anisotropic properties and microstructure of the valve leaflet, several studies have investigated methods of introducing multiple layers to the valve leaflet design. In the past, studies focused on first developing single-layer designs, as fabrication processes were limited. With the advancement of fabrication techniques and materials science, there have been several groups that developed and tested multilayered scaffolds for TEHVs. For instance, the electrospinning technique using materials such as poly-ε-caprolactone (PCL) enables the formation of aligned nanofibers [129]. These aligned scaffolds introduce anisotropic properties similar to native valve leaflets. Modification to electrospun scaffolds and addition of other materials have since been introduced to generate more complex structures that resemble the three layers of the leaflet [118, 130]. An example of this is a trilayer elastomeric scaffold created by Masoumi et al., where poly (glycerol sebacate) (PGS) was molded into a diamond-like shape using microfabrication processes. This scaffold was then assembled to generate a PGS scaffold with electrospun PGS/PCL sandwiched in between. This generated a tunable, elastic, anisotropic scaffold that supported cellular function and activity. The scaffold was tested functionally in an *ex vivo* model, where the trilayer leaflet outperformed the single layer PCL-only scaffold [118].

When generating complex structures composed of different materials, the interaction between layers is another important consideration. One study demonstrated that a trilayer hydrogel quasilaminate can be generated using poly (ethylene glycol) diacrylate (PEGDA) and a sandwich fabrication method [131]. The scaffold was composed of two stiff hydrogel outer layers and one soft hydrogel component to represent the spongiosa layer. The quasilaminate scaffold did not experience any issues between the interface of the layers and did not vary in bending moduli compared to its single layer counterpart. However, a main takeaway from this study is that when cells were introduced to the trilayer scaffold, the modulus decreased [131]. Another fabrication process that enables structure and anisotropic properties to be introduced is the application of 3D printing. Additive 3D printing can enable scaffolds of intricate designs to be fabricated, where the microstructure and alignment of fibers can be printed with spatial placement of specific cell types [132]. While 3D printing enables significant complexity to be introduced to the scaffold, this process is still in the development phase. The biomaterials needed to create these scaffolds must first be optimized for the 3D printing process.

There are several different fabrication processes used to generate biomimetic scaffolds resembling the three layers of the valve leaflet. While some techniques, such as electrospinning, introduce the anisotropic properties, the fabrication process may not suitable for generating a scaffold with cells encapsulated within it. Therefore, when designing the structure of the TEHV, the method in which scaffolds will be fabricated have to be carefully considered, as it can affect overall mechanical properties, anatomical structure of the scaffold, and cellular activity.

3.7 Function

Healthy heart valves are essential for proper heart function. In an average lifetime, a person’s heart valves will open and close nearly 3 billion times, allowing 3-5 L of blood to

circulate through the body [85, 133]. Valves rely on the inertial forces from blood flow to open and close, passively ensuring unidirectionality during the cardiac cycle. The semilunar valves (pulmonary and aortic) prevent blood from flowing back into the ventricles, while the atrioventricular valves (tricuspid and mitral) prevent blood from flowing back into the atria from the ventricles. To sustain such an important function in the cardiac cycle, heart valves must be able to withstand many forces of the hemodynamic environment within the heart, a feat made possible as a result of its structure.

3.7.1 *Hemodynamics*

In the aortic valve, the leaflets of the valve are closed during diastole, slightly overlapping in a region called the lunula to allow the filling of the left ventricle. The valve annulus then expands in radius until a small orifice is present, and blood begins to flow through the orifice as the ventricle contracts during systole [85]. During this contraction, the aortic valve opens, and blood flows through the valve, traveling up to 1.35 ± 0.35 m/s [134]. At the end of systole, the deceleration of blood flow allows for the coaptation of the valve cusps. The aortic sinuses are particularly important in this function. Pressure differences cause blood along the aortic wall to reverse direction, creating vortices on the leaflets facing the aorta, leading to the closure of the valve leaflets. In addition, vortices create a small pressure gradient across the leaflets and push them into their closed position [85, 133].

3.7.2 *Biomechanics of heart valve function*

During the cardiac cycle, valves experience stresses and strains as a result of blood flow and pressure gradients between the chambers of the heart. Arjunon et al. described three mechanical stimuli experienced by heart valves: shear stress, pressure, and leaflet strain (Figure 3) [42].

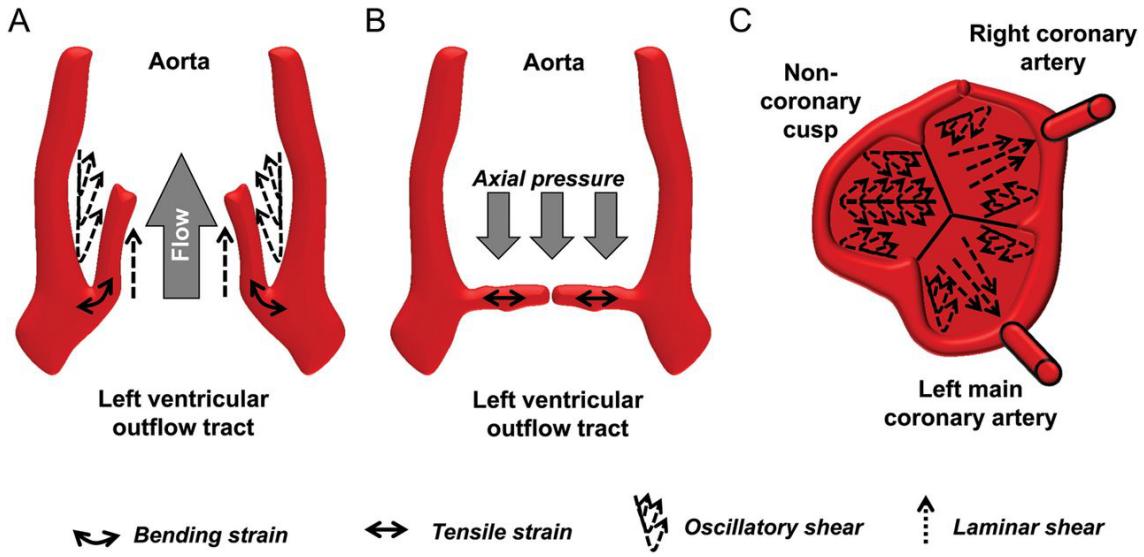

Figure 3. Shear stresses and strains experienced by aortic valve leaflets.

Stress and strain during a) systole, b) diastole, and c) diastole, from a top view. Adapted under the terms of the Creative Commons Attribution License [1]. Copyright 2013, Back et al.

Shear stress in valves is defined as the frictional stresses that the leaflets experience due to blood flow during the cardiac cycle. While shear stresses on the walls of the aorta, proximal to the leaflets, are well described, only a few attempts to measure shear stresses on aortic valve leaflets have been reported. One group conducted studies on the shear stresses experienced by the different surfaces on aortic valve leaflets. They reported that shear stresses experienced by the ventricularis were unidirectional, whereas those experienced by the fibrosa were oscillatory and dependent on hemodynamics [135, 136]. In these studies, they reported that the highest shear stresses experienced by the ventricularis were 80 dynes/cm^2 during systole, and during diastole, the fibrosa experienced shear stresses of about 23 dynes/cm^2 [135, 136]. In a diseased or defective state, leaflets may experience higher levels of shear stress due to altered hemodynamics

[42]. It is also suggested that reduced shear stresses can lead to calcification of the leaflet [137].

During diastole, heart valves experience transvalvular pressure gradients ranging from 10 mmHg to 120 mmHg [133]. The aortic valve, in particular, experiences a transvalvular diastolic pressure gradient of 80 mmHg [42]. The ability to sustain this pressure is due to circumferentially aligned collagen fibers in the fibrosa layer of the leaflets [138]. In the case of varying degrees of aortic stenosis or hypertension, transvalvular pressure gradients can increase depending on the severity of the disease [42].

Strain, a measure of deformation, in aortic valve leaflets is largely determined by tissue structure. In the circumferential direction, collagen fibers provide tensile strength. Alternatively, elastin fibers mainly oriented in the radial direction lead to greater strain experienced in this direction. Strain in the circumferential and radial directions were reported to be 10% and 40%, respectively [139-141].

3.7.3 *Design Criteria*

TEHVs must be designed to offer a significant increase in function compared to the diseased valve while simultaneously integrating with the patient's body, a task not yet accomplished by mechanical or biological valve implants. Above all, TEHVs must ensure the functionality of the valve by passively maintaining unidirectional blood flow. In order to achieve this functionality, TEHVs must be designed with several considerations in mind. First and foremost, TEHVs must be able to withstand the inertial forces of blood flow in the hemodynamic environment of the heart, using them to open and close passively. Blood flow out of the left ventricle during systole should passively open the TEHV. By mimicking the general anatomy of the valve leaflets and sinuses, vortices due to back flow of blood at the end of systole, in addition to those as a result of pressure gradients between heart chambers, should cause the TEHV to close fully.

In the closed state during diastole, TEHVs must be able to withstand a transvalvular pressure gradient of 80 mmHg. Upon opening, TEHV leaflets will experience unidirectional shear stress on the ventricularis surface and oscillatory shear stress on the fibrosa surface, and such shear should not cause damage to the leaflets, nor should it stimulate the progression of disease, such as calcification. Lastly, leaflets should display anisotropic properties, particularly regarding strain in the circumferential and radial directions, as these properties are important in ensuring valve functionality and preventing pathological conditions from developing on the cellular level [42].

3.7.4 *Functionality of TEHVs*

Because healthy human heart valves are difficult to obtain, the mechanical properties of valve leaflets and the mechanical stimuli they experience have yet to be fully investigated. In comparison, studies in the functionality of TEHVs are even more lacking, as complete, functional valve structures have yet to be fabricated. Some groups that have investigated the functionality of their tissue engineered scaffolds include Engelmayr et al. [142], Driessen et al. [143], and Alavi et al. [144]. A few studies of TEHV implantation into animal models have been conducted by Sodian et al. [145]. Hoerstrup et al. [146], and Kluin et al. [147].

Engelmayr et al. created a bioreactor to simulate cyclic flexure to test heart valve scaffolds made of PGA fibers and a 50:50 blend of PGA and PLLA fibers, coated in P4HB to allow molding into different shapes. From this study, they determined that dynamic flexure significantly decreases the stiffness of their scaffolds after 1 week compared to those in static conditions, due to fiber fragmentation observed in SEM images of the scaffolds [142]. This suggests that dynamic testing is necessary to evaluate the functionality of TEHVs in a physiological setting, as TEHV behavior may not be truly represented in static testing conditions. Driessen et al. aimed to model the mechanics

TEHV leaflets and created scaffolds PGA coated in P4HB seeded with human cells and conditioned in a diastolic pulse duplicator. Over 4 weeks, the conditioned leaflets became thinner. Uniaxial tensile tests were performed on the conditioned leaflets, and the results were used to develop a model to analyze TEHV mechanics. In addition to less coaptation of the engineered scaffolds, these results indicated that the tissue engineered leaflets were stiffer and less anisotropic compared to native porcine valve leaflets [143]. Alavi et al. designed many different nitinol mesh leaflets, conditioned in a pulse duplicator to determine which leaflets functioned most similarly to the native valve. Accelerated wear tests were then conducted on the best scaffolds to determine their durability, and computer simulations revealed that scaffold design may result in abnormal valve function [144]. These studies demonstrate the importance of testing the functionality of TEHVs in dynamic conditions and indicate a need for more appropriate scaffold designs to replicate the functionality of native valves.

Only a few studies involving TEHV implantation into animal models have been conducted to date. Sodian et al. created polyhydroxyoctanoate (PHO) scaffolds with ovine carotid arterial cells and implanted the scaffolds into 6 sheep. These valve scaffolds resulted in no stenosis or thrombosis for 20 weeks, but they degraded slowly, resulting in prolonged bioabsorption of PHO [145]. Hoerstrup et al. created a PGA mesh coated with P4HB, which resulted in faster degradation of the scaffold that was higher in strength and flexibility. These valve scaffolds resembled native heart valves in structure, mechanics, and composition, and they remained functional in sheep for 5 months [146]. More recently, Kluin et al. implanted an electrospun polycarbonate bis-urea (PC-BU) valve into the pulmonary position of sheep for up to 12 months. During this time, the subjects did not show signs of valve failure, and the implanted scaffolds had cell infiltration into the porous microstructure. The evidence of collagen, GAGs, and elastin deposition similar to native valves was thought to contribute to the successful functionality of these valves [147].

While the field of TEHVs is rapidly advancing, many TEHVs have yet to be studied for functionality. As more groups are successful in designing functional TEHV scaffolds, studies regarding the mechanical properties and the effect of hemodynamics on these scaffolds must be conducted to determine their suitability for implantation in humans.

3.8 Evaluation of TEHVs

3.8.1 *Bioreactors*

To create functional TEHVs, it is important that TEHV scaffolds experience physiological hemodynamic conditions, as the stresses and strains on valves during the cardiac cycle is essential to inducing proper cellular behavior. Dynamic bioreactors serve an important role in this process. In addition to making it possible to observe initial leaflet functionality, they can also condition scaffolds over time, allowing cells to produce ECM that may enhance mechanical properties prior to implantation. Because hemodynamic behavior around valves is quite complex, many different bioreactors have been created to mimic the conditions that native valves experience, including cyclic stretch and flexure, oscillatory shear stress, and pressure, and more are in development.

In 2000, Hoerstrup et al. developed a pulsatile flow bioreactor in order to stimulate TEHV scaffolds to increase in mechanical strength through ECM production, while enabling a more complete degradation of the polymeric scaffold. This bioreactor consisted of an air chamber and a fluid chamber separated by a silicone rubber diaphragm, which caused pulsatile flow when displaced periodically [148]. For less mechanically robust TEHVs made of materials such as hydrogels, Jockenhoevel et al. created a bioreactor consisting of a laminar flow chamber to introduce shear stress to fragile scaffolds [149]. Soon following, Engelmayr et al. reported a bioreactor design to provide cycle flexural stimulation to TEHV scaffolds in order to observe changes in effective stiffness of the

scaffold due to unidirectional cyclic flexure [142]. To study the effects of conditioning scaffolds with only some of the mechanical cues present during the cardiac cycle, Mol et al. designed a diastolic pulse duplicator, a bioreactor that only mimics the diastolic phase of the cycle and conditions scaffolds using a strain-based approach [150]. Alternatively, Engelmayr et al. designed the Flex-Stretch-Flow (FSF) Bioreactor in order to study the coupled effects of cyclic flexure, stretch, and flow on TEHVs [151]. In addition, Syedain et al. created a cyclic stretch bioreactor consisting of the TEHV mounted in a latex tube that is cyclically pressurized by culture media, stretching the valve root and leaflets with the latex.

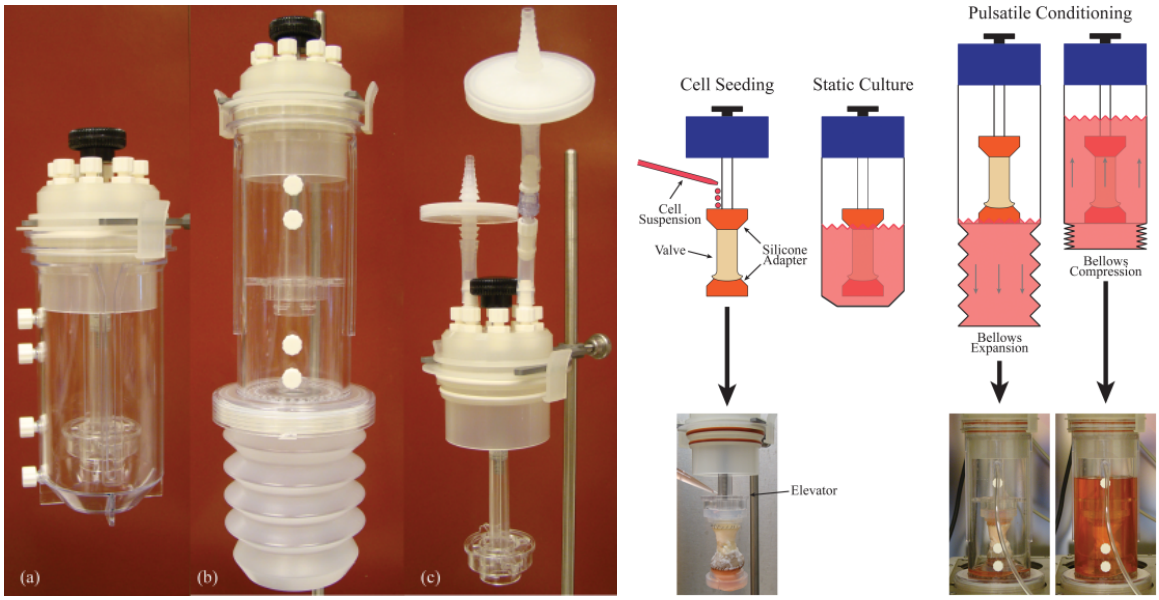

Figure 4. Disposable bioreactor designed by Converse et al. This bioreactor design consists of (a) the seeding chamber, (b), the pulsatile chamber, and (c) the cap. TEHV conditioning in the disposable bioreactor is shown on the right. Reproduced with permission [2]. Copyright 2015, Wiley.

More recently, Ramaswamy et al. designed a more physiologically relevant bioreactor that would allow for higher fluid velocities and subject scaffolds to higher shear stress while maintaining laminar flow [152]. Converse et al. identified a problem with bioreactors in that most of the ones that have been developed are complex and suited for

bench research, rather than clinical application. Current bioreactors utilize flow-loops to mimic circulation, which increases system complexity, and they are designed to be re-sterilized and re-used. From a regulation standpoint, this is undesirable because re-sterilization and re-use increases the risks of disease transmission in between scaffolds during seeding and conditioning. This serves as a hindrance for the clinical development of patient-specific TEHVs, so alternative designs must be pursued to make this process clinically translatable. To address this issue, Converse et al. developed a disposable bioreactor system consisting of three parts: a seeding chamber where cells can attach to the scaffold, a pulsatile chamber for mechanical condition, and a cap where the scaffold attaches to allow movement between chambers. A screw driven actuator compresses and expands a bellows to generate pulsatile flow of culture medium (Figure 4) [153]. Alongside the rapid development of TEHVs, bioreactors have also been improved to better mimic physiological hemodynamics and to be more applicable outside of bench research, as TEHVs come closer to reaching the clinic.

3.8.2 *In vivo evaluations*

Prior to implantation in humans, TEHVs must be evaluated in animal models to ensure that they can function long-term with matrix remodeling and tissue growth without entering a diseased state. Ideally, primates would serve as the best models to observe TEHVs *in vivo* long-term because they closely resemble humans anatomically and physiologically, but they are expensive to purchase and maintain, and their use is heavily restricted by ethics [154]. For this reason, smaller mammals are used, such as pigs, calves, and sheep. The most commonly used animal model for studying TEHVs is the adult sheep. Sheep have been widely used because they have high calcium metabolism, making them valuable for observing TEHVs for durability and sustained performance under "worst case" conditions [155]. However, this characteristic of ovine models may lead to increased fibrosis of the valve, and therefore, sheep are not a proper representation of valve tissue

remodeling and regeneration in humans [156]. In addition, sheep have reduced platelet activity compared to humans, which may result in the failure to reveal the thrombogenic potential of TEHVs scaffolds [157]. *In vivo* studies of TEHVs are limited, but the majority of them have been conducted in ovine models [39, 117, 147, 158].

More recently, Gallo et al. reported on the potential use of the Vietnamese pig to evaluate TEHVs because they possess anatomic features that are very similar to those of humans. Compared to common farm pigs, Vietnamese pigs are smaller and do not grow as rapidly; they reach about 70 kg during adulthood. Vietnamese pigs are also suitable because their cardiac output, stroke volume, mean arterial pressure, heart rate, and myocardial blood flow are all comparable to humans, as well as their immune response and mechanism of blood coagulation. However, these pigs were reported to be more susceptible to endocarditis [159]. While Vietnamese pigs show promise, for now, there is not a standard animal model for the evaluation of TEHVs *in vivo*.

3.9 TEHV fabrication techniques

Before highlighting different biomaterials used for TEHVs, there are three main techniques for fabricating natural or synthetic scaffolds that will be covered throughout this section: molding, fiber spinning, and bioprinting (Figure 5). Scaffolds can be fabricated through molding, which is a process where precursor solution is dissolved, poured into a mold, and then gelled. This technique is often utilized to generate tubular or planar scaffolds [160]. Another mechanism utilized for generating fibrillar scaffolds is electrospinning. This fabrication process involves subjecting a polymer solution to an electric field. A charged polymer solution is generated when the electrostatic repulsion overcomes the surface tension between the polymer and syringe. Once this occurs, jets of polymer travel towards a surface, during which the solvent evaporates to generate continuous filaments of natural or synthetic material [161]. Bioprinting is a more recent

approach used to generate scaffolds for heart valve tissue engineering. 3D bioprinting is an additive manufacturing technique that enables complex 3D structures to be generated through layer-by-layer deposition of biomaterials, cells, and growth factors [162, 163]. The most common types of 3D bioprinting are inkjet, extrusion-based, and laser-assisted printing [162].

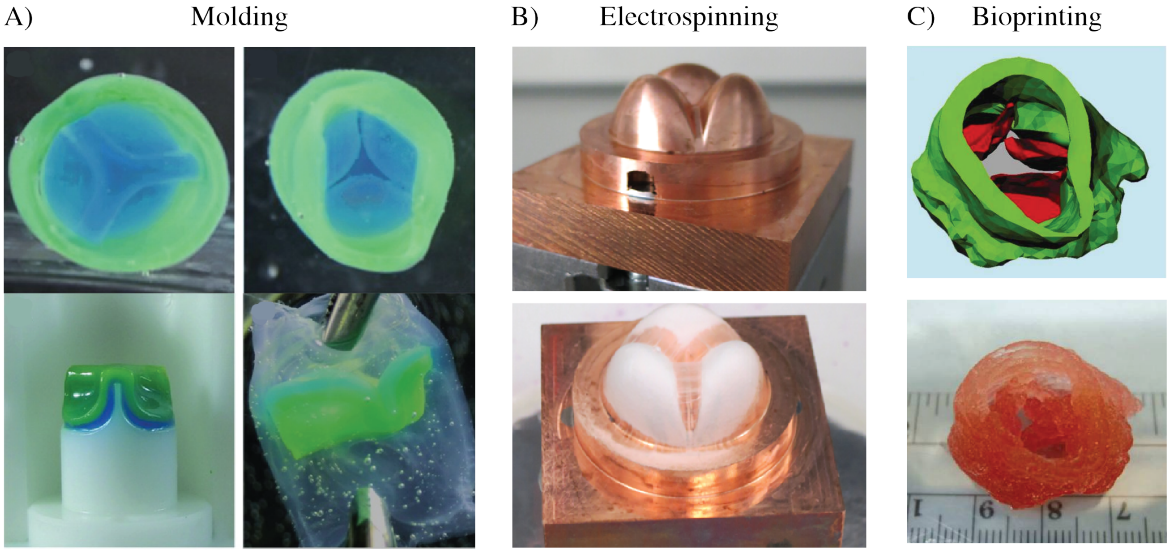

Figure 5. Fabrication methods for TEHVs. A) Molding can be used to generate heart valve conduits. A multi-step injection molding technique was utilized to generate a fibrin valve with leaflets and aortic root. Color was added for visualization of leaflets. Bottom images demonstrate the ability to create two-layered leaflets. Reproduced under the terms of the Creative Common Attribution Noncommerical License [99]. Copyright 2015, M. Weber et al. B) Copper valve mold was used as the collector for electrospinning PEGdma-PLA to create valve conduit. Reproduced with permission [71]. Copyright 2014, Elsevier. C) Top image shows a 3D model of a reconstructed aortic valve. The color difference is to distinguish different cell sources used for 3D printing scaffold: green represents SMCs and red is for VICs. Bottom image is the 3D bioprinted valve. Reproduced with permission [72]. Copyright 2013, Wiley.

3.10 Natural biomaterials

The application of natural biomaterials has been used in a variety of tissue engineering applications such as wound healing, sutures, bone regeneration, drug delivery, and medical devices [164]. Natural materials can be in the form of polysaccharides, proteins, and polyesters and are derived from a number of animal sources, plants, algae, and fermentation of microorganisms [165-167]. The advantage of natural biomaterials over other materials is that they have similar biological macromolecules that are important for guiding cells in tissue homeostasis and repair. In addition, the material properties can minimize chronic inflammation and immunological reactions. In this section, ECM-derived natural biomaterials and their applications in heart valve tissue engineering are discussed. GelMA will be further discussed in reference to its application to this thesis project.

3.10.1 *Collagen*

Collagen is the most abundant protein in the body, with more than 28 genetic variants [168]. The most common type of collagen is collagen type I, which has been extensively studied in tissue engineering applications [169]. The other types of collagen are II, III, and V, and they make up components of skin, muscle, bone cartilage, and tendons. All variants of collagen are characterized by a triple-helix structure, where each single polypeptide chain is composed of a repeating sequence, Gly-Xaa-Yaa. Glycine is the smallest amino acid that is found in every third amino acid of the peptide sequence, and any amino acid can be found in the Xaa or Yaa positions. More frequently, proline occupies the Yaa position, and it is often found as hydroxyproline due to post-translational modification. Aside from the frequency of proline and hydroxyproline, there are hydrogen bonds that stabilize the triple-helix structure, thus enabling the structure to remain stable at

body temperature [170]. When synthesized *in vivo*, collagen self-assembles into fibrillar structures to form collagen fibers that make up the matrix surrounding the cells.

With collagen being one of the most abundant proteins found in the body, there have been many applications in the cosmetic, medical, pharmaceutical, and food industry [171]. Collagen can be fabricated into several different forms such as collagen sheets, sponges, hydrogels, pellets, or nanospheres. In the case for heart valve tissue engineering, collagen is of high interest mainly because the leaflets of the valve are primarily composed of collagen type I. Collagen can be extracted and purified from different tissue sources [160]. It is also possible to obtain human recombinant collagen; however, the mechanism for doing so is expensive and not yet scalable for clinical translation [172].

Collagen hydrogels are fabricated by using collagen type I monomers that self-assemble into fibrillar structures to form a viscoelastic hydrogel. The mechanical properties of collagen hydrogels can be tuned through the concentration of monomer, temperature, pH, and ionic strength [160, 173]. These conditions can influence the diameter of collagen fibers and the overall mechanical properties of the hydrogel [174]. Although the mechanical properties are tunable, the elastic moduli of collagen hydrogels are limited to 10-30 kPa and have an ultimate tensile strength of 5-10 kPa [175]. These properties of collagen hydrogels are not representative of natural ECM because lower protein concentrations must be used to ensure proper diffusion of nutrients to the surrounding cells [85, 176].

In heart valve tissue engineering, collagen scaffolds were molded in 2D or 3D hydrogels to better understand heart valve biology and the progression of valve disease [177, 178]. To develop a scaffold with physiological properties, the temperature, pH, and crosslinker concentration has been utilized to modulate the scaffold properties [179-181]. In several studies, collagen gels were used to examine cellular behavior and changes that

mimic physiological conditions. In one study, collagen gels were used to understand the metabolic activity of VICs and VECs co-cultured in the presence of chondroitin sulfate [182]. The results of this study demonstrated that collagen constructs were capable of contracting similar to mitral valve tissue and were ideal for understanding valve biology. In a different study, 3D collagen gels were generated to determine the effects of anisotropic strain on VIC phenotype and fibroblastic behavior [183]. This study led to a better understanding of how VICs respond to strains, where the phenotype of VICs was modulated by anisotropic biaxial strain [183].

While electrospinning has been widely applied to tissue engineering, collagen electrospinning alone has yet to be applied to heart valve tissue engineering [161, 184]. However, collagen in combination with synthetic polymers have been used to generate nanofibers scaffolds for tissue engineering [185-187]. Meanwhile, extrusion-based 3D bioprinting has been used to create collagen scaffolds for tissue engineering applications but these scaffolds are less common than scaffolds of other biomaterials such as alginate, methacrylated polymers, and synthetic hydrogels [14, 188]. 3D bioprinting is possible with collagen only if the pH or temperature are properly controlled [160]. With ideal conditions, collagen can take up to half an hour for complete gelation [189]. The most common application of collagen for 3D bioprinting is for cartilage or skin tissue engineering and not as often for heart valve tissue engineering [190, 191]. Collagen is rarely bioprinted by itself but rather with a combination of other materials such as Pluronic, which is used to improve the viscosity needed for extrusion [189, 192, 193]. While collagen was not used directly in 3D bioprinting a heart valve, Duan et al. 3D bioprinted a heterogeneous heart valve using gelatin and alginate hydrogels [106]. Gelatin is a denatured form of collagen and has similar properties to native collagen.

There are many advantages and disadvantages to using collagen as a biomaterial for tissue engineering heart valves. One advantage of collagen is that it is a native

biomaterial in which cells can recognize and interact with. For instance, collagen has a peptide sequence Arg-Gly-Asp (RGD) that cells can recognize through integrin-binding. This interaction can result in activation of several signaling pathways that can promote proliferation, migration, and prevent apoptosis [194, 195]. In addition, VICs are known to secrete matrix metalloproteinases (MMPs) that can control collagen scaffold degradation [196, 197]. Collagen, a native material found in heart valve leaflets, would be the ideal scaffold for tissue engineering heart valves. Although there are several advantages to using a natural biomaterial, collagen has major setbacks that limit its capabilities to be used as a biomaterial for clinically translatable valves.

One of the major disadvantages of collagen is the lot-to-lot variation from different animal sources and from different tissue samples [171]. Another concern is that collagen from other species or even other humans can elicit an immunogenic reaction if there are antigens present [160]. Collagen, when exposed to blood, can activate blood coagulation pathway through platelet adhesion and aggregation [198]. There are surface treatments to make the collagen less thrombogenic or methods to recruit endothelial cells that can prevent thrombogenesis [199]. However, a major limitation is the mechanical properties of collagen scaffolds. It does not meet the design criteria for heart valve tissue engineering by itself and thus modifications or combination with other materials are required to utilize collagen as a material for heart valve tissue engineering.

3.10.2 *Gelatin*

Gelatin is partially hydrolyzed collagen that was originally investigated for its application as a cell culture platform. Soluble gelatin retains many of the bioactive features of collagen; however, to form hydrogels, the gelatin solution must be cooled to temperatures below physiological conditions. As a result, this prompted chemical modifications to gelatin to generate a robust tunable hydrogel. The most common

modification to gelatin is methacrylation, where methacrylic anhydride is mixed with gelatin solution to generate gelatin methacrylate (GelMA) [200]. The ability to tune the mechanical properties of gelatin using photopolymerization has led to its application in bone, cartilage, tissue culture platforms, and tissue engineering [201-203]. Gelatin scaffolds have been designed to be either porous or fibrous, depending on application.

As for TEHV, GelMA has been incorporated into polymer blends to improve the viscosity for 3D extrusion-based printing and to introduce biological active sites for enhanced cell viability [106]. Another application of GelMA is to study VIC behavior and the effects of different biomolecules. For example, different fibrotic growth factors were incorporated into the 3D hydrogel [204]. VICs were able to exhibit a fibroblast-like phenotype within two weeks of cell culture. When TGF-B1 was incorporated into the GelMA, VICs differentiated into a myofibroblast phenotype with upregulation of α-SMA, MMPs, and migration [204]. These two applications of GelMA demonstrate that gelatin can be modified and tuned for *in vitro* studies and possibly for the development of a 3D valve conduit. The advantage of using gelatin is similar to collagen in that it contains bioactive molecules that promotes cell adhesion, proliferation, and migration. However, gelatin is mechanically weak and requires chemical modification or addition of other materials for it to form a hydrogel. Thus, the best application of gelatin is to introduce biological activity to a scaffold or to be used as an additive for modifying physical properties of a polymer blend for 3D bioprinting.

3.11 Synthetic biomaterials

Due to the inadequate mechanical properties, lack of tunability, and batch-to-batch variation of natural biomaterials, synthetic biomaterials have been pursued for TEHV fabrication. Two main categories of synthetic polymers have been used extensively for this

purpose, those that can be crosslinked into hydrogel scaffolds, and those that can be made into mechanically stiffer scaffolds that degrade by hydrolysis.

3.11.1 *Hydrogel polymers*

Hydrogels are studied extensively in the field of tissue engineering due to their elasticity, high water content, and biocompatibility. As opposed to hydrogels made of natural materials, synthetic hydrogels have been pursued in tissue engineering endeavors for their tunable mechanical properties. Two types of synthetic hydrogels have been used widely to fabricate heart valves: poly(ethylene glycol) (PEG) and poly(vinyl alcohol) (PVA). In particular, PEGDA will be further discussed in reference to its application to this thesis project.

3.11.2 *Poly (ethylene glycol)*

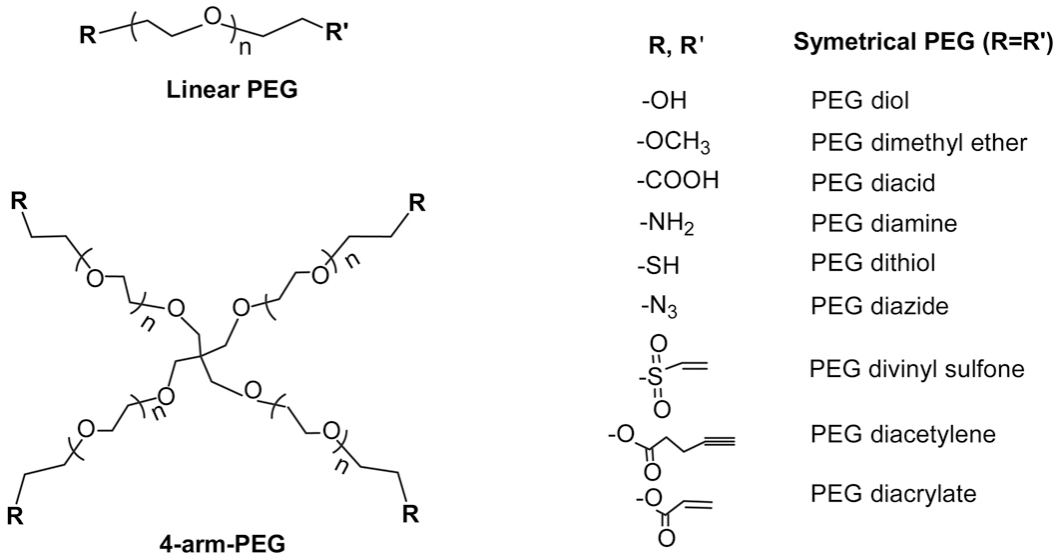

Figure 6. The chemical structure of linear and branched PEG with functional groups, represented by R and R'. Reproduced with permission [225]. Copyright 2010, Elsevier.

Poly(ethylene glycol) (PEG), also known as poly(ethylene oxide) (PEO), is the most commonly studied synthetic hydrogel for TEHVs. PEG is formed by the polymerization of ethylene oxide, and in its most basic form, contains hydroxyl groups on each end. It is hydrophilic and can be linear or branched. In place of the hydroxyl groups, PEG polymers can be functionalized with different groups such as methoxy, carboxyl, amine, thiol, azide, vinyl sulfone, acetylene, and acrylate (Figure 6) [205]. PEG-diacrylate (PEGDA) is particularly useful, as PEGDA can be photocrosslinked, and it is formed by the reaction of PEG with acryloyl chloride. For TEHV applications, PEG hydrogels are commonly fabricated by crosslinking PEGDA with exposure to UV or white light in the presence of their respective photoinitiators: 2-hydroxy-4′-(2-hydroxyethoxy)-2-methylpropiophenone (Irgacure 2925) for UV light, and triethanolamine, Eosin Y, and N-vinyl pyrrolidone for white light [206]. PEGDA undergoes a rapid and random free radical propagation and termination, known as chain-growth polymerization [205, 207]. This polymerization method results in a heterogeneous polymer network. Photo-crosslinked PEG hydrogels are not readily degradable in their most basic form, but PEG-based block polymers with terminating acrylate groups can be both crosslinked and degradable, depending on the composition of the block copolymers [208].

PEG hydrogels are popular for various tissue engineering purposes because they are biocompatible, non-immunogenic, and FDA approved for internal use. They are also very versatile as their mechanical, structural, and degradation properties can be tuned using a variety of methods [206]. However, PEG hydrogels are bioinert due to their hydrophilicity, meaning cells will not readily attach to the surface. Therefore, tissue engineering using PEG hydrogels requires the addition of bioactive molecules to the hydrogel, such as RGD, a peptide found on fibronectin that promotes cell adhesion and migration [205].

In recent years, many studies have been conducted on the ability of PEG hydrogels to maintain the phenotype of native cells in heart valves, as well as promote the production of ECM. Wang et al. demonstrated that VICs from porcine aortic valves maintain their quiescent fibroblast phenotype much better when cultured on PEG hydrogels as opposed to stiff plastics and suggest that the fibroblasts sense the elasticity of the surfaces by the PI3K/AKT pathway [209]. This is an important observation, because the maintenance of quiescent VICs is essential to normal valve function; VIC differentiation into myofibroblasts can lead to valvular fibrosis [209]. In a similar study, VIC differentiation was moderated by VECs cultured on PEG hydrogels of different stiffnesses, and it was found that preservation of the quiescent VIC phenotype was most effective on softer hydrogels [79]. Kang et al. studied the effects that modifying different photocrosslinking variables, such as photoinitiator concentration and light intensity, had on different valvular cell types encapsulated and 3D printed in a mixture of GelMA, PEGDA, and alginate to determine the conditions that would optimize cell viability and morphology [210]. Another study reported that soft PEG hydrogels (4.3 kPa) could revert VICs from their activated, myofibroblastic phenotype into a quiescent phenotype and that the addition of ascorbic acid could promote ECM remodeling, including the deposition of collagens I and III, without activation of the myofibroblast phenotype [211]. These recent studies have all presented the benefits of using soft PEG hydrogels for cell encapsulation in the development of healthy valve leaflets as opposed to stiffer materials.

In addition to obtaining the correct cellular behavior in PEG hydrogel scaffolds, several studies have also been conducted regarding the structure and functionality of PEG hydrogels in TEHVs. Durst et al. was the first group to study the bending mechanics of PEG hydrogels. They conducted three-point bending tests using a custom designed bending tester on cell-seeded PEG hydrogels of different concentrations and molecular weights and reported the flexural stiffness of these constructs, some of which matched the flexural

stiffness of native valve leaflets [212]. Tseng et al. identified the importance of designing valve leaflet scaffolds that mimicked the trilayer structure of native leaflets and used the mechanical tunability of PEG hydrogels to fabricate quasilaminate gels using a "sandwich" layering method [131]. Hockaday et al. also utilized the mechanical tunability of PEG hydrogels, as well as a 3D printing technique, to rapidly fabricate mechanically heterogeneous aortic valve scaffolds [98]. Jin et al. recognized the importance of patterning PEGDA hydrogels in such a way that the anisotropic properties of native leaflets could be preserved. This group simulated different patterns of scaffolds created by photolithographic patterning in order to guide the design of PEGDA hydrogels to advance the structure of TEHVs [213]. The incorporation of anisotropic properties into PEG hydrogel scaffolds is currently being improved to better mimic native valve leaflets to develop more functional TEHVs.

3.11.3 *Hydrolytically degradable polymers*

Hydrolytically biodegradable polymers such as poly(glycolic acid) (PGA), poly(lactic acid) (PLA), polycaprolactone (PCL), poly(glycerol sebacate) (PGS), and polyurethanes (PU) have shown promise for their use in TEHVs, as they are biocompatible and exhibit good mechanical properties suitable for withstanding the stresses and strains experienced by valves in a hemodynamic environment. Using techniques such as electrospinning, these polymers can be fabricated into fibrous scaffolds similar to native valve ECM structure [214]. These materials have been widely studied for TEHVs due to these characteristics. PCL will be further discussed in reference to its application to this thesis project.

3.11.4 *Polycaprolactone*

With a lower melting point and a slower rate of degradation *in vivo* compared to PLA, polycaprolactone (PCL) has also been used to contribute mechanical stiffness to tissue engineered valve leaflets. PCL is a semicrystalline polymer, highly soluble in organic solvents and easy to blend with other polymers [215]. It is commonly synthesized by the ring opening polymerization of the cyclic monomer ε-caprolactone [215]. It is elastic and has a tensile strength of approximately 23 MPa [216]. These properties make PCL suitable for tissue engineering leaflets by methods such as electrospinning or 3D printing. However, its slow rate of degradation can be both advantageous and disadvantageous, as the scaffold may not be resorbed as new tissue is formed.

An early study to use PCL as a valve scaffold was conducted by Lieshout et al., in which a PCL filament was knitted into round leaflet patches, which were sutured into a tube made of the same knitted PCL. The knitted structure was fitted on a mold and a fibrin solution was poured over the mold. Once the fibrin gelled, the PCL-fibrin knitted scaffold was placed in a pulse duplicator system. While the knitted scaffolds showed complete coaptation and durability over 10 million cycles, correct valve function was not obtained as there was significant leakage, a backflow 39% of the forward flow, likely due to areas of the scaffold where the fibrin detached [217]. Another study compared PCL scaffolds to P4HB-coated PGA scaffolds in terms of compaction and degradation over time. Rectangular and trileaflet scaffolds of PGA and PCL were fabricated, seeded with human and ovine vascular-derived cells, and cultured for 4 weeks. The PCL scaffolds only showed up to 10% compaction, whereas the PGA scaffolds showed up to 50% compaction due to the quick degradation of PGA in 4 weeks [218]. A similar comparison was conducted between these two types of scaffolds in a study of the rate of tissue formation in relation to the degradation rate of the scaffold. Seeded and unseeded scaffolds of PGA-P4HB and PCL were fabricated and cultured for up to 6 weeks. The scaffold-to-tissue ratio was

measured, and uniaxial tensile tests were conducted on these scaffolds each week. From this study, they determined that PCL scaffolds resulted in the most tissue formation over 6 weeks, and the formation of tissue also increased the stiffness of the scaffolds. The tissue that formed on PCL scaffolds contained ECM components in amounts similar to those in native leaflets [219]. A different study fabricated highly porous PCL scaffolds using a jet-spraying method to create anisotropic nanofibers and seeded human adipose derived stromal cells (hADSC) and human VICs (hVIC) into the anisotropic scaffolds. They found that the anisotropic nanofibers caused the cells to develop an elongated morphology without causing differentiation of hADSC. The cells also produced ECM, maintained the anisotropy, and improved the mechanical properties of the scaffolds over 20 days [129].

3.12 Future Direction in TEHVs

While the field has progressed significantly, a TEHV has yet to be translated into the clinic. As highlighted in this review, researchers have access to several different classes of biomaterials, each with its own advantages and disadvantages. While fabrication techniques have evolved to develop more complex structures closely resembling native valves, a main takeaway point is that a single biomaterial may not be sufficient for TEHVs. The combination of several biomaterials may be the solution to addressing the limitations of using a single biomaterial. The possibility to use several biomaterials with advanced fabrication techniques has led to the development of TEHVs using two main approaches, an "off-the-shelf" or a patient-specific approach (Figure 7). Both strive to fulfill the requirements of an ideal TEHV; however, each approach is unique in the fabrication process and the target patient population.

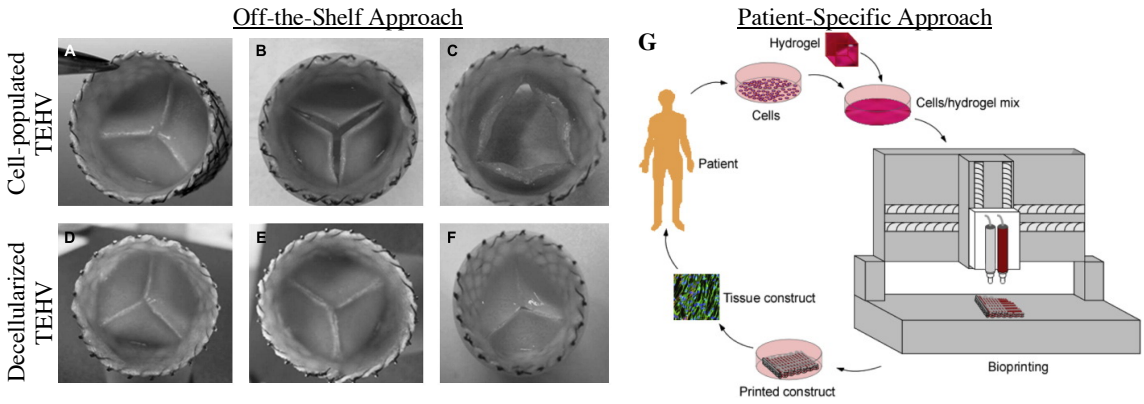

Figure 7. There are two main approaches for TEHVs, off-the-shelf and patient-specific. A-C) Using the off-the-shelf approach, homologous valves were made from biodegradable synthetic materials and homologous cells, followed by 4 weeks of in vitro dynamic strains. D-F) Homologous valves were decellularized after culturing. A,D) Represent the macrostructure of valve. B,E) Valves after leaflet separation, where the cell-populated TEHV experienced tissue retraction. C,F) Valve leaflets after 24 hours of exposure to pulmonary conditions. Reproduced with permission [264]. Copyright 2012, Elsevier. G) The concept of generating patient-specific heart valve involves autologous cells combined with a biomaterial suitable for 3D bioprinting. The scaffold is then maintained or conditioned under mechanical stimulus before being transplanted back into the patient. Reproduced with permission [2]. Copyright 2015, Elsevier.

3.12.1 *Off-the-shelf approach*

An "off-the-shelf" approach involves a scaffold with the ability to remodel and form new tissue in the body through its recruitment of endogenous cells. This approach is advantageous over the traditional *in vitro* approach because it does not require preconditioning of the scaffold before implantation, which can take up to 6 weeks. During this preconditioning time, there are risks of bacterial and fungal contamination. The

logistics of maintaining good manufacturing practice and infrastructure for translating an *in vitro* scaffold comes with an enormous cost [220].

There are two main methods for developing off-the-shelf TEHVs, *in situ* heart valve scaffolds formed through foreign body reaction, and decellularized TEHVs. Kishimoto et al. developed an autologous heart valve scaffold using in-body tissue architecture technology. This involves placing a mold into the subcutaneous space, where the body forms a fibrous scaffold surrounding the mold [221]. The stentless mold was tested in a goat model, where the valve performed well under systemic circulation. This approach enables off-the-shelf scaffolds to be created; however, it is in the initial stages of preclinical animal work. More assessment of the immune reaction to a foreign scaffold such as this one is needed along with its long-term performance in physiological conditions.

The concept of decellularized TEHVs was developed, in part, to address the issue of cell-mediated contraction observed with cell-populated TEHVs. Decellularization of TEHVs involves first creating a biodegradable synthetic scaffold seeded with homologous cells. Then scaffolds are subjected to decellularization, in which the process is gentle enough to not alter the collagen or tissue structure. Dijkman et al. demonstrated that decellularized TEHVs can be stored for up to 18 months without any alterations to the tissue structure [222]. In addition, these off-the-shelf scaffolds have the ability to be reseeded with stem cells and maintain good cell viability through the crimping process for minimally invasive procedures [117]. Following this new approach, researchers demonstrated the feasibility and long-term functionality of homologous off-the-shelf TEHVs in a sheep and non-human primate model [39, 223]. The concept of off-the-shelf TEHVs may be the fastest method to clinical application. While this approach is promising, more research is needed on the recellularization, remodeling, and growth potential of off-the-shelf scaffolds. Concerns with thrombogenicity and calcification long-term will also need to be assessed.

Other research groups have used hybrid tissue engineering approaches to develop off-the-shelf scaffolds with biological and mechanical properties capable of active remodeling post-implantation. Janhavi et al. developed a Bio-hybrid valve using electrospinning to create aligned nanofibrous scaffolds composed of decellularized bovine pericardium and PCL-chitosan. The scaffold was optimized to mimic the anisotropic and microstructure properties of native valves. The Bio-hybrid scaffold was 20 times the strength of the native valve and demonstrated ECM deposition and cell proliferation when seeded with human VICs [224]. While promising, this hybrid TEHV must be evaluated under physiological conditions and tested for its regenerative potential.

In another study, the concept of a biohybrid scaffold capable for eliciting endogenous tissue remodeling and repair was developed using rapid manufacturing approach. Using jet spinning, a fibrous scaffold of 60/40 ratio of P4HB:gelatin was produced using a rapid and automated fabrication technique. JetValves were fabricated in less than 15 minutes and demonstrated comparable hydrated shelf-life to fibrin-based scaffolds [225]. The JetValve was assessed *in vitro* and *in vivo* for its functionality. The scaffold demonstrated structural integrity and *in vivo*, the leaflets demonstrated proper coaptation with minor regurgitation [225]. The scaffolds also promoted VIC infiltration, but further evaluation is necessary to determine its ability to fully regenerate *in vivo*. This study demonstrates that jet spinning is a fabrication technique that can rapidly generate scaffolds of various different diameters. Furthermore, this technique is flexible in that growth factors or bioactive molecules can be incorporated into the scaffold to further promote endogenous cell and tissue regeneration.

The off-the-shelf approach using molding and electrospinning has truly advanced the potential to translate TEHVs into a clinical viable product. However, the off-the-shelf approach may not directly address the need for valves that can undergo somatic growth for pediatric patients. Another important aspect to consider is that each individual will have a

different endogenous reaction and regeneration to bioactive TEHVs and thus a more personalized approach may be necessary.

3.12.2 *Patient-specific approach*

The patient-specific approach is the concept of generating a scaffold that is specific to the recipient of the valve implant, consisting of autologous cells, biomaterials, and an anatomical 3D model generated from imaging modalities. The patient-specific approach to TEHVs involves the more traditional *in vitro* method, which can be time-consuming and challenging for clinical translation. However, generating a patient-specific valve can have significant impact on patients with complications that limit their quality of life, and most importantly, younger patients in need of a valve capable of growing and integrating with their circulatory system.

The most relevant method for developing patient-specific TEHVs is the use of 3D bioprinting. There are several different methods for 3D bioprinting, such as inkjet, laser-based, stereolithography, and extrusion-based printing [14, 226]. Each method has advantages and disadvantages, but researchers have extensively used extrusion-based printing of hydrogels for TEHVs [226]. Often times, computer-aided models can be generated using patient CT data to create an anatomical representative implant. With advancement in the field of bioprinting, researchers have the ability to control the placement of different cell types and biomaterials. This enables complex hybrid scaffolds to be generated with anisotropic and heterogeneous properties [98, 106]. These complex, patient-specific scaffolds can be fabricated in a record time of less than 45 minutes [98]. However, the complexity of 3D bioprinting has led to challenges in identifying a suitable set of bioinks that provide good cell viability and mechanical tunability, while having shear-thinning and viscous properties to be "printable".

While many studies have been able to generate anatomical living conduits, most have not been tested in physiological conditions. Another concern with this fabrication technique is the resolution needed for constructs to be created. While electrospinning enables nanostructures to be tailored, 3D bioprinting is limited to micro-scale printing. However, other printing process such as stereolithography can enable higher resolution printing, but this process comes with several limitations. This approach does not seem to have progressed as rapidly as off-the-shelf approaches mainly because researchers are still developing and engineering biomaterials for the 3D bioprinting process. The complexity of this multiple variable process is the main cause for the delay in progression of this fabrication technique for TEHVs. Similar to the off-the-shelf approach, there are several milestones that researchers need to reach before successfully developing a TEHV. The ideal TEHV may eventually combine the benefits of both approaches.

CHAPTER 4 HUMAN IPSCS-DERIVED MSCS ENCAPSULATED IN PEGDA HYDROGELS MATURE INTO VIC-LIKE CELLS [ii]

4.1 Summary

Despite recent advances in tissue engineered heart valves (TEHV), a major challenge is identifying a cell source for seeding TEHV scaffolds. Native heart valves are durable because valve interstitial cells (VICs) maintain tissue homeostasis by synthesizing and remodeling the extracellular matrix. In this study, the goal is to demonstrate that induced pluripotent stem cells (iPSC)-derived mesenchymal stem cells (iMSCs) can be derived from iPSCs using a feeder-free protocol and then further matured into VICs by encapsulation within 3D hydrogels. The differentiation efficiency was characterized using flow cytometry, immunohistochemistry staining, and trilineage differentiation. Using our feeder-free differentiation protocol, iMSCs were differentiated from iPSCs and had CD90+, CD44+, CD71+, αSMA+, and CD45- expression. iMSCs underwent trilineage differentiation when cultured in induction media for 21 days. iMSCs were encapsulated in poly(ethylene glycol) diacrylate (PEGDA) hydrogels, grafted with adhesion peptide (RGDS), to promote remodeling and further maturation into VIC-like cells. VIC phenotype was assessed by the expression of alpha-smooth muscle actin (αSMA), vimentin, and collagen production after 28 days. When MSC-derived cells were encapsulated in PEGDA hydrogels that mimic the leaflet modulus, we observed a decrease in αSMA expression and increase in vimentin. In addition, iMSCs synthesized collagen type I after 28 days in 3D hydrogel culture. Thus, the results from this study suggest that iMSCs may be a promising cell source for TEHV.

4.2 Introduction

Heart valve disease is an increasing clinical burden associated with high morbidity and mortality [14, 16]. The prevalence of valvular disease is expected to triple by 2050 due to age-dependent degeneration of heart valves and rheumatic fever in developing countries [7, 8]. Congenital heart defects also contribute to the incidence of heart valve disease and occur in 1 to 2% of births [227].

With limited biological diagnostics or drugs to prevent heart valve disease, treatment is restricted to valve repair, valve replacement, or the Ross procedure. Valve replacement is often performed in older patients using either a mechanical or biological valve prosthesis [228]. While these implants improve survival and quality of life, the lack of cells is considered to be the main source of failure for mechanical or glutaraldehyde-fixed biological valves [10] and the main reason for their inability to grow and repair. Without the potential for somatic growth, pediatric patients are required to undergo several surgeries for valve refitting [4, 31]. Tissue engineered heart valves (TEHV) can potentially address the shortcomings of current implants by incorporating biomaterials with autologous cells to enable growth and biological integration [156].

Native heart valves are durable because valve cells maintain tissue homeostasis [19], and without these cells, mechanical or biological prostheses fail over time [10]. Within the valve there are two primary cell types: valve endothelial cells (VECs) and valve interstitial cells (VICs). The primary focus of this study will be on VICs, which are found throughout the three layers of the leaflet and are known to synthesize and remodel the extracellular matrix [19, 72, 229]. These cells are believed to mediate long-term valve durability but

could play a role in heart valve disease progression [10]. Other cell types such as fibroblasts and smooth muscle cells are also believed to populate the leaflets and play a role in active matrix remodeling [44].

Despite recent advances in the field of TEHV, the challenge to identify a suitable cell source for seeding 3D scaffolds still remains [10, 44]. To ensure the success of the TEHV, various cell types have been investigated. These include xenogeneic, allogenic, and autologous cells. Example of these cell types include bone marrow-derived cells, adipose-derived cells, and amniotic fluid cells from porcine, sheep, and human sources [230-232]. Xenogeneic and allogenic cells have been shown to evoke an immune response and may only be suitable for preclinical research [14, 233]. Meanwhile, autologous cells are the most appropriate cell source for seeding TEHV because they are patient-specific and depending on the cell source, they have the potential to be expanded and differentiated into other cell types.

More recently, mesenchymal stem cells (MSCs) derived from various sources such as bone marrow (BM) and adipocytes have been investigated as a potential cell source for TEHV [44, 95, 234]. This is because of their similar characteristics to smooth muscle cells and fibroblasts and their ability to differentiate into several cell types. While initial studies demonstrated promising results, a major limitation of MSCs derived from sources like bone marrow is a decrease in differentiation potential with expansion of *in vitro* cultures [235-237], which results in limited therapeutic efficacy.

An alternative cell source that maintains a higher level of stemness and can be readily expanded for clinical translation is induced pluripotent stem cells (iPSCs). Previous studies

have shown that MSCs derived from human embryonic stem cells have the same cell surface phenotype compared to BM-derived MSCs [236]. Meanwhile, iPSC-derived MSCs (iMSCs) demonstrate trilineage differentiation [238]. With minimal senescence and higher telomerase activity potential [236, 239], iMSCs from iPSCs can be a potential cell source for TEHV. While only a few other groups have generated iMSCs from iPSCs, there is a need for safer transgene-free iPSCs and a feeder-free differentiation protocol for a more clinically translatable cell source.

While the outcomes of a TEHV depends on the cell source, the scaffold in which the cells are seeded can be utilized to direct cell phenotype and function. To recapitulate the ECM architecture in valve leaflets, a variety of natural and synthetic biomaterials have been explored. An ideal scaffold for TEHV is one that provides the biological cues to promote cell migration, proliferation, differentiation, and spreading [199]. The scaffold should also allow for the exchange of oxygen and cellular waste, and stimulate ECM production and remodeling [240].

In particular, poly(ethylene glycol) hydrogels can be designed to promote proper cell phenotype, proliferation, ECM production, and proteolytic degradation of the ECM. The goal is to generate a hydrogel that can enable cell adhesion and stimulate iMSCs to actively remodel the scaffold with ECM production [10]. Thus, the hydrogel network must accommodate the initial activation of iMSCs for active remodeling of the matrix, but over time, it must maintain cells in a quiescent fibroblast phenotype to prevent a pathological phenotype. Several groups have investigated PEG-diacrylate (PEGDA) as a hydrogel scaffold for TEHV applications [33, 204, 212, 241]. Thus, we investigated the maturation

of iMSCs into VIC phenotype by encapsulating iMSCs into a 3D PEGDA hydrogel mimicking the microenvironment found in native valve leaflets.

The objective of aim 1 is to develop a feeder-free protocol for differentiating iMSCs from integration-free iPSCs and to introduce these cells into a three-dimensional hydrogel to promote VIC phenotype and ECM matrix production and remodeling. We hypothesize a feeder-free protocol for differentiating embryonic stem cells can be modified to differentiate iPSCs into iMSCs. The introduction of iMSCs into a 3D hydrogel commonly utilized to study VIC phenotype and ECM production will enable us to identify the potential of iMSCs as a cell source for TEHV.

4.3 Materials and Methods

All media components were purchased from Thermo Fisher Scientific (Waltham, MA, US) unless otherwise stated.

4.3.1 *iPSCs differentiation into iMSCs*

The differentiation protocol used in this study was modified from a protocol originally used to differentiate human embryonic stem cells (hESCs) [242]. The differentiation process was modified to be feeder-free. Human integration-free iPSCs (supplementary information) were cultured for two passages in mTesR™1 media (StemCell Technologies) on Geltrex-coated plates (Gibco) before being harvested for MSC differentiation. Once confluent, iPSCs were passaged using collagenase IV at 200 U/mL for 5 minutes at room temperature. During differentiation, cells were cultured in differentiation media (DM), consisting of knock-out DMEM (KO-DMEM), 0.1 mM β-mercaptoethanol (Sigma

Aldrich, MO), 1 mM L-glutamine, 20% fetal bovine serum (GE Healthcare Lifescience, UT), 1% non-essential amino acids, and 1% penicillin and streptomycin for 3 days in suspension petri dish (Corning, MA) to promote formation of cell aggregates. Afterwards, cells were transferred to gelatin-coated plates and cultured for 9 days. When cells became confluent, they were passaged by incubating 2 mg/mL of collagenase type II in PBS for 30 minutes at 37°C. Cells were maintained on gelatin-coated plates, plated at a seeding density of 2 x 10^4/ cm^2, and had media changed every 2 to 3 days. After this stage, cell media was replaced by iMSC media, which is composed of KO-DMEM, 2 mM L-glutamine, 10% fetal bovine serum (GE Healthcare Lifescience, UT), 1% nonessential amino acids, and 1% penicillin and streptomycin. Media was changed every 2 days. Cell phenotype was characterized after the fourth passage.

4.3.2 *Flow Cytometry*

To characterize MSC surface antigens in iMSCs, cells were harvested, rinsed with PBS, and fixed with 4% paraformaldehyde at 0.5 x 10^6 /mL for 10 minutes at room temperature. Afterwards, cells were incubated in 10% goat serum for 10 minutes at room temperature. Primary antibodies were diluted in BD Brilliant Flow Buffer and incubated for 30 minutes at room temperature. The cells were washed with flow buffer several times before being resuspended in 500 μL of flow buffer and analyzed using flow cytometer (BD LSR II, BD Bioscience, CA). The conjugated antibodies included mouse anti-human CD90 BUV395 (1:25, BD Biosciences), rat anti-human CD44 v450 (1:25, Tonbio), and mouse anti-human CD45 PE (1:25, Tonbio). For non-conjugated antibodies, rabbit anti-human CD71 (1:100, Santa Cruz Biotechnology) and mouse anti-human αSMA (1:100, ABCAM) were used. Secondary antibodies included anti-rabbit and anti-mouse Alexa fluorophore

488 (1:300, Life Technologies). The panel of markers were controlled by unstained cells, human MSCs, and for CD45, a negative marker, fluorescein-5-Maleimide (1mg/mL) was used as positive control. For cells that were stained with primary and secondary antibodies, a similar protocol for conjugated antibodies was used. However, antibodies were diluted in 1% bovine serum albumin (Sigma), and after cells were stained with primary antibodies, they were washed several times before incubation in the secondary antibodies for 30 minutes at room temperature.

4.3.3 *Trilineage Differentiation*

To evaluate iMSC trilineage differentiation, cells were harvested and plated in triplicates at a seeding density 3.15 x 10^4 cells/cm^2. For adipogenic differentiation, cells were cultured in iMSC media until 80-90% confluency, when the media was replaced by adipogenic induction media (Amsbio). To differentiate iMSCs into chondrocytes, a monolayer differentiation approach was utilized. Once cells reached 100% confluency in iMSC media, hMSC chondrogenic media (Vitrobiopharma) supplemented with 10% FBS was used. Osteogenic differentiation was conducted with cells at 100% confluency using osteoblast differentiation medium (Amsbio). Cells were cultured for 21 days with media changes every three days. Caution was necessary to not disturb cell monolayers. All differentiation medias were supplemented with 1% penicillin and streptomycin. iMSCs maintained in iMSC media during the trilineage protocol was the negative control.

After differentiation, iMSCs treated with adipogenic and osteogenic induction media were fixed with 4% v/v paraformaldehyde in PBS for 10 minutes at room temperature. To stain for adipocytes, a working solution of 3 parts Oil Red O (Sigma) stock solution (0.3%

w/v of Oil Redo O in isopropanol) with 2 parts DI water was filtered and incubated with cells for 5 minutes at room temperature. Multiple wash steps were necessary until washes were clear. The nuclei were stained with Hematoxylin following manufacturer's protocol. For staining chondrocytes, toluidine blue stain (Sigma) was used after cells were fixed with cold methanol for 2 minutes. Cells were incubated with 0.5% v/v toluidine blue and washed with PBS. Cells treated with osteogenic media were stained with 1% w/v Alizarin Red S (Ricca Chemical Company) solution for 30 minutes at room temperature in the dark. Multiple washes were needed after incubation in the staining solution. Samples were stored at -20°C until dye extraction. A microplate reader (BioTek Instruments) was used to measure absorbance at 492 nm, 603 nm, and 409 nm for Oil Red O, Toluidine Blue, and Alizarin Red S, respectively. Cells were imaged using the Olympus IX71 microscope.

4.3.4 *Immunostaining and Cell Viability*

To characterize cell phenotype of iMSCs in comparison to MSCs, cells were cultured on glass coverslips for 24 hours at a 2 x 10^4 cells/cm^2 concentration. Immunofluorescence staining of αSMA and Phalloidin were performed following standard protocols. iMSCs were incubated with primary antibody mouse anti-human αSMA (1:250, Abcam), and secondary antibody anti-mouse Alexa Fluor 488 for secondary antibody (1:500). Rhodamine phalloidin at 25 µL/mL (Life Technologies) was used to stain for F-actin and DAPI (1 µg/mL; Sigma) stained the cell nuclei. For negative controls, only secondary antibody was incubated with cells. Cells were fixed with 4% v/v paraformaldehyde for 20 minutes, permeabilized with 0.2% Triton X-100 followed by 1-hour incubation in 1% BSA, all samples were performed at room temperature. The primary and secondary antibodies

were incubated overnight at 4°C and 2 hours at room temperature, respectively. Phalloidin and DAPI were added to cells for 20 minutes at room temperature. At each step, three washes with PBS were performed for 5 minutes each wash. Samples were imaged using Olympus IX71 microscope. Human MSCs were used a control cells and all samples were conducted as triplicates.

The ECM component was characterized in 3D PEGDA hydrogels by encapsulating 1 x 10^6 cells/mL iMSCs in 5% w/v PEGDA with 5 mM RGDS for 28 days. DAPI was used to image cell nuclei and fluorescein-5-Maleimide (10 μg/mL) was utilized to image the cell surface. Hydrogels were stained for collagen type I, αSMA, vimentin, periostin, and calponin using primary antibodies: mouse anti-human collagen type I (1:100; Abcam), mouse anti-human αSMA (1:100; Abcam), rabbit anti-human vimentin (1:100; Santa Cruz), rabbit anti-periostin (1:100; Abcam), and mouse anti-calponin (1:100; Abcam). The following secondary antibodies were used: goat anti-mouse Alexa Fluor 647 conjugate (1:200), and goat anti-mouse Alexa Fluor 488 (1:200). The protocol mentioned above for 2D cell culture was utilized for cell-laden hydrogels. iMSCs characterization was performed using an Olympus IX81 for confocal microscope imaging. To control for immunostaining, PEGDA blank hydrogels and secondary only antibody stained cell-laden hydrogels were used. Primary VICs (DV Biologics) and human dermal fibroblasts (HDFs) were utilized as a phenotype control. The level of fluorescence was quantified using ImageJ. First, a threshold was applied to images and then, using particle analysis function in ImageJ, the % area coverage of the marker of interest was determined.

4.3.5 *Preparation of PEGDA hydrogels*

Poly(ethylene glycol) diacrylate (PEGDA; ESI BIO) of molecular weight 3400 Da was used to make hydrogels. A prepolymer solution of 5% w/v PEGDA, 10 μM Eosin Y (Santa Cruz Biotechnology), 0.375% v/v 1-vinyl-2-pyrrolidinone (NVP; Sigma), 1.5% v/v triethanolamine (TEOA; Sigma) was crosslinked using a white-light source (LED Light; Braintree Scientific, Inc.) for 1 minute. Hydrogels were soaked in PBS and then in media. Hydrogels with no cells were used for mechanical tests.

Hydrogel functionalization was performed by conjugating Arg-Gly-Asp-Ser (RGDS) peptide (Cayman Chemical, MI) to acrylate-PEG-succinimidyl valeric acid (ACR-PEG-SVA; Laysan Bio, Inc., AL) in 50 mM sodium bicarbonate buffer solution at pH 8.5 (Sigma). RGDS peptide was incorporated into the PEG mesh network to enable cell adhesion. ACR-PEG-SVA was combined with RGDS at a 1:1.2 molar ratio (ACRY-PEG-SVA: RGDS) and reacted overnight at room temperature under constant agitation. PEG-RGDS was then dialyzed with MWCO membrane 3400 against 4 L of ultrapure water for 3 days with 4-5 water changes per day. Samples were then lyophilized into a dry powder. Conjugation was confirmed using NMR and MALDI-TOF.

To create cell-laden PEGDA hydrogels, a prepolymer solution of 5% w/v PEGDA with the white-light crosslinking components stated above was sterile-filtered using a 0.22-um syringe filter (EMD Millipore). Cells were then added to the prepolymer solution at 1.0 x 10^6 cells/mL (cell viability and mechanical testing) or 1.5 x 10^6 cells/mL (ECM production studies). To generate hydrogel disks, 15 μL of prepolymer solution was injected into molds consisting of a SigmaCote glass slide (Sigma), silicone spacers of 0.381 mm

thickness (McMaster-Carr), and an 18-mm round coverslip (Fisherbrand). The prepolymer solution was crosslinked under LED white-light (Braintree Scientific) for 1 minute and gels were then soaked in PBS, followed by iMSC media. The media was changed every 2 days.

4.3.6 *Characterization of PEGDA hydrogels*

The overall properties of PEGDA hydrogels was characterized by compression testing using a TA Instruments ElectroForce 3100 Mini. Before performing compression testing, hydrogels were soaked in PBS for at least 24 hours and the diameter of each hydrogel was measured using a caliper. The thickness of the hydrogels was about 0.85 mm. Quasi-static compression testing was performed on a group of hydrogels, sample size n = 8, with a 1 N load and maximum displacement of 0.4 mm at a rate of 0.02 mm/sec. The linear portion of the stress-strain curve between 5-15% strain was used to calculate the least-squares fit slope to determine Young's modulus.

4.3.7 *Cell Viability*

To determine cell viability, cell-laden hydrogels were stained with Live/Dead™ assay with calcein-AM and ethidium homodimer at 4 μM and 2 μM concentrations, respectively. Both components of Live/Dead™ assay were diluted in DAPI solution and incubated with hydrogels at 37°C for 20 minutes before imaging. Cell viability was measured at day 1 and day 7. Confocal microscopy (Olympus IX81) and ImageJ software was used to image hydrogels and quantify cell viability, respectively.

4.3.8 *ECM Analysis*

Before digestion of hydrogels, each construct was weighed, and excess water was removed by using weighing paper. PBE buffer was prepared by weighing out 7.1 g Na_2HPO_4 and 1.86 g Na_2EDTA in 500 mL of ddH_2O and pH corrected to 6.5. The solution was sterile-filtered with a 0.22 um filter before use. Constructs were digested and homogenized in a papainase solution composed of 1.67 mg per mL of L-Cysteine (Sigma-Aldrich), PBE buffer, and 0.5% v/v papain (Sigma-Aldrich). Samples were incubated in this solution for 15-18 hours at 60°C. Samples were then frozen at -20°C until analysis. The cell density in each construct was quantified using the Quant-iT™ PicoGreen® assay following manufacturer's instructions.

To determine collagen content, samples were first homogenized in ultra-pure water and then equal volume of 10N HCl was added to a glass PTFE-lined vial. Samples were hydrolyzed for 3 hours at 120°C. Once cooled, 5 mg of activated charcoal was added to samples. The supernatant was recovered by centrifugation. Samples were stored at -20°C until analysis. Using the manufacturer's instruction for the hydroxyproline assay (Sigma-Aldrich), samples were mixed with Chloramine T/Oxidation buffer and diluted DMAB reagent. Samples were incubated in these two components for 90 minutes at 60°C before absorbance was recorded at 560 nm. Data was normalized to the wet weight of the hydrogel.

4.3.9 *Statistical Analysis*

All quantitative data was expressed as the mean ± standard deviation (SD). Statistical analysis was performed using Graphpad Prism 7 (La Jolla, CA). One-way ANOVA with post-hoc Tukey-Kramer test was used to determine statistical significance in flow

cytometry experiments for surface marker expression. Student t-tests were utilized for statistical analysis of absorbance levels in trilineage differentiation and cell viability assays and for marker quantifications. A one-way ANOVA with post-hoc Dunnett's test was performed for collagen production. Sample size was determined by preliminary data and a Monte-Carlo simulation using Prism 7. In general, sample size n = 3-5 and technical replicates were used. Statistical significance was considered at a value of $p < 0.05$.

4.4 Results

4.4.1 *iMSCs derived from iPSCs using a feeder-free approach demonstrate phenotypic similarity to human MSCs*

To address the need for a suitable cell source for seeding TEHVs, integration-free iPSCs were first generated from human dermal fibroblasts derived from a healthy child (Supplementary Figure 28), then differentiated into iMSCs using a feeder-free protocol. The surface marker profile of iMSCs was characterized by the expressions of CD90, CD44, CD71, αSMA, and CD45 using flow cytometry. Figure 8 shows that iMSCs have a 99.3%, 98.8%, 99.6%, and 95.9% positive expression of CD90, CD44, CD71, and αSMA, respectively. Meanwhile, there was a 0.020% expression of CD45, a hematopoietic marker. The expression of $CD90^+$, $CD44^+$, $CD71^+$, αSMA^+, $CD45^-$ phenotype suggests that iMSCs have a similar surface marker profile to MSCs.

In addition to surface marker analysis, cells were cultured in adipogenic, chondrogenic, and osteogenic induction media to verify their multipotency. After 21 days in induction media, iMSCs demonstrated the capability to undergo trilineage differentiation **(**Figure 9). iMSCs cultured in adipogenic induction media led to

intracellular lipid vesicles stained by Oil Red O dye. The levels of Oil Red O staining were quantified by measuring the absorbency at 492 nm. iMSCs treated with induction media resulted in a significantly higher absorbency of the dye compared to cells in MSC media.

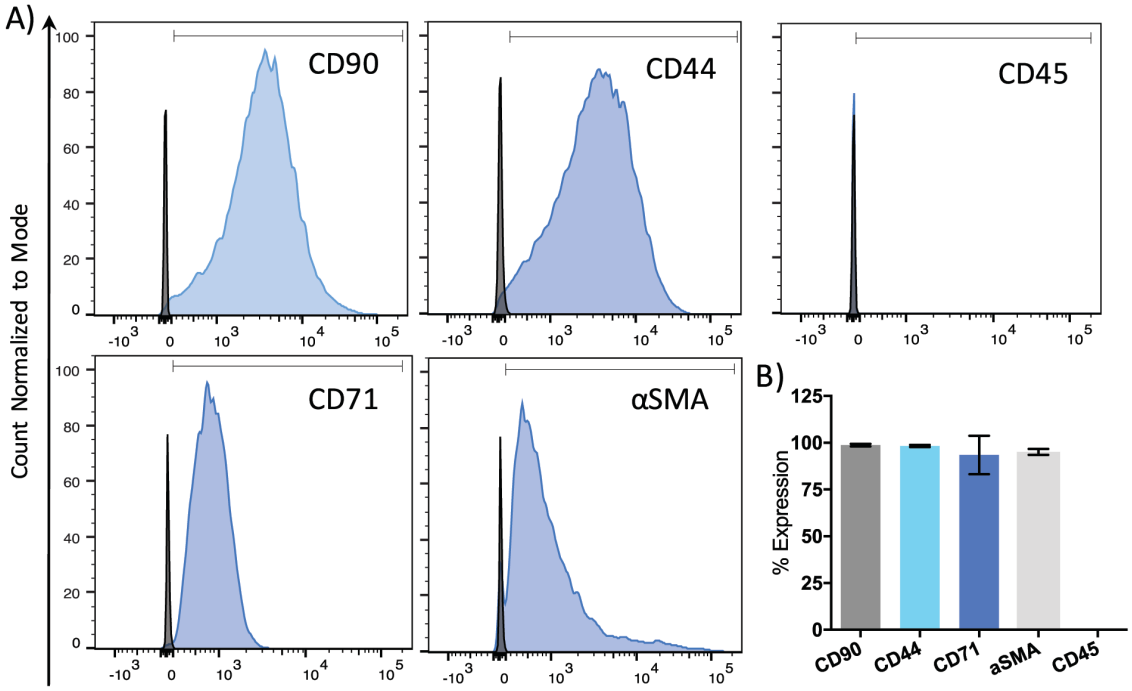

Figure 8. Characterization of iMSCs differentiation efficiency via flow cytometry. A) iMSCs were stained for positive expression of CD90, CD44, CD71, and αSMA surface markers. No expression of CD45 was observed. Blue peaks - stained cells. Black peaks - unstained cells. B) The expression of each marker was quantified by gating population of iMSCs and comparing to non-stained cells. N = 3-4.

Furthermore, iMSCs cultured in osteogenic media led to statistically higher levels of extracellular calcium deposits, stained bright red using Alizarin Red S, as compared to cells in MSC media. Meanwhile, iMSCs cultured in chondrogenic induction media began to form aggregates that stained purple-blue with toluidine blue stain, suggesting that iMSCs have differentiated into chondrocytes. The measured absorbency of toluidine blue dye was

also statistically higher than cells without induction media.

Furthermore, immunocytochemical staining was used to assess the localization of marker proteins αSMA and F-actin in iMSCs compared to control, human MSCs. Figure 10 shows iMSCs have stress fibers of αSMA and F-actin similar to human MSC controls. The cell morphology is also observed to be similar between iMSCs and human MSCs, where cells are fibroblast-like, bipolar, and elongated.

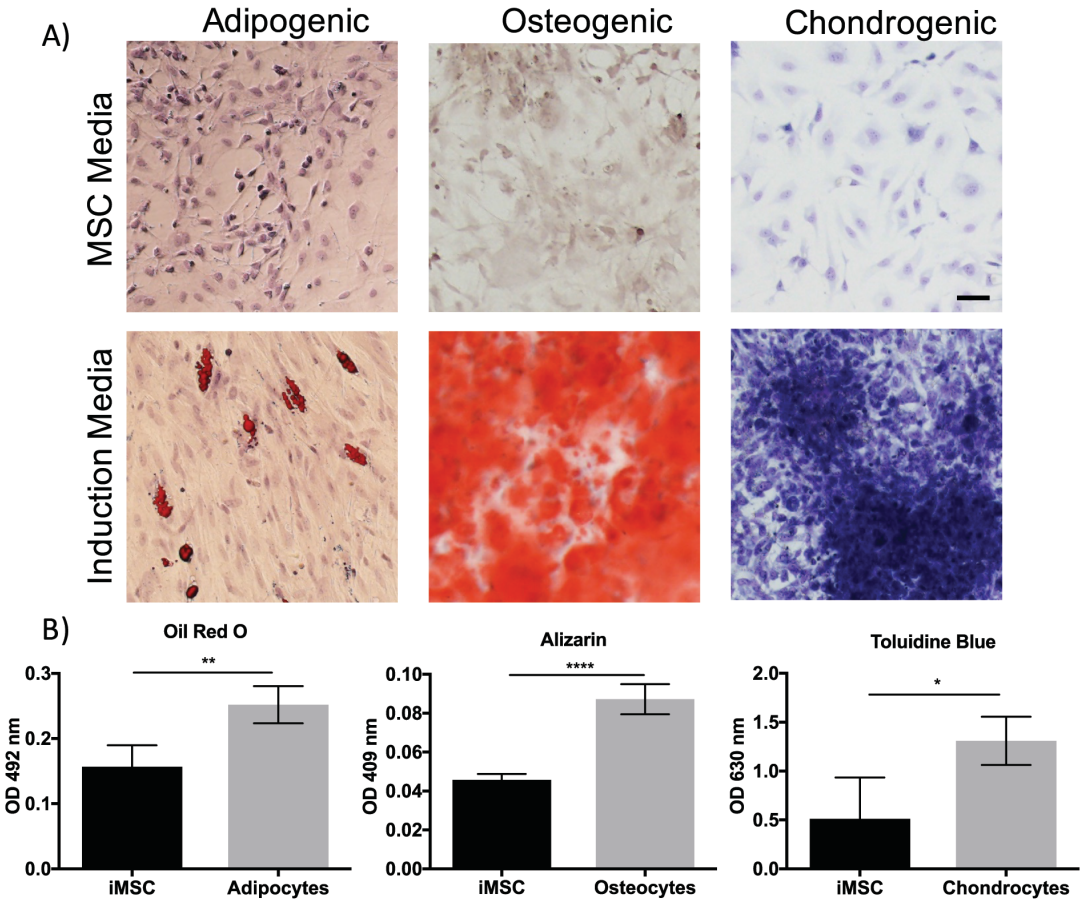

Figure 9. Trilineage Differentiation of iMSCs. A) iMSCs were cultured in adipogenic, osteogenic, chondrogenic induction media for 21 days. Control iMSCs were cultured in MSC media. iMSCs demonstrate the ability to differentiate into adipocytes by evidence of

intracellular fat deposits stained by Oil Red O. iMSCs cultured in osteogenic media led to high levels of extracellular calcium deposition stained in bright red using Alizarin Red S. High levels of toluidine blue staining in observed in iMSCs treated with chondrogenic media. B) The absorbency of each stain was quantified. *p<0.05; **p<0.01; ***p<0.001; t-test. Scale bar 50 μm.

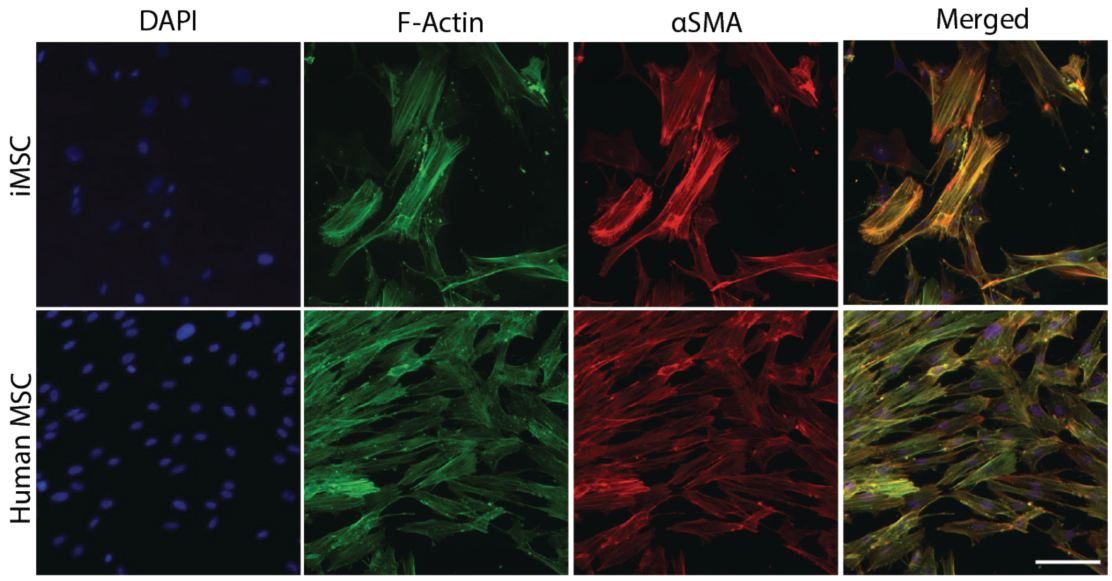

Figure 10. Characterization of iMSC phenotype. iMSCs and human MSCs (control) were immunostained with DAPI, F-Actin, and αSMA after 24 hours. iMSCs had comparable expression of αSMA and F-actin stress fibers to human MSCs. Scale bar 50 μm.

4.4.2 *Mechanical characterization of PEGDA hydrogels*

Before encapsulating iMSCs in PEGDA hydrogels, RGDS, an adhesion peptide sequence, was conjugated to acrylate-PEG-succinimidyl valerate (SVA) with a molecular weight of 3.5 kDa using an established protocol [243]. This peptide sequence is conserved in fibronectin, an extracellular matrix protein that enables cellular interaction through

integrin binding. The ^{1}H NMR spectra in (Supplementary Figure 29) demonstrates that RGDS was conjugated to PEG via peaks at 4.4 nm, 4.2 nm, and 3.10 ppm. The conjugation was also verified by a shift in mass, 3673 Da for the acrylate-PEG-SVA to 3956 Da for PEG-RGDS, using MALDI-TOF **(**Supplementary Figure 30**).**

To determine the PEGDA hydrogel properties, PEGDA hydrogels with and without iMSCs were characterized through compression testing. Using the molds described under the methods section, PEGDA hydrogel discs of 5% w/v ratio following 1-minute of white-light exposure were created. Compression testing demonstrated the average modulus of PEGDA hydrogels at 1-minute white-light exposure to be 5.6 kPa (Figure 11). Meanwhile, cell-laden hydrogels had a significantly higher modulus of 30 kPa, and after 28 days of encapsulation, there was a significant decrease to 3.7 kPa. The overall modulus of blank PEGDA and 28 day hydrogels were still within the modulus of leaflet layers (~5-13 kPa) that native valve cells experience [125].

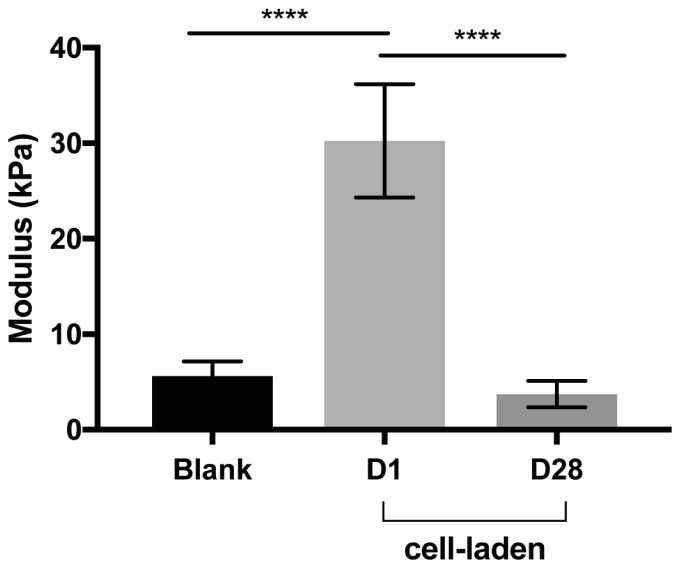

Figure 11. Mechanical properties of PEGDA hydrogels. Compression testing was used to

determine the bulk modulus of 5% v/w PEGDA hydrogels with 5mM RGDS, crosslinked with white-light for 1- minute. The elastic modulus in PEGDA only hydrogels was an average of 5.6 kPa. While cell-laden PEGDA hydrogels had a modulus of 30 kPa, which decreased to 3.7 kPa after 28 days. One-way ANOVA. ****$p<0.0001$; N = 8 -10.

4.4.3 *Cell Viability in PEGDA hydrogels*

The cell viability of iMSCs encapsulated in 5% v/w PEGDA hydrogels with 5 mM RGDS was assessed after 1 and 7 days using the Live/Dead assay. After 1 day of encapsulation, iMSCs remained viable at 93% with a round cell morphology (Figure 12). Meanwhile, the cell viability decreased to 77% at day 7, though this was not statistically significant. In addition, there was a noticeable difference in cell morphology when iMSCs were encapsulated within the hydrogel or near hydrogel surface at day 7 as shown by calcein AM staining. Near the surface of the hydrogel, the cells showed signs of spreading and elongation. In contrast, within the hydrogel the cells-maintained a round morphology.

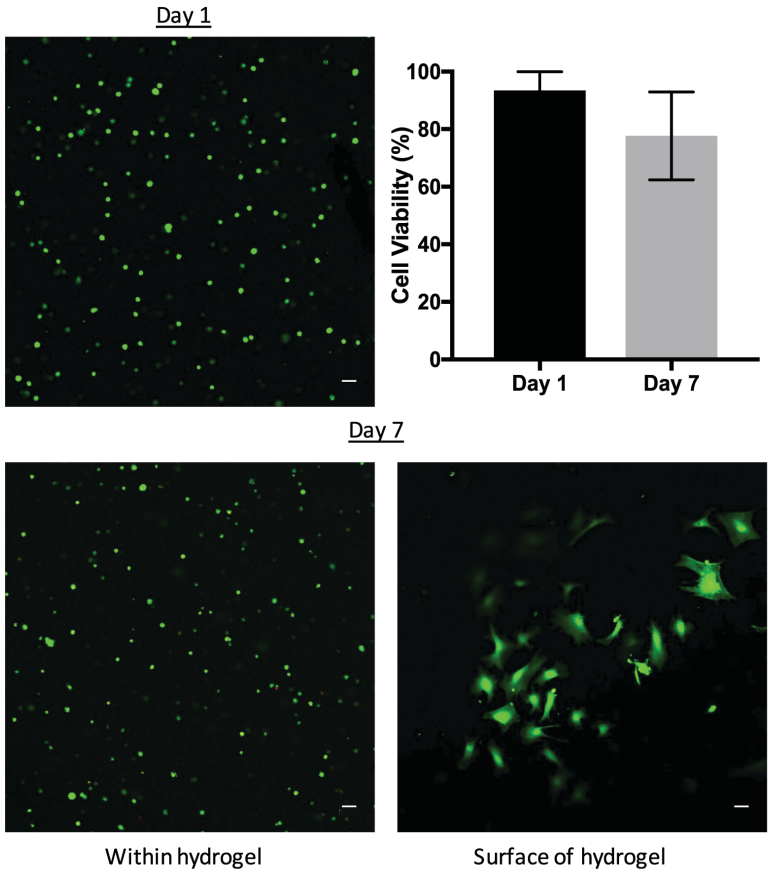

Figure 12. Cell viability of iMSCs encapsulated in 5% PEGDA hydrogels. iMSCs were encapsulated into PEGDA hydrogels 5% w/v with 5 mM RGDS. Hydrogels were cultured for 1 or 7 days. Cell viability was 93% after 1 day of encapsulation and maintained at 77% after 7 days. There was no statistical significance between day 1 or day 7. Green is Calcein AM. Red represents ethidium homodimer. Student t-test; no significance. N = 3. Scale bar 50 μm.

4.4.4 *Maturation of iMSC into VIC-like phenotype within PEGDA hydrogels*

To assess iMSCs maturation into VIC-like cells, iMSCs were encapsulated in 5% w/v PEGDA hydrogels with 5 mM RGDS. Primary VICs and HDFs were also encapsulated into PEGDA as phenotype controls. As shown in Figure 13, cells within hydrogels were stained for αSMA and vimentin at 1- and 28-days post-encapsulation. At day 1, diffuse staining of αSMA (red) with no distinct stress fibers or staining for vimentin (green) was observed. At day 28 post-seeding, there was a distinct difference in staining patterns of αSMA and vimentin compared to day 1, where there was significantly less diffuse staining

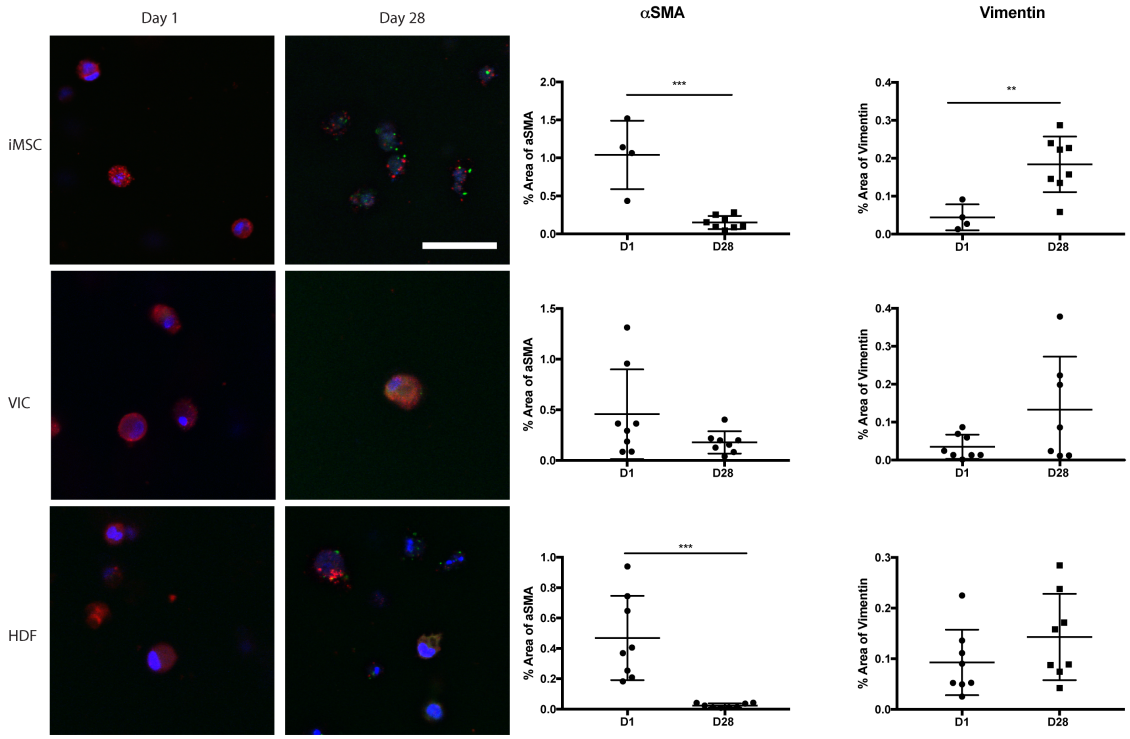

Figure 13. iMSC expression of αSMA and vimentin after 28 days. iMSCs, VICs, and HDFs were encapsulated into PEGDA hydrogels 5% w/v with 5 mM RGDS for 28 days. Fluorescence for αSMA and vimentin was quantified for each cell type at day 1 and day 28. Student t-test was conducted to comparing day 1 to day 28. DAPI - Blue; Vimentin - Green; αSMA - Red. **p<0.01; ***p<0.001; t-test; N = 4-8. Scale bar 50 μm.

of αSMA and more staining for vimentin. In comparison, primary VICs and HDFs had higher expression of αSMA at day 1, followed by a decrease in expression by day 28. When the levels of αSMA and vimentin were compared at day 28 between the three cell types, iMSCs expression of αSMA and vimentin were most similar to VICs (Supplementary Figure 32).

To further examine VIC-like differentiation, gels were stained with both calponin and periostin. While quantitative analysis of iMSCs showed that there was a small decrease in these 2 markers from day 1 to day 28, this was not statistically significant (Figure 14**)**. VICs had a significant increase in periostin over time, while calponin remained at a similar level throughout the experiment. Meanwhile, HDFs showed no changes in either marker over time **(**Figure 14). When the levels of expression for periostin and calponin were compared at day 28 for all 3 cell types, iMSCs had similar levels of expression of periostin compared to VICs and HDFs; however, the level of calponin was significantly reduced compared to VICs (Supplementary Figure 31).

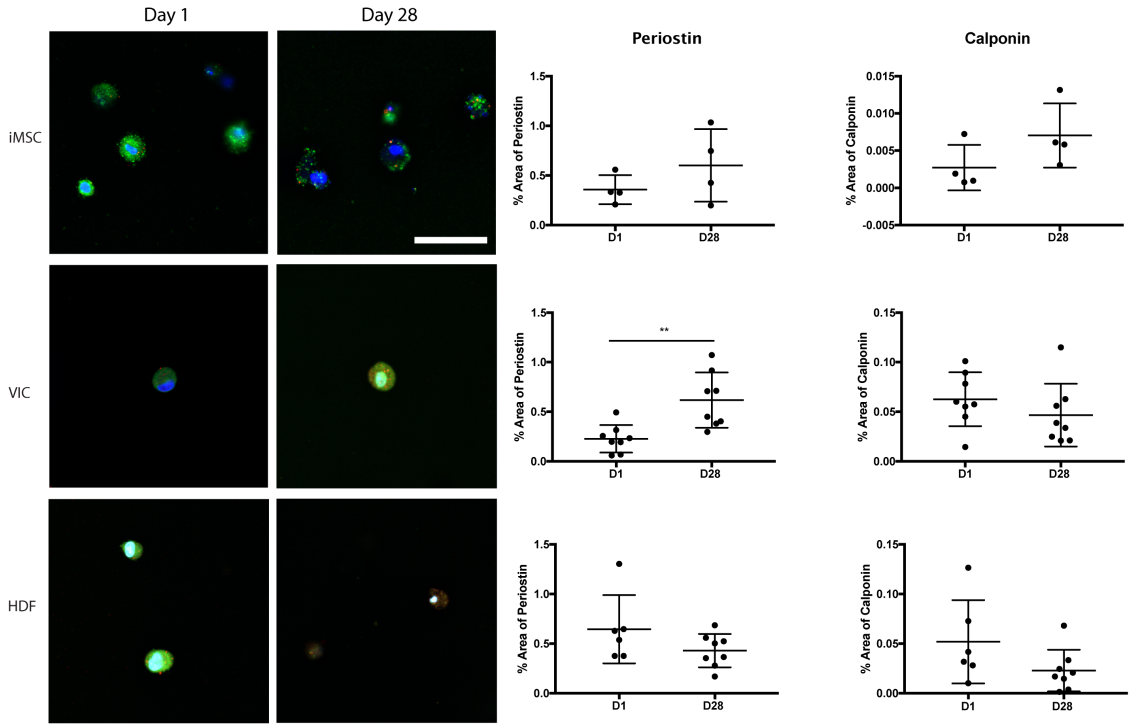

Figure 14. iMSC expression of periostin and calponin after 28 days. All three cell types, iMSCs, VICs, and HDFs were encapsulated into 5% w/v PEGDA hydrogels with 5 mM RGDS for 28 days. Fluorescence for periostin and calponin was quantified for each cell type at day 1 and day 28. Student t-test was conducted to compare changes in expression over time. DAPI - Blue; Periostin - Green; Calponin - Red. **p<0.01; t-test; N = 4-8. Scale bar 50 μm.

4.4.5 *Collagen deposition in 3D PEGDA hydrogels with encapsulated iMSCs*

To determine if matured iMSCs had the capacity to deposit collagen, an important ECM component necessary to maintain valve homeostasis, hydrogels were fluorescently stained for collagen type I overlaid with the cell membrane (Figure 15). When iMSCs were initially encapsulated, there was minimal intracellular staining of collagen and some collagen deposits at the edge of the cell membrane. At the subsequent time point, collagen deposition surrounded the cell membrane as observed by the extracellular red staining.

Quantitative analysis of collagen staining was significantly increased at day 28 compared to day 1. Meanwhile, there was no change in collagen production in either VIC or HDF hydrogels. When all 3 cell types were compared at day 28, iMSCs had significantly higher levels of collagen type I staining when compared to VICs and HDFs (Supplementary Figure 31).

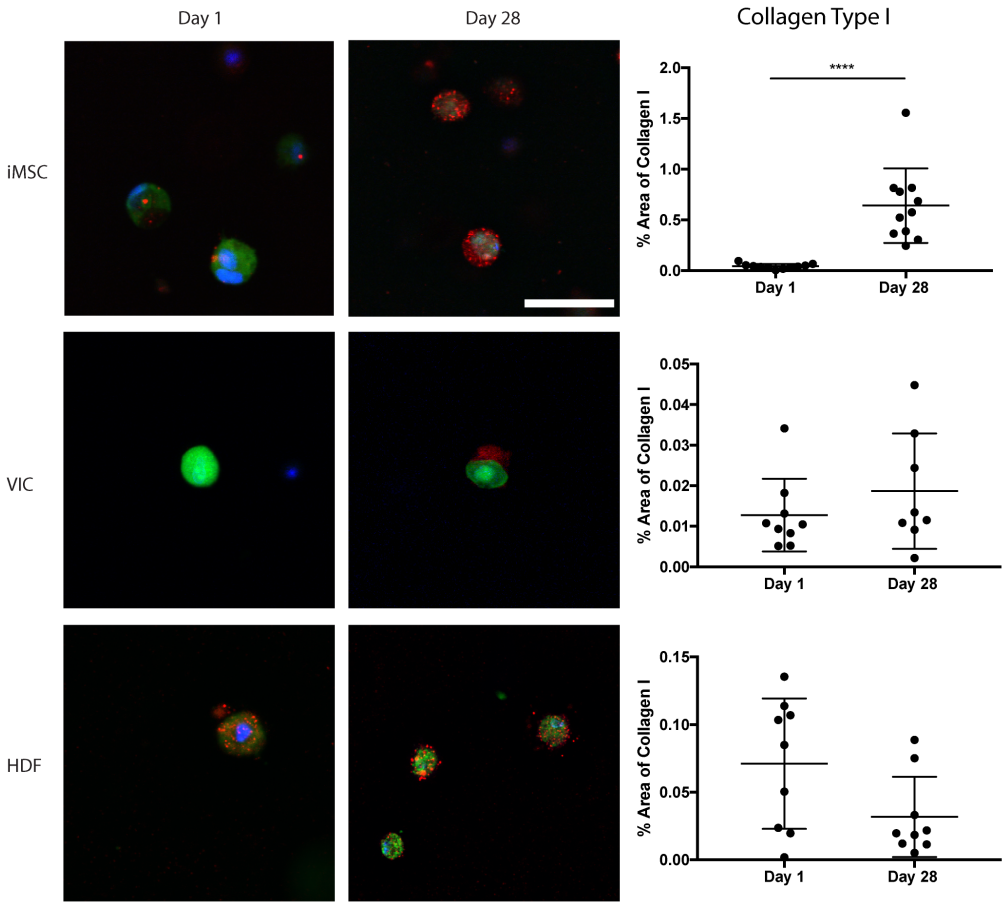

Figure 15. iMSC Collagen Type I Deposition in PEGDA Hydrogels. iMSCs, VICs, and HDFs were encapsulated into PEGDA hydrogels 5% w/v with 5 mM RGDS. Hydrogels were cultured for 1 and 28 days before being stained for collagen type I. Over time, iMSCs begin to deposit collagen. Student t-test was conducted to compare changes in expression over time. DAPI - Blue. Cell membrane - Green. Collagen type I - Red. ****$p<0.0001$ t-test; N = 3. Scale bar 50 µm.

In separate experiments, the amount of collagen was quantitatively measured using the hydroxyproline assay, as hydroxyproline is a major component of collagen that stabilizes the helical structure (Figure 16). To control for changes in cell viability and/or number, total DNA was measured using Quant-iT™ PicoGreen® and used for normalization. While there was no significant change in DNA content with time, there was a statistically significant increase in normalized collagen deposition in day 28 hydrogels compared to day 1. However, no statistical difference was detected between day 1, 7, and 14 days.

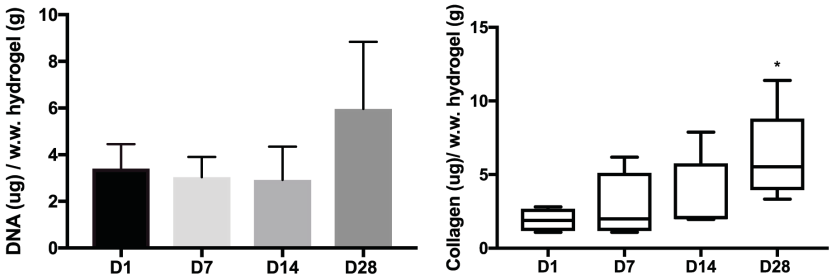

Figure 16. Quantification of DNA content and collagen in cell-laden PEGDA hydrogels. iMSCs were encapsulated into 5% w/v PEGDA hydrogels with 5 mM RGDS for 1, 7, 14, and 28 days. A) Using the PicoGreen assay, the DNA content remained unchanged at all time points. N = 4. B) Collagen content was determined by hydroxyproline assay and normalized by wet weight of hydrogel. *$p<0.05$ vs day 1; ANOVA followed by Dunnett's post-test. N = 4-5.

4.5 Discussion

A major shortcoming for current valve prostheses is the absence of cells required for active repair and remodeling of the scaffold [10]. Valve cells play an important role in the tissue homeostasis, in particular VICs, which synthesize and remodel the extracellular

matrix [19, 72, 229]. In aim 1, we attempted to generate a patient-specific cell source for adequate seeding of TEHVs. Cells were generated using a feeder-free differentiation protocol that had been previously used for embryonic stem cell differentiation [244], in order to differentiate induced-pluripotent stem cells (iPSCs) into iPSC-derived mesenchymal stem cells (iMSCs). iMSCs had similar expression in surface markers, phenotype, and functionality to adult human MSCs. These iMSCs were capable of trilineage differentiation as shown via staining and quantitative assays, and when cultured in a PEG hydrogel, differentiated further in to a VIC-like phenotype.

The advantage of using MSCs derived from integration-free iPSCs is the reduced risk associated with genome-integrating viruses [245]. Other protocols using iPSCs to derive iMSCs, use genome integrating viral vectors [246], which pose the risk of mutations that can alter differentiation potential and tumorigenesis, often caused by c-Myc oncogene reactivation [247]. Furthermore, using iPSCs as the main source for iMSCs presents the opportunity to differentiate iPSCs into other cell types from the germ layers: ectoderm, mesoderm, and endoderm. iMSC derived from iPSC has the ability to expand indefinitely without senescence and to differentiate into different cell types such as chondrocytes, osteoblasts, adipocytes, smooth muscle cells [238, 248]. In contrast, MSCs derived from sources like bone-marrow have limited differentiation potential and capabilities after extended *in vitro* culture [236, 237]. Thus, the feeder-free protocol and integration-free iPSCs reported here, presents advantages such as the inexhaustible autologous cell source, potential differentiation into several cells types, and the reduced risk for carcinogenicity compared to other protocols [236, 239, 248, 249].

After generating iMSCs, we hypothesized that introducing iMSCs into a 3D culture

decorated with RGDS, an adhesion peptide, would promote cells to mature into VIC-like phenotype. A previous study by Zhang et al. demonstrated that RGDS concentration can regulate VIC phenotype [33]. Furthermore, VICs encapsulated within degradable PEG-RGDS hydrogels for 21 days produced ECM such as fibronectin and collagen type I, suggesting that RGDS is an important peptide for regulating and promoting VIC phenotype and ECM production [33]. Before encapsulating iMSCs, we first characterized the properties of the PEGDA hydrogels to verify that it closely mimicked the microenvironment in native valve leaflets. Using compression testing, the Young's modulus of PEGDA blank hydrogels was within the physiological modulus of 5-13 kPa [125], interestingly there was an increase in modulus after cell encapsulation. A possible reason for a 6-fold increase could be due to the formation of a denser polymer network surrounding cells. To assess this, a hydrogel swelling test and scanning electron microscopy (SEM) can be used to assess the changes in the polymer crosslinking such as the mesh size. After 28 days, the modulus decreased either because of non-enzymatic degradation of PEGDA or cell death. Based on previous studies the modulus of heart valve leaflets is estimated to about 2 MPa and 15 MPa in the radial and circumferential direction, respectively [250, 251]. While this is several orders of magnitude higher than our study, the hydrogels utilized here were not intended to replicate the overall leaflet modulus but rather the microenvironment in which the valve cells experience.

The viability of iMSCs was characterized using Live/Dead assay. iMSCs encapsulated into PEGDA hydrogels demonstrated over 93% cell viability after day 1, this value then decreased to about 77% after 7 days in culture. A possible reason for the decrease in cell viability is the exposure to free radical from the polymerization process

[252]. Furthermore, there was a distinct difference between cells on the surface compared to those encapsulated in the hydrogel. This difference can be explained by the fact that iMSCs may have been unable to spread through a non-degradable hydrogel, resulting in a round morphology. Thus, we also created a hydrogel containing a slow-degrading PEG-LGPA-PEG sequence (MALDI-TOF shown in Supplementary Figure 31**)** [253], iMSCs did not assume a spindle-like morphology but rather formed large aggregates of cells, either through proliferation or migration, both of which are not favorable for a tissue engineered heart valve scaffold (Supplementary Figure 32,Figure 33,Figure 34,Figure 35). The LGPA linker was chosen due to slower degradation kinetics as linkers such as GPQ degrade on the order of days and were likely unfavorable. Additionally, we examined the mechanical properties of the degradable hydrogel (Supplementary Figure 36) and found that these hydrogels at baseline were much softer than non-degradable hydrogels. Thus, future studies will examine degradation linkers of different rates or a combination of degradable natural polymers, to generate a more suitable 3D environment for iMSCs to spread and mature into VICs.

VICs are known to be a heterogeneous cell population with various sub-phenotypes that can resemble fibroblasts, smooth muscle cells, and MSCs [19, 48, 72]. Previous studies have demonstrated that VICs can be categorized into several phenotypes such as embryonic progenitor MSCs, quiescent VICs, activated VICs, progenitor VICs, and osteoblastic VICs [48]. The ideal phenotype for TEHVs is one that can be initially activated to remodel the scaffold and then transition into a quiescent phenotype, where cells maintain the scaffold structure. If VICs remain in an activated state, there could be issues with scaffold contraction and potential transdifferentiation of VICs into osteoblast-like cells [73, 254].

Activated VICs demonstrate high levels of αSMA with distinct fiber formation, which in our study was observed in the 2D culture when immunostaining for αSMA and F-actin and comparing it to human MSCs. At the initial encapsulation of iMSCs into 3D PEGDA hydrogels, there was diffuse staining of αSMA with no staining of vimentin present at day 1. There was a significant decrease in αSMA expression thereafter, and the staining transitioned from diffuse to punctate staining of αSMA after 28 days. The decrease in αSMA was accompanied by an increase in vimentin and low levels of periostin and calponin expression. Periostin is a protein involved in cell adhesion and robustly expressed in cardiac fibroblasts [255], and calponin is a calcium binding protein often found in smooth muscle cells or myofibroblast-like cells [256] and thus low levels of these proteins is desirable. These results suggest that by introducing iMSCs into a 3D hydrogel system, iMSCs express less αSMA, more of vimentin, and low levels of periostin and calponin. This can be interpreted as cells are transitioning from an activated phenotype to a more quiescent phenotype, which is characterized by the expression of vimentin, a marker for fibroblasts [44, 48].

To determine whether iMSCs are more VIC-like or fibroblast-like, the expression of αSMA, vimentin, periostin, and calponin was compared to VICs and HDFs after 28 days of encapsulation (Supplementary Figure 32). iMSCs had similar expression of αSMA, vimentin, periostin markers compared to VICs. The only significant difference in marker expression was calponin, which was higher in VICs. Although, the iMSCs were not identical to VICs, they may not need to be as VICs are heterogeneous in nature [257]. Furthermore, a previous study demonstrated that it was feasible to use MSCs as a cells

source for heart valve tissue engineering [110]. The results of that study showed MSCs having comparable levels of collagen, αSMA, and vimentin when introduced to different scaffolds [110].

While iMSCs appear to transition into a quiescent phenotype, it is important to discuss some of the limitations of the current hydrogel platform that could be resulting in the observed phenotype. iMSCs were cultured in non-degrading PEGDA hydrogels, which can result in a round-like morphology and "quiescent" state mainly because cells are unable to spread and degrade the hydrogel. However, when iMSCs were introduced into a slow-degrading PEGDA hydrogel cells did not spread throughout the hydrogel but rather formed aggregates of cells after 28 days of encapsulation (Supplementary Figure 33, Figure 34, Figure 35). In fact, the decrease in αSMA and increase in vimentin was not observed in the slow-degrading PEGDA hydrogels, further suggesting that the non-degrading hydrogel may be the more ideal environment for iMSCs to transition into a quiescent phenotype and produce collagen type I.

Collagen is a major extracellular matrix component that makes up the valve leaflet, along with proteoglycans and elastin [138]. Using immunostaining of iMSCs within hydrogels, there was little evidence of collagen type I at day 1, and as time progressed, collagen deposition significantly increased and was localized surrounding the cells. When compared to VICs and HDFs, iMSCs had significantly higher levels of collagen (Figure 32). Quantitative hydroxyproline assay confirmed the immunostaining of collagen as there was significant increase at 28 days compared to day 1. Interestingly, while DNA levels rose progressively during the interim time points, it was not statistically significant. Again,

similar to above, this could be due to the fact that the cells were unable to degrade the hydrogel and thus replace it with their own matrix, or that specific signals need to be added to the hydrogel to induce matrix secretion. Another explanation for an increase in DNA content at day 28 is that cells could have been in a "recovery state" post-encapsulation and only after 28 days were cells able to proliferate and produce collagen. However, a limitation of this study is that cells from the surface were not removed before homogenization. Overall, these findings suggest that iMSCs have the capacity to synthesize collagen type I when introduced into a 3D microenvironment mimicking the valve leaflet layers.

In future studies, we plan to investigate the potential for iMSCs to produce proteoglycans, elastin, and secrete matrix metalloproteinases. The use of PEGDA is to demonstrate, that as a simplified model, iMSCs can progress towards a VIC-like phenotype. However, further work is necessary to study these cells long-term as a potential cell source for tissue engineering. The role of mechanical stimuli is also worth investigating as it is a known to impact VICs phenotype and function [19].

4.6 Conclusion

Developing a suitable cell source for tissue engineering is a critical component for the success and durability of TEHVs. In this study, we attempt to address this problem by differentiating iMSCs from iPSCs and then further maturing these cells into VIC-like cells by introducing these to a 3D culture designed to mimic the layers of the valve leaflets. First, a modified differentiation protocol was utilized to differentiate into iMSCs using a feeder-free approach. Next, the PEGDA hydrogel was characterized and tuned to match the mechanical properties observed in valve leaflets. iMSCs were then encapsulated into

PEGDA hydrogels to study the effects of a 3D culture in the maturation of iMSCs into VIC-like cells. Encapsulated iMSCs demonstrated a transition from an activated VIC-like phenotype to a more quiescent state. In addition, collagen deposition was identified in cell-laden PEGDA hydrogels, corresponding to the potential use of iMSCs as a cell source for TEHV. As such, these experiments contribute a potential new cell source for seeding TEHVs as well as highlight the importance of a 3D culture environment to influence cell phenotype and function.

CHAPTER 5 A MULTILAYERED VALVE LEAFLET DEVELOPED FROM PCL AND GELMA/PEGDA HYDROGEL

5.1 Summary

For children with heart valve disease, valve replacement is often the only possible treatment. However, valve implants are incapable of growth, so multiple surgeries are often needed for valve refitting. Patient-specific, tissue engineered heart valves (TEHV) may address this issue, but mechanically functional TEHVs have yet to be developed. This study aims to recreate native valve structure using PCL and cell-laden GelMA/PEGDA hydrogels in order to generate a valve scaffold capable of growth and regeneration while maintaining proper valve function. Two main layers (fibrosa and spongiosa/ventricularis) were developed individually before being combined and evaluated together. The PCL fibrosa layer was 3D printed to be 40-50 μm thick with circumferential, radial, and diagonal strand alignments. These scaffolds were evaluated for their mechanical properties, degradation over time, and their compatibility with iMSCs. Uniaxial testing indicated anisotropy can be accomplished via strand orientation and under physiological conditions, there was evidence of initial degradation of these scaffolds over 8 months. Immunostaining also indicated that iMSCs on PCL scaffolds treated with poly(methacrylic acid) (PMAA) begin to transition toward a more VIC-like phenotype. Next, a combination of 7.5% w/v GelMA and 5% w/v PEGDA was used to encapsulate iMSCs within a hydrogel spongiosa/ventricularis layer. Cell-laden hydrogels were mechanically evaluated for degradation and assessed for survival within the hydrogel. While cell-laden hydrogels were significantly lower in storage and loss moduli compared to blank hydrogels, they did not

exhibit a change in moduli over 28 days, indicating that the hydrogels were not undergoing short-term degradation. Cells encapsulated within the hydrogel remained 80% viable after day 7. To combine the layers, the hydrogel layer was crosslinked onto treated PCL scaffolds. These scaffolds were assessed under aortic pulsatile shear stress conditions, and iMSC expression of VIC markers, as well as production of collagen type I, was quantified by immunostaining. These results indicated that pulsatile shear stress did not induce a VIC-like phenotype. However, encapsulated cells did begin to deposit collagen I.

5.2 Introduction

An estimated two to three million children live with heart disease, about 5% of whom have heart valve disease [4-6]. This is mainly due to congenital heart defects in industrialized countries and the persistence of rheumatic fever in underdeveloped regions [7-9]. Valve disease is treated by replacement or valve repair. In most cases, valve repair is not possible, and valve implants have a number of risks, such as thrombogenicity and calcification. A significant issue for pediatric patients is the lack of small implants capable of growing, often requiring several surgical interventions for valve refitting [4, 10]. Tissue engineered heart valves (TEHVs) have the potential to address limitations with current implants through their self-repairing and remodeling capacity.

Although there have been recent advancements in the field of TEHVs, the challenge to develop a mechanically functional aortic TEHV for long-term implantation remains. Ideally, a TEHV should be biocompatible, durable, and anti-thrombogenic, while exhibiting physiological hemodynamic profile. A TEHV that meets all these criteria and is capable of functioning under physiological aortic conditions has not yet been created.

The aortic heart valve opens and closes approximately 4 million times a year, with minimal transvalvular pressure gradient [10]. The mechanical strength of valves is attributed to the unique microstructure of each leaflet layer. The orientation of ECM of these layers are believed to enable the constant loading and unloading of the valve leaflets [19]. A challenge with tissue engineering an aortic valve is the difficulty to replicate the trilayer leaflet structure, which is comprised of the fibrosa, spongiosa, and ventricularis [10, 41, 120]. The fibrosa provides mechanical strength through circumferentially aligned collagen fibers. The spongiosa is the middle layer, rich in glycosaminoglycans, while the ventricularis is composed of radially aligned elastin. The leaflet layers are surrounded by valvular interstitial cells (VICs) that maintain tissue homeostasis of the valve [19]. With the native valve leaflet structure and function as a guide, the goal is to design a scaffold that closely mimics this structure to develop a functional aortic TEHV.

To develop a TEHV, the biomaterials and the approach used is vital to ensure a mechanically functional heart valve. The biomaterial requirements for our TEHV are the ability to integrate cells and promote physiological phenotype and cellular function, compatibility with 3D bioprinting, tunable mechanical properties, and most importantly, undergo slow degradation over time. Considering these requirements, we have opted for two types of biomaterials: biodegradable poly-ε-caprolactone and a formulation of gelatin methacrylate and polyethylene diacrylate. The combination of these two types of biomaterials is hypothesized to enable us to incorporate cells into the leaflet scaffold and replicate the microstructure of the leaflet layers using 3D printing. Furthermore, since the geometry and design are key components for a functional TEHV, 3D bioprinting and molding will be the primary approach used.

While other methods have been used to generate heart valve conduits, these approaches have been limiting in their ability to incorporate different materials in customized patterns while enabling spatial placement of cells. Another major advantage of 3D printing is the ability to easily generate patient-specific valves of different geometries and sizes. The concept of using 3D bioprinting to generate a TEHV has been tested by various other groups [14, 106]; however, the combination of the proposed biomaterials, geometry, and valve design has not yet been investigated.

The objective of aim 2 is to develop a multilayered valve leaflet using PCL and a hydrogel-based bioink to generate a mechanically functional aortic TEHV that has the ability to promote VIC-like phenotype, ECM matrix production, as well as undergo slow degradation. We hypothesize that a leaflet composed of 3D printed PCL and a hydrogel layer can be combined in a specific spatial orientation to recapitulate the ECM orientation observed in native leaflets, and that under physiological shear conditions, leaflets will have positive expression of VIC markers and demonstrate initial ECM production.

5.3 Methods and Materials

All media components were purchased from Thermo Fisher Scientific unless otherwise stated.

5.3.1 *Cells*

Human induced mesenchymal stem cells (iMSCs) derived from a feeder-free induced pluripotent stem cell protocol were used for experiments [11]. Cells were maintained in iMSC media containing KO-DMEM, 2mM L-glutamine, 10% fetal bovine serum (Atlanta

Biologics), 1% nonessential amino acids, and 1% penicillin and streptomycin. The media was changed every 2 days.

5.3.2 *3D printing PCL*

For this study, poly-ε-caprolactone (PCL; Sigma-Aldrich) of molecular weight of 80,000 Da was used. Scaffolds were 3D printed to a thickness of 40-50 μm using the EnvisionTEC 3D Bioplotter (Gladbeck, Germany). PCL pellets were first melted in the high temperature cartridge to 180°C for 20-30 minutes before starting a print. Once melted, the PCL was extruded out of the metal cartridge through a 22G stainless steel Luer lock needle tip (EnvisionTEC). The metal needle was calibrated, and scaffolds were printed at 4.0 bar and at a speed of 1.0 mm/s. Scaffolds of various different sizes were 3D printed while maintaining the thickness previously mentioned. The inner pattern design of the PCL scaffolds was controlled by the strand orientation. For instance, the circumferentially aligned scaffold has the bottom layer strands aligned at 90° and the top layer strands at 180°. Meanwhile, the radially aligned scaffold consisted of the bottom layer at 180° and the top layer at 90°. The diagonal orientation was achieved by printing a bottom layer at 30° follow by the top layer at 150°. All strands were printed at a 0.4 mm distance.

5.3.3 *Uniaxial tensile testing of PCL*

To perform uniaxial tensile testing, PCL scaffolds were 3D printed into dogbone specimens following the ASTM D1708 – 13 guidelines. The dogbone specimen was designed using SOLIDWORKS to have a total length of 37.5 mm, gauge length of 15 mm, and a width of 5.5 mm. The thickness of the PCL scaffolds ranged from 60 to 160 μm. For

uniaxial testing, a sample size of 4-7 samples were tested. To characterize the degradation properties of PCL scaffolds, the dogbone scaffolds were scaled down by a factor of 1.5 and were maintained in PBS solution at 37°C for up to 8 months. The thickness of these samples ranged from 30 to 50 μm. The uniaxial tensile properties of degraded samples were tested at 6.5 months and 8 months. A sample size of 3-6 samples was used. Degraded samples were compared to control samples from day 0. Before uniaxial testing, graphite markers were placed along the gauge length of the samples and sand paper was attached to the end of the dogbone specimen to enhance grip. Uniaxial testing was performed on the TestResources SM-500-294 with a 25 lb-f load cell at a rate of 12 mm/min and 8 mm/min for the dogbone with a 37.5 mm and 25 mm length, respectively. The upper and lower tangent moduli and the ultimate tensile strength and elongation were determined using MATLAB code (MathWorks), as previously described [258].

5.3.4 *Surface treatment of PCL and cell metabolism assessment*

The hydrophobicity of the PCL surface and its ability to crosslink with other biomaterials can be modulated by grafting hydrophilic poly(methacrylic acid) (PMAA) onto PCL via a modified two-step protocol [259]. After rinsing PCL scaffolds in ethanol and deionized water, samples are submerged in 30% hydrogen peroxide solution (Sigma-Aldrich) and exposed to UV light at 37°C for 6 hours. Next, samples were rinsed with deionized water and placed into a 4% weight-to-volume (w/v) solution of methacrylic acid (MAA) in deionized water for 2 hours under UV exposure at 37°C. PCL-MAA scaffolds were then rinsed with deionized water for 24 hours before use. Cell compatibility and adhesion onto the PCL-MAA scaffolds was assessed using the alamarBlue assay and

immunostaining (detailed below). Using non-treated 12-well plates, iMSCs were seeded onto PCL-MAA scaffolds at a density of 25 x 103 cells/mL. After day 1 and day 7, samples were thoroughly rinsed in PBS and alamarBlue was added as 10% of the sample media volume and incubated at 37°C. A fluorescence excitation wavelength of 560 nm was used and the fluorescence emission was read at 590 nm using the BioTek Synergy 2 plate reader (BioTek Instruments). The following experimental groups were utilized: PCL-MAA, PCL only, and controls of media only with alamarBlue were used. After the alamarBlue assay, samples were rinsed with PBS and then fixed in paraformaldehyde for immunostaining.

5.3.5 *Hydrogel formulation and fabrication*

Poly(ethylene glycol) diacrylate (PEGDA; ESI BIO) of molecular weight 3400 Da and gelatin methacrylate (GelMA; Cellink) were used to make hydrogels. A prepolymer solution of 5% w/v PEGDA, 10 µM Eosin Y (Santa Cruz Biotechnology), 0.375% v/v 1-vinyl-2-pyrrolidinone (NVP; Sigma-Aldrich), and 1.5% v/v triethanolamine (TEOA; Sigma-Aldrich) was dissolved in PBS of 80% the total volume. The prepolymer solution was sterile-filtered using the Spin-X Tube Filter (Corning). Subsequently, 7.5% w/v sterile GelMA was added to the prepolymer solution and incubated at 37°C for 30 minutes with periodic vortexing prior to use. Cells were added to the solution at a concentration of 5 x 106 cells/mL to complete the remaining 20% of the total volume. Hydrogels were made by sandwiching 15 µL of prepolymer solution between a hydrophobic glass slide and a cover slip suspended by thin silicone rubber spacers (McMaster Carr) of 0.381 mm thickness on each side. After assembly, the hydrogels were incubated at 4°C for 5 minutes and then crosslinked using a white-light source (LED Light; Braintree Scientific, Inc.) for 5

additional minutes. Hydrogels were removed from the glass with a spatula and placed in media.

5.3.6 *Rheology*

Rheological assessment for mechanical properties and hydrogel degradation was conducted on blank hydrogels and cell-laden hydrogels (5 x106 cells/mL) at the following time points: 1, 7, 14, 21, and 28 days. This assessment was performed on the Anton Paar MCR 302 stress-controlled rheometer with a 9 mm diameter, 2° measuring cone. The storage and loss moduli of the hydrogels were measured using dynamic oscillatory strain and frequency sweeps. The hydrogels were loaded on the plate, and the cone was lowered to the thickness of the hydrogel. An initial strain amplitude sweep was performed at ω = 10 rad/s to determine the linear viscoelastic range of the samples. Oscillatory frequency sweeps between 0.5 to 30 rad/s were performed to determine the storage and loss moduli at 1.6% strain [260]. All samples had 5-6 technical replicates.

5.3.7 *Cell Viability*

Hydrogels were collected at day 1 and day 7 timepoints for assessment of cell viability. A dead control was created by collecting and incubating one hydrogel in 70% methanol for 30 minutes at 37°C. All hydrogels were first rinsed with PBS and stained with the Live/Dead™ assay, consisting of a solution of 10 µM calcein AM and 5 µM ethidium homodimer, for 25 minutes at 37°C. They were then collected, rinsed with PBS, and placed back in media. Confocal microscopy (Olympus FV100) was utilized to image the gels, and cell viability was quantified using an automated counter in CellProfiler. A total of 5 biological replicates were used with a minimum of 3 technical replicates in each set.

5.3.8 *Preparation of multilayered valve leaflet*

3D printed PCL-MAA and GelMA/PEGDA hydrogel were combined in a multilayered scaffold for testing under pulsatile shear stress (PSS) conditions. For samples tested under PSS, PCL-MAA was cut into rectangular scaffolds of 12 x 14 mm dimension. Then, 8 μL of prepolymer GelMA/PEGDA hydrogel was added to the scaffold with silicone spacers (McMaster Carr) of 0.381 mm thickness. The spacers were used to control the thickness of the hydrogel. Then, a circular glass coverslip (18 mm diameter) treated with Rain-X® Original glass repellent (RainX) was placed on top of the hydrogel with the spacers on each side. Prepolymer solution contained crosslinking components as previously mentioned with a cell concentration of 5 x 10^6 cells/mL. Before crosslinking, samples were placed at 4°C for 5 minutes followed by white-light crosslinking for 5 minutes at 4°C.

5.3.9 *Pulsatile shear stress testing*

To study the multilayered scaffold and assess the VIC phenotype and ECM production under the shear stress condition, a cone-in-plate bioreactor was used as previously described [261]. Using this system, 9 multilayered samples were loaded into the cone-in-plate bioreactor and tested for up to 7 days under PSS with constant flow of iMSC media throughout the bioreactor. Control samples were multilayered scaffolds at day 0. The media was changed halfway through experiment. The PSS profile reached a peak shear stress of 80 dynes/cm^2 with a cycle duration of 800 ms consisting of an acceleration and deceleration phase to represent the systole and diastole phases of the cardiac cycle [262].

5.3.10 *Immunostaining*

The VIC phenotype and collagen I production was characterized in the multilayered scaffolds by using immunofluorescence staining and confocal microscopy (Olympus FV1000). For PCL scaffolds, only VIC phenotype was assessed. To stain the nucleus, 4′,6-Diamidine-2′-phenylindole dihydrochloride (DAPI, Sigma-Aldrich) at 1 ug/mL was used and fluorescein-5-Maleimide at 10 µg/mL (FITC-MAL; Cayman Chemical Company) was used to stain the cell membrane. Hydrogels were fixed with 4% v/v paraformaldehyde for 20 minutes, permeabilized with 0.2% Triton X-100, and incubated for 1-hour incubation in 1% bovine serum albumin (BSA; Sigma-Aldrich). All incubations were performed at room temperature thus far. Hydrogels were stained for collagen type I, αSMA, and vimentin using primary antibodies at 4°C overnight: mouse anti-human collagen type I (1:100; Abcam), mouse anti-human αSMA (1:100; Abcam), rabbit anti-human vimentin (1:100; Santa Cruz biotechnology). The following secondary antibodies were used: goat anti-mouse Alexa Fluor 647 (1:200), and goat anti-mouse Alexa Fluor 488 (1:200). Blank and cell-laden hydrogels were stained with secondary-only antibody as a control. The amount of fluorescence was quantified using CellProfiler 3.1.8, where images for each stain were used to quantify presence of nuclei and the VIC marker using the IdentifyPrimaryObjects function. Afterwards, RelateObjects and FilterObjects were used to determine the number of cells positive with the VIC marker of interest. The percent of cells positive for the VIC marker was calculated using the calculateMath function. Collagen type I staining was quantified using a modified similar approach, as used for VIC markers, the only difference being that the percent area was calculated rather than the percent of positive cells. A total of 3 biological samples were used, and a minimum of 6

images were taken from different x,y, and z locations on the PCL or the multilayered scaffolds.

5.3.11 *Statistical Analysis*

All quantitative data were expressed as the mean ± standard deviation (SD). Statistical analysis was performed using Prism 8 (Graphpad) and all experiments were tested for normality using the Shapiro-Wilk test. For uniaxial tensile testing and degradation experiments of PCL scaffolds, if samples were normally distributed, an unpaired ordinary one-way ANOVA with Holm-Sidak's multiple comparisons test was used, while for samples not normally distributed, a Kruskal-Wallis ANOVA test with Dunn's multiple comparison test was performed. As for cell compatibility and cell viability, an unpaired t-test and paired t-test were used to compare between day 1 and day 7, respectively. To quantify the percent of cells with positive αSMA and vimentin expression an ordinary one-way ANOVA and a Tukey's multiple comparison test was used. For the shear stress studies, an unpaired t-test was used for comparing the cells positive for αSMA and vimentin expression, as well as for the percent area covered by collagen type I. For all experiments, unless otherwise stated, sample size n = 3-5 and technical replicates were used. Statistical significance was considered at a value of $p < 0.05$.

5.4 Results

5.4.1 *Mechanical properties of PCL scaffold*

The mechanical properties of PCL scaffolds of three strand orientations (circumferential, radial, and diagonal) were evaluated, as shown in Figure 17a. The Cauchy-Green stress-strain curve demonstrates a similar shape among the different strand orientations, where there is an initial phase up to 7-12% Green strain, followed by a plastic deformation phase thereafter. In Figure 17b, the upper tangent modulus (UTM) and lower tangent modulus (LTM) were calculated for all three strand orientations. The average UTM was 5.2 MPa for circumferential strand alignment, 3.7 MPa for radial strand alignment, and 4.1 MPa for the diagonal strand alignment on PCL scaffolds. The circumferential scaffolds were statistically significant when compared to the radially aligned scaffolds, and no significance was determined when compared to diagonal scaffolds. As for the LTM, no statistical significance was determined among all three alignments, and the average LTM was 139.8, 204.2, and 137.6 MPa for the circumferential, radial, and diagonal scaffolds, respectively. Furthermore, the ultimate tensile strength, which describes the materials capacity to withstand the loads with a tendency to elongate the scaffold, was the highest for the radially aligned scaffolds at 168.1 MPa, while the circumferential UTS was 155.2 MPa followed by 92.8 MPa for the diagonal scaffolds. There was no statistical difference between the UTS of circumferential and radial scaffolds; however, the diagonal scaffold was statistically lower when compared to the radial scaffolds. Lastly, the UTE for the radial scaffolds was significantly higher than the other two strand orientations with a strain of 26.6, while circumferential and diagonal scaffolds were 19.7 and 14.8, respectively.

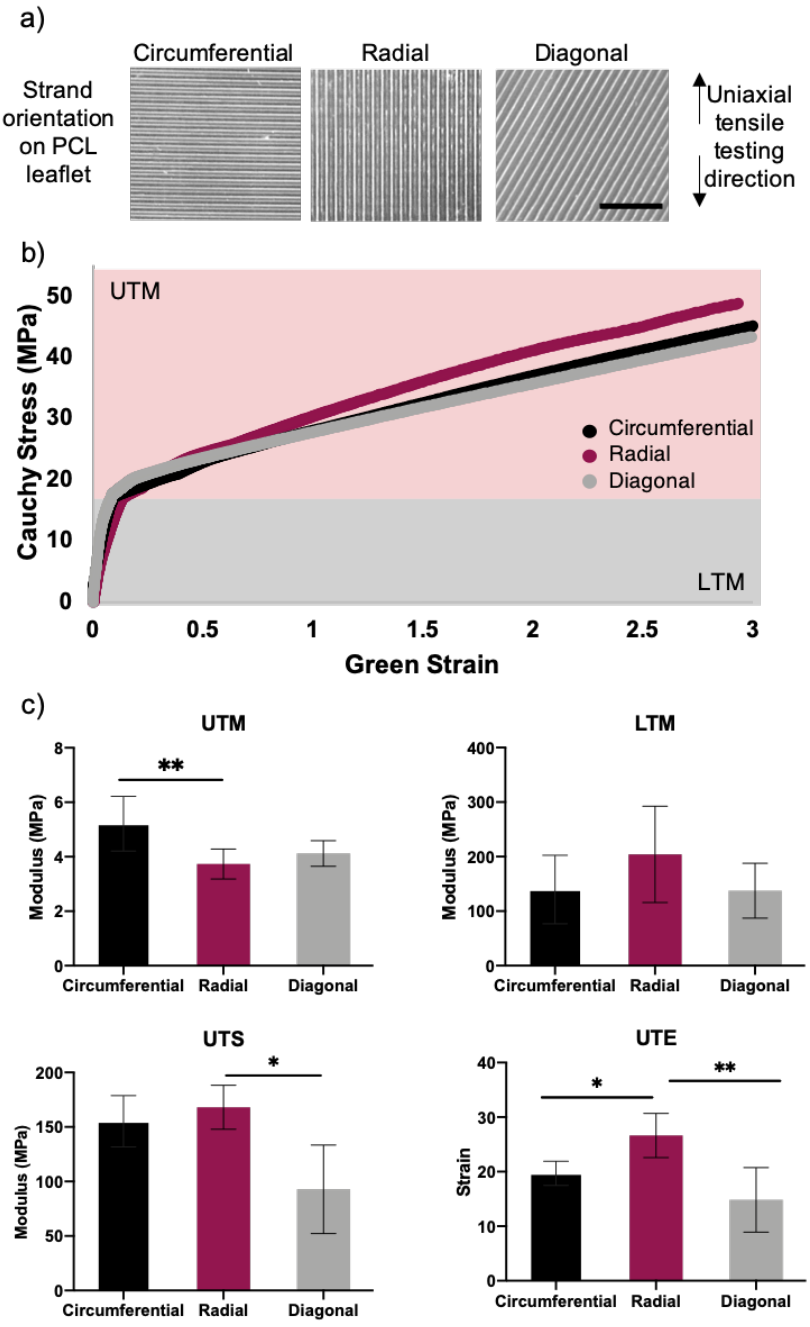

Figure 17. Mechanical properties of PCL scaffolds of three different strand orientations. A) Representative images of the strand orientation of 3D printed PCL scaffolds used for tensile testing. The direction in which samples were subjected to tensile testing is

demonstrated on the right. B) Cauchy-green stress-strain curve for the circumferential, radial, and diagonal scaffolds, where the moduli for PCL scaffolds was calculated from two different regions, the upper and the lower tangent modulus (UTM and LTM). C) The mechanical properties of the PCL scaffolds were characterized by four properties: the UTM, LTM, ultimate tensile strength (UTS), and ultimate tensile elongation (UTE). N = 4. *p<0.05; ** p<0.01; ***p<0.001. Scale bar = 5 mm.

5.4.2 *Degradation properties of PCL scaffolds*

The mechanical properties of PCL scaffolds of circumferential strand orientation were assessed to determine changes in bulk properties due to degradation (Figure 18). Circumferential PCL scaffolds did not show evidence of degradation based on their UTM and LTM properties; however, there was a significant decrease in UTS and UTE when comparing 0 to 8 months. The UTS significantly decreased from 155.2 MPa to 62 MPa after 8 months, while the UTE also significantly decreased from 19.7 MPa to 8.9 MPa. Additionally, a decrease in sample thickness was observed after 8 months of degradation as shown in Supplementary Figure 37.

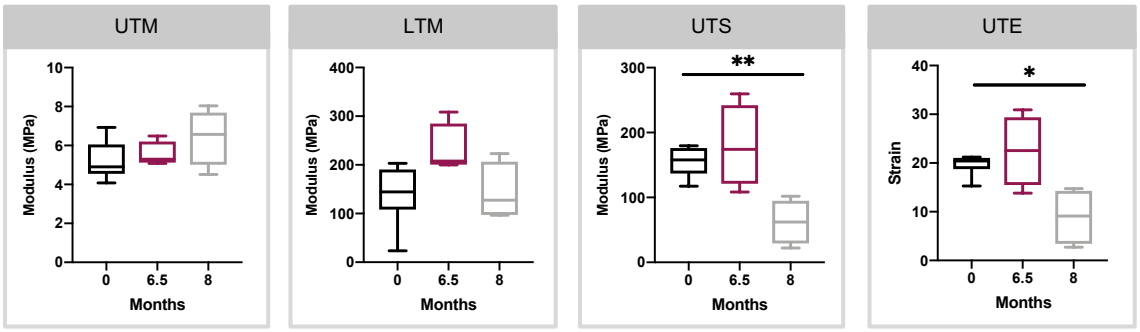

Figure 18. Characterization of degradation of PCL scaffolds of circumferential strand orientation. The UTM, LTM, UTS, and UTE were characterized from uniaxial tensile testing post-degradation. Samples were maintained at 37°C in PBS for degradation studies

and at 6.5 and 8 months the mechanical properties were characterized and compared to month 0 scaffolds. N = 3-7. One-way ANOVA comparing 0 to 8 months. * $p<0.05$; ** $p<0.01$.

5.4.3 *iMSC metabolism when seeded on PCL scaffolds*

The cellular health and metabolic function of iMSCs seeded on either PCL-MAA or PCL scaffolds were assessed at day 1 and day 7 as shown in Figure 19. Using alamarBlue, the level of fluorescence was normalized to day 1 and then compared between the two samples. PCL scaffolds treated with methacrylic acid (PCL-MAA) were statistically higher than PCL scaffolds, where there was 4 times more fluorescence.

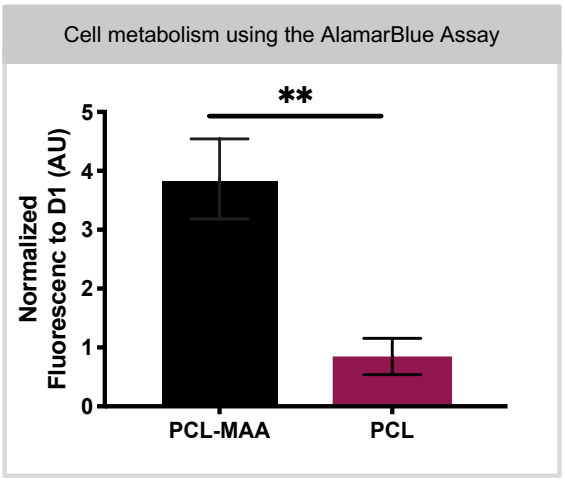

Figure 19. iMSC metabolism when seeded on PCL scaffolds. PCL-MAA and PCL were seeded with iMSCs and alamarBlue reagent was used to assess the cellular health and metabolic function of adhered cells. The level of fluorescence was normalized to day 1 and an unpaired t-test was used for statistical analysis. N = 3. Unpaired T-test. **$p<0.01$.

5.4.4 *Cell phenotype assessment on PCL scaffolds*

In addition to assessing whether or not cells adhered onto the PCL scaffold, the effects of the scaffold on the iMSC phenotype was important to characterize. Scaffolds were stained for αSMA and vimentin and the number of positive cells with αSMA and vimentin expression were quantified. On average, 30% of the iMSCs seeded on PCL stained positively for αSMA, regardless of surface treatment of MAA. Meanwhile, 70% and 50% of cells stained for vimentin when seeded on PCL-MAA and PCL, respectively. While, 30% of the cells seeded on tissue culture (TC) expressed vimentin. In Figure 20c, iMSCs seeded on PCL-MAA scaffolds have positive diffuse staining of vimentin in most of the cells, with a few cells staining for αSMA stress fibers. Cells seeded on the PCL only scaffold also have diffuse staining of vimentin, except cells do not demonstrate distinct stress fibers of αSMA and rather have αSMA staining at the focal adhesion sites. On the TC plate, iMSCs have minimal staining of vimentin and staining of very distinct stress fibers of αSMA.

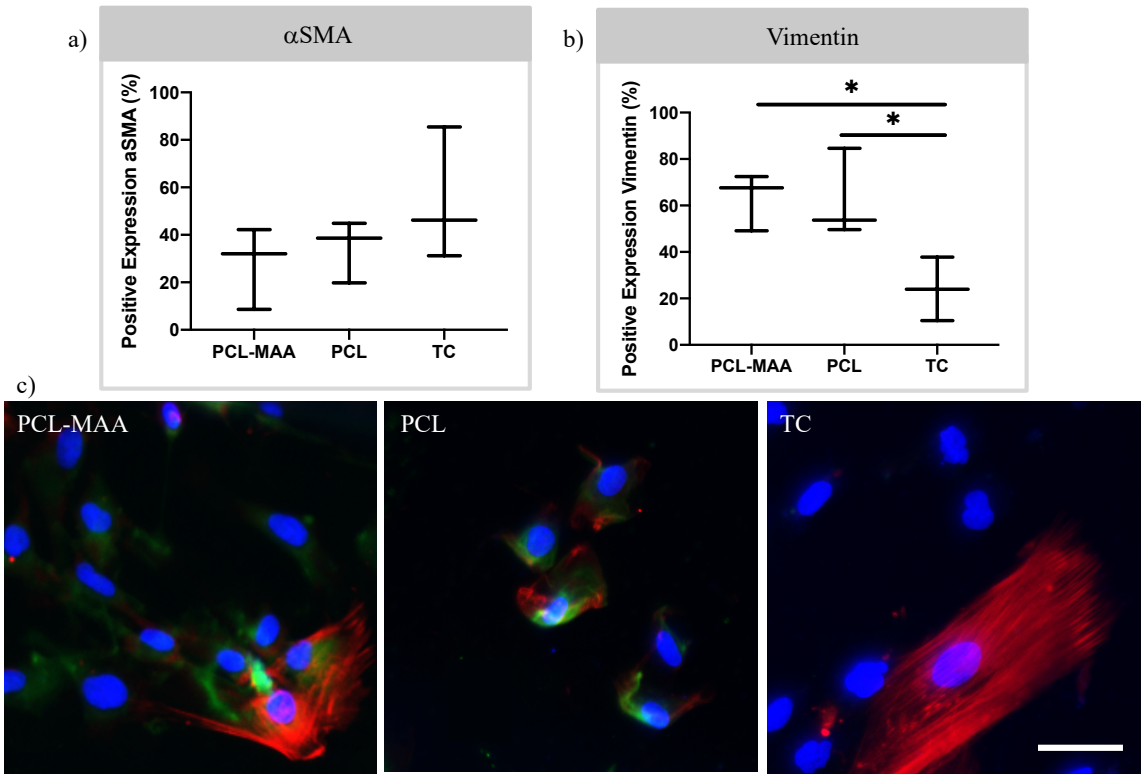

Figure 20. Quantification of αSMA and vimentin expression of iMSCS seeded on PCL-MAA, PCL, and tissue culture plate (TC). A,B) Percentage of cells that stained positive for αSMA and vimentin was determined from immunostaining images using CellProfiler software. A total of 3 biological samples were used, and a minimum of 6 images were taken from different x, y, and z locations on the PCL. C) Immunostaining images of iMSCs seeded on PCL-MAA, PCL, and TC. N = 3. One-way ANOVA comparing all experimental groups. *p <0.05. DAPI – blue, vimentin – green, and αSMA – red. Scale bar 50 μm.

5.4.5 *Mechanical properties of GelMA/PEGDA hydrogels*

For the spongiosa/ventricularis layer of the valve scaffold, hydrogels of GelMA and PEGDA were used. The mechanical properties of cell-laden hydrogels are important because they should be representative of what native cells experience on the leaflets.

Mechanical properties were also used as a measure of degradation over the course of 28 days. The storage and loss moduli of blank and cell-laden hydrogels were measured over a range of frequencies, as shown in Supplemental Figure 38, and measurements taken at 1.6 Hz were compared across groups, as shown in Figure 21. The storage moduli of blank and cell-laden hydrogels indicated a significant difference, with cell-laden hydrogels exhibiting a lower storage modulus on average compared to that of blank hydrogels. However, comparisons of storage moduli across 28 days showed no significant changes over the experimental time period in either group. Similarly, a significant decrease in loss modulus was also observed between blank and cell-laden hydrogels. In loss moduli, significant differences over time were observed between hydrogels, specifically between day 7 and day 28 of blank hydrogels. These results indicate that while variations in storage and loss moduli exist between groups, cell-laden hydrogels are not degrading within the course of 28 days.

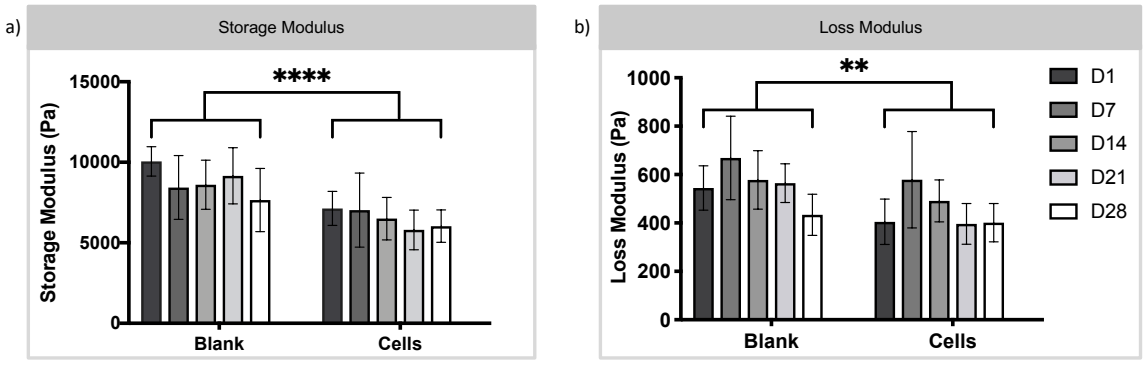

Figure 21. Rheological characterization. Storage moduli (a) and loss moduli (b) of blank GelMA/PEGDA hydrogels and cell-laden GelMA/PEGDA hydrogels over 28 days measured by rheology. N = 5 - 6. Two-way ANOVA comparing Blank vs. Cells. ** $p < 0.001$, **** $p < 0.0001$.

5.4.6 *Cell viability of GelMA/PEGDA hydrogels*

Evaluating cell viability within these hydrogels is important to ensure that they are able to produce ECM components to remodel and regenerate the leaflet. As shown in Figure 22, iMSCs encapsulated in 7.5% w/v GelMA and 5% w/v PEGDA hydrogels remained viable at 92% by day 1. By day 7, iMSC viability decreased to 80%. While the decrease from day 1 to day 7 was significant, iMSCs still remained viable encapsulated within the hydrogels.

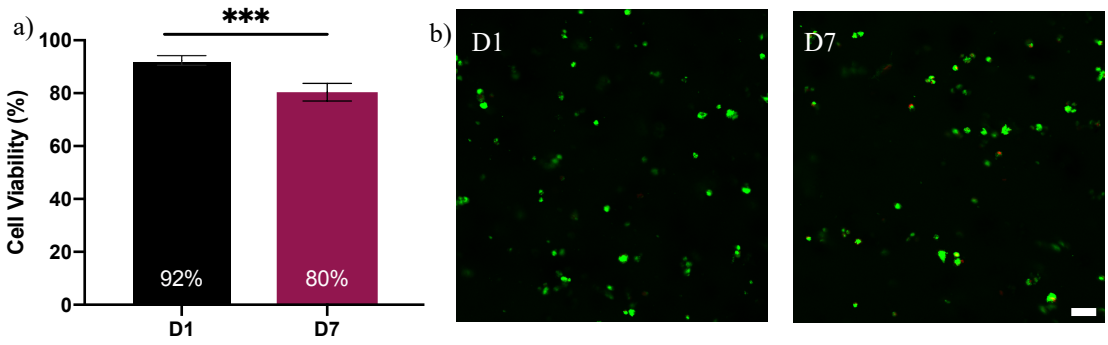

Figure 22. Assessment of cell viability using Live/Dead assay. A) Cell viability of iMSCs encapsulated in GelMA/PEGDA hydrogels at day 1 and day 7. Cell viability decreased from 92% to 80% over 7 days. B) However, cells still remained viable within the hydrogels up to 7 days. N = 5. Paired t-test, *** $p < 0.001$. Green – Calcein AM. Scale bar 50 µm.

5.4.7 *VIC phenotype and collagen type I production in multilayered leaflet scaffolds under PSS*

To create a multilayered leaflet, the PCL and GelMA/PEGDA components were crosslinked together. Samples were loaded into the cone-in-plate bioreactor for assessing the effects of pulsatile shear stress on VIC phenotype and collagen type I production in

cell-laden scaffolds. In Figure 23a, the expression of αSMA and vimentin was quantified and compared between day 0 and day 7 PSS. In the multilayered scaffolds, 18% of the encapsulated cells were positive for αSMA at day 0. After day 7 of PSS, this number increased to an average of 23% of the cells positively expressing αSMA. When staining for vimentin, 16% and 28% of the cells expressed vimentin in the multilayered scaffolds at day 0 and at day 7 PSS, respectively. There was no statistical difference between the day 0 and day 7 PSS for both αSMA and vimentin expression. Representative images of the immunostaining of αSMA and vimentin are demonstrated in Figure 23b. At day 0, there is diffuse staining of αSMA present and then cells have a combination of diffuse and punctate staining of αSMA and punctate staining of vimentin after 7 days of PSS conditions. No evidence of background staining is present in the secondary antibody only images for αSMA and vimentin (data not shown).

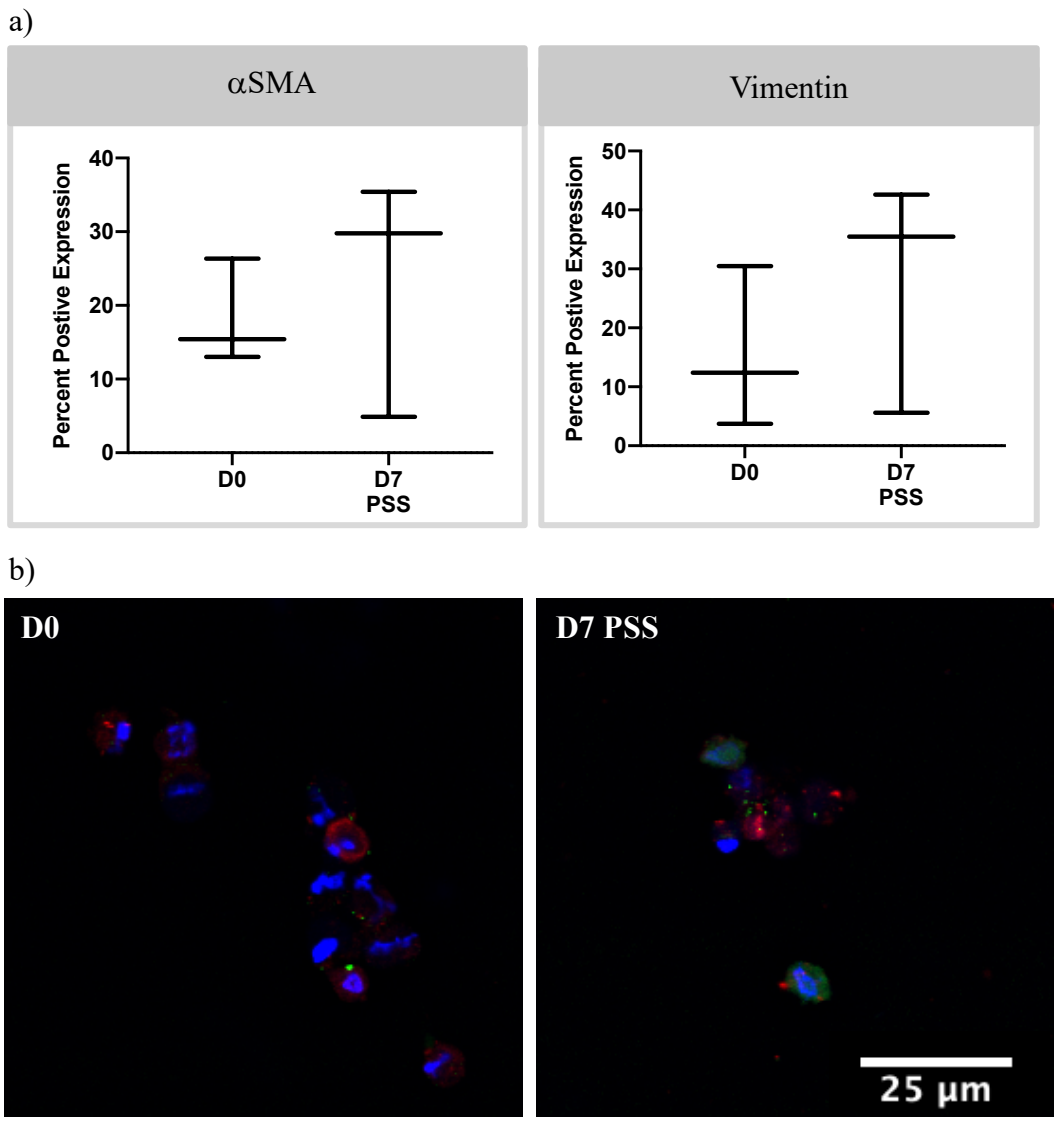

Figure 23. Quantification of αSMA and vimentin expression in cell-laden multilayered scaffolds. A) αSMA and vimentin expression was quantified by determining the number of positive cells with αSMA and vimentin expression at D0 and post-D7 in PSS conditions. A total of 3 biological samples were used, and a minimum of 6 images were taken from different x, y, and z locations on the multilayered scaffold. B) Confocal images of

immunostaining of αSMA and vimentin at D0 and D7 PSS. N = 3. Unpaired t-test – no significance. DAPI – blue, αSMA – Red, and vimentin – Green. Scale bar 25 μm.

Collagen type I deposits were also quantified through immunostaining and compared between day 0 and day 7 PSS in Figure 24a. At day 0 there was minimal evidence of collagen type I and by day 7 PSS 0.34% of the imaged area was stained positively for collagen type I. This increase in collagen type I was determined to be statistically higher when compared to day 0. In Figure 24b, immunostaining demonstrates minimal to no staining of collagen type I, at day 0 and at day 7 PSS, we observe diffuse collagen type I staining surrounding the cell membrane (stained in green). In control samples stained only with secondary antibody, no collagen type I staining is observed (image not shown).

a)

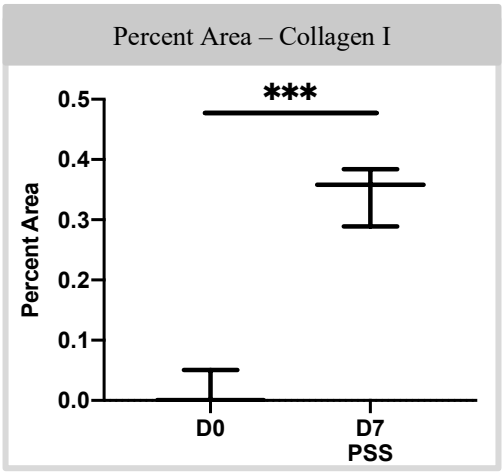

b)

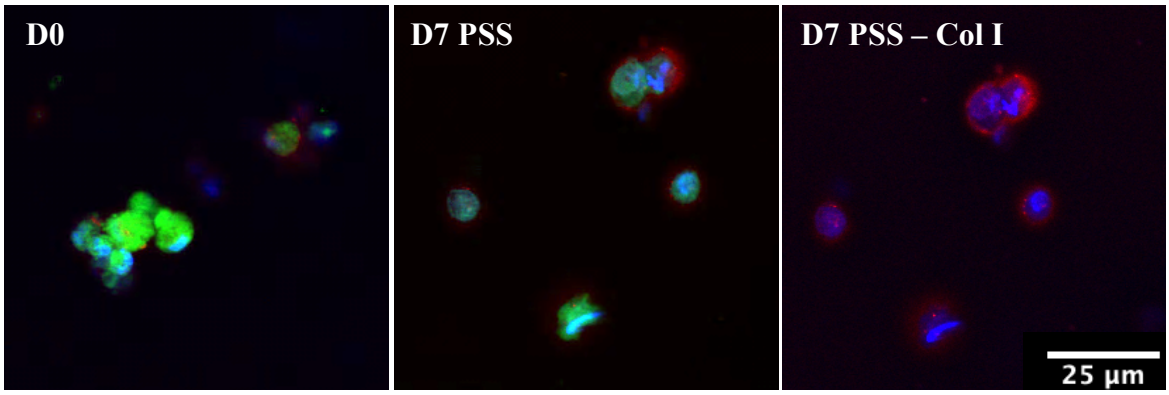

Figure 24. Quantification of collagen type I deposits in cell-laden multilayered scaffolds. A) Collagen type I was quantified by determining the percent area of collagen type I staining over the area of total image. A total of 3 biological samples were used, and a minimum of 6 images were taken from different x, y, and z locations on the multilayered scaffold. B) Confocal images of immunostaining of Collagen type I at D0 and D7 PSS. N = 3. Unpaired t-test. $p<0.0001$. DAPI – blue, Collagen type I – Red, and cell membrane (FITC-MAL) – Green. Scale bar 25 μm.

5.5 Discussion

Heart valve tissue engineering has the potential to address the limitations of current mechanical and bioprosthetic heart valve implants. Most importantly, TEHVs could tremendously impact the pediatric population, who currently rely on heart valve implants that were designed and made for adults. In this aim, our goal was to develop a multilayered valve leaflet using PCL and a hydrogel-based bioink to generate a mechanically functional aortic TEHV that has the ability to promote healthy VIC-like phenotype and ECM production, and is capable of degrading over time. To engineer a functional aortic TEHVs, a rationally-designed heart valve leaflet composed of both synthetic and natural polymers was developed.

The heart valve leaflet was designed considering the structural and mechanical properties of the fibrosa layer in native leaflets, where the collagen fibers are circumferentially aligned, and the mechanical properties are anisotropic [263]. In this aim, PCL was 3D printed in three different strand orientations to determine which scaffold would yield mechanical properties similar to native leaflets. The stress-strain curve of the

PCL scaffolds was observed to have two phases with distinct tangent moduli and the shape of the curve suggests the scaffold is not relatively elastic. The UTM of the PCL scaffolds were within the physiological range of 4 – 13 kPa [122], and the circumferential UTM was statistically higher compared to the radial. This suggests that strand orientation can produce anisotropy because at different orientations, a significant difference in the UTM is observed. At the UTM, it is important to notice the PCL scaffolds undergo plastic deformation. The LTM, regardless of the strand orientation, was much higher than native tissue, where there was no statistical difference among the different strand orientations. Given that native leaflets have a modulus of 4 – 13 kPa [122], it suggests that under physiological conditions it is unlikely that the PCL scaffolds will undergo any major deformation or fracture.

A reason why the PCL scaffolds have two different tangent moduli could be due to the manufacturing process used. PCL scaffolds were 3D printed using strands of melted polymer which created "crosslinking" between strands, yielding a very high initial tangent modulus. This can describe why we observe a stiffer material reinforced by the crosslinking of the strands, regardless of strand orientation. Once the crosslinks have unlinked, then we observe the true modulus, where the PCL scaffold is more compliant. The statistical difference between all three strand orientations for the UTE indicates that the introduction of different orientations can affect the overall UTE of the scaffold, which suggests that strand orientation can introduce anisotropic properties to the scaffolds. Overall, PCL scaffolds have some resemblance to the native leaflet. For further studies, only circumferentially aligned PCL scaffolds were investigated, as these strands most closely resemble collagen fiber alignment. Given that we are engineering a TEHV that has the

capacity to degrade and remodel over time, it was important to assess short-term degradation to ensure that this material would not degrade quickly. Degradation of the PCL scaffolds is characterized to be slow and not evident in the UTM and LTM properties of the circumferential PCL scaffolds after 8 months. However, there was evidence of some degradation through the significant decrease in UTS and UTE. Some evidence of degradation is to be expected as PCL has slow degradation of 24-36-months [264].

Next, the PCL scaffold was surface-treated with poyl(methacrylate acid) in order to reduce hydrophobicity and to ensure that this material can be crosslinked with the hydrogel biomaterial. The health of iMSC metabolism post-surface treatment was important to assess to ensure cells interacting with the PCL remained viable and healthy. AlamarBlue data demonstrated that iMSCs have higher metabolic activity compared to PCL-only scaffolds, suggesting that decreasing hydrophobicity led to more cellular metabolic activity. It could also suggest that more cells were able to adhere onto the PCL-MAA scaffold compared to PCL scaffolds. Previous studies have demonstrated that when hydrophobicity is decreased, more cell adhesions are observed [265]. Furthermore, it was important to characterize the VIC-like phenotype of iMSCs seeded on PCL-MAA scaffolds given the stiffness of PCL and its potential to elicit an activated myofibroblast-like phenotype. On average, 35-40% iMSCs adhered on PCL scaffolds were positive for αSMA expression, regardless of MAA treatment. Interestingly, iMSCs were 50-60% positive for vimentin expression, suggesting that iMSCs, when seeded on PCL, are more VIC-like cells. If iMSCs remain activated through long-term expression of αSMA, an alternative is to utilize ascorbic acid to modulate the cell phenotype while promoting ECM remodeling [211].

The next component of the multilayered leaflet is the hydrogel-based bioink composed of GelMA/PEGDA. The degradation of this material is important to characterize as this material should ideally degrade slowly to enable cells to remodel and produce ECM. Overall, there was significant difference in the storage and loss modulus between blank and cell-laden hydrogels. A lower modulus for cell-laden hydrogels could be caused by a high seeding density, which can reduce the number of crosslinking sites available. In a previous study, when cells were introduced into a quasilaminate scaffold, composed of varying stiffness of PEGDA, a similar decrease in modulus was observed [131]. However, no difference was observed over different time points suggesting low to minimal degradation of the GelMA/PEGDA hydrogels short-term. If necessary, slow MMP-cleavable degradation peptides may need to be introduced into the GelMA/PEGDA bioink to control degradation [266]. The cell viability of iMSCs was assessed in cell-laden hydrogels of GelMA/PEGDA, and while there was a decrease in cell viability, 80% viability was considered acceptable for future experiments. Thus, suggesting that overall, the GelMA/PEGDA hydrogel is suitable for use in the valve leaflet.

The VIC-like phenotype and collagen type I production was studied in the multilayered scaffolds under pulsatile shear stress conditions for 7 days. To assess whether there were any changes to the phenotype of iMSC and whether iMSCs were capable of producing collagen type I, scaffolds were immunostained for αSMA, vimentin, and collagen type I. We have previously shown that iMSCs in PEGDA hydrogels transition from an activated VIC-like phenotype to a more quiescent state, and that these cells have the capacity to produce collagen type I shortly after 7 days under static conditions [11]. Under PSS, we did not observe any changes in αSMA and vimentin expression, where

there were 20% positive cells for αSMA and vimentin. The lack of significance could be explained by biological variation and a small sample size. Results from immunostaining suggests that under PSS and in the multilayered scaffold, we do not observe an activated VIC-like phenotype nor expression of vimentin. It is worthwhile noticing that this is only day 7 and that a longer time point may be necessary. While no changes in cell phenotype were observed, the amount of collagen type I produced was significantly higher at day 7 under PSS compared to day 0. Furthermore, the diffuse staining appears to be surrounding the cells suggesting that collagen type I production is possible under PSS and in the cell-laden multilayered leaflet scaffold. While the percent of collagen of the overall area imaged is low (0.34%), it is important to recognize the amount of collagen produced is influenced by the number of cells present. A limitation for assessing collagen I is the small amounts of cells visualized during imaging, and thus a possible reason for the 0.34% of the area positively stained for collagen I. In future studies, collagen type I content can be measured by hydroxyproline assay; however, the amount of hydrogel collected will need to be increased to be able to detect collagen using this assay. Another component to consider for future studies is increasing the duration of this experiment, because through previous studies we have demonstrated that cells produce large amounts of collagen at day 28 [11]. This may be a challenge with the cone-in-plate bioreactor as it is not built for time points longer than 7 days. An alternative to evaluate the production of collagen is to use a heart valve bioreactor, where longer time points can be sustained.

5.6 Conclusion

In this aim, we demonstrated a multilayered heart valve leaflet can be composed of 3D printed PCL and a hydrogel layer to recapitulate structural features of native leaflets.

Each material used for the multilayered leaflet was assessed for its mechanical properties and its interactions with iMSCs to ensure that cells remained viable and maintained a healthy VIC-like phenotype. Furthermore, the multilayered leaflet under pulsatile shear stress conditions resulted in collagen type I production suggesting the leaflet is capable of ECM production over time. While our results are promising, future studies are necessary to evaluate the multilayered leaflet under aortic valve conditions as well as assess its growth and remodeling potential long-term.

CHAPTER 6 PCL TEHVS FUNCTION UNDER PHYSIOLOGICAL AORTIC VALVE FLOW CONDITIONS

6.1 Summary

Most TEHVs have been developed for the pulmonary position as TEHVs capable of withstanding aortic valve conditions are required to be more durable. In this aim, a 3D printed PCL leaflet of circumferential strand orientation was assembled onto a valve stent to evaluate whether this layer of the TEHV leaflet, which is designed to be the load-bearing layer, can withstand aortic valve flow and pressure conditions. Using a left-ventricle flow loop, the hemodynamic profile of the PCL-TEHVs was tested under aortic heart valve conditions and the following parameters were computed: the effective orifice area, mean and max transvalvular pressure gradient, regurgitation volume, and leakage volume. Hemodynamics studies of the PCL-TEHV resulted in similar EOA and mean transvalvular pressure gradient to commercially available valves. In addition, there was no evidence of leakage or regurgitation suggesting the PCL-TEHV properly functions under aortic valve conditions. While the PCL-TEHV is promising, future studies are necessary to evaluate the multilayered leaflet under aortic valve conditions, fatigue properties, and overall remodeling potential in a bioreactor.

6.2 Introduction

Thus far in the TEHV field, numerous valve constructs have been created from decellularized tissue, molding, electrospinning, and 3D bioprinting [10, 41, 267]. Several of these conduits have been tested for feasibility in preclinical animal models [147, 268, 269]. Universally, these TEHVs lost their functionality due to leaflet retraction and valvular incompetence caused by maladaptive cellular remodeling - often observed after 8-12 week *in vivo* [39, 117, 223, 270-272]. This issue has only been recently investigated by a study conducted by Emmert et al., where computational modeling was used to better design heart valves using data on cellular remodeling due to mechanical forces, valve leaflet geometry, and hemodynamic conditioning of valves [273]. In Emmert et al.'s study, a functional and biological competent pulmonary valve conduit was placed in a relevant sheep model for over 1 year [273]. While the results from Emmert et al. study are exciting, a cell-laden aortic TEHV with long-term functionality has yet to be developed and tested in physiological flow conditions for long-term use. Thus, there is a need to develop a multilayered 3D scaffold with the microstructure of each leaflet layer for improved mechanics, and cellular integration for remodeling potential.

3D printing enables every component of the TEHV to be customized and easily adapted to a patient. CAD modeling from CT scans can be easily implemented to generate a 3D model of the patient's aorta. With those dimensions, a valve ring can be 3D printed using biodegradable materials and subsequently the leaflet can be mounted onto the valve ring. Combined, the valve ring and valve leaflets will be biodegradable and designed to facilitate biological integration with the host during its slow degradation process. In addition to designing the valve ring, we have also developed a rapid assembly method to

mount valve leaflets onto the valve ring. This method involves a single scaffold for the valve leaflet which is then fixed to the aortic valve ring using either sutures or cyanoacrylate. The use of 3D printing and our assembly method enables aortic heart valves to be manufactured as fast as six hours.

Our approach takes advantage of 3D bioprinting to replicate the collagen alignment in the fibrosa layer. The use of different biomaterials allows us to develop a functional valve that promotes controlled remodeling to minimize leaflet retraction. As observed previously by Emmerts et al. work, the design of the leaflet as well as the properties of the material are crucial for proper cellular remodeling. The scaffolds we will test strategically utilize 3D printed strands that capture the anisotropic properties at the micro-level, and as for the macro-geometry we are able to rapidly test different leaflet geometries to quickly identify an ideal environment for cellular remodeling. This detail-oriented engineering approach will create a new pathway for patient-specific valves to be developed.

For clinical translation of our TEHV, the multilayered scaffold will need to be assessed under physiological flow conditions before *in vivo* studies. This is a critical step in determining the hemodynamic profile of the TEHV as well as the capacity for it to undergo ECM remodeling. At this point, most TEHVs are tested under pulmonary flow conditions as the flow profile is similar to the aortic valve, but at a lower magnitude [133]. Under pulsatile flow conditions, TEHVs are assessed for potential clinical stenosis or regurgitation and for the level of ECM deposition. While the pulmonary flow conditions are similar, our goal is to develop an aortic valve. Thus, we will utilize a pulsatile flow loop mimicking the aortic valve position. We hypothesize that when our multilayered scaffold is assembled onto a valve ring and tested under aortic valve conditions, the TEHV

will have similar hemodynamic profile to clinically available valve protheses and have the capacity to induce ECM remodeling by the encapsulated valve cells. To test this hypothesis, we will 3D print the valve ring, assemble the multilayered leaflet to the ring, and test the valve under pulsatile aortic valve conditions.

6.3 Methods

6.3.1 *Aortic heart valve prototype*

To build a heart valve prototype, the two components necessary are the valve stent and the valve leaflet. Using SOLIDWORKS, a valve stent of 17 mm inner diameter and 19 mm outer diameter was designed referencing Thubrikar's work [274]. The valve stent was 3D printed using the Stratasys Objet30 Pro and the following two materials, the Objet RGD875 (VeroBlackPlus; Stratasys) and the FullCure 705 (Support Resin; Stratasys). A single valve leaflet composed of PCL-MAA scaffold was attached to the valve stent via cyanoacrylate (Loctite® 404) ensuring that 2 mm of excess PCL remained above the valve stent posts.

6.3.2 *Hemodynamic profile of heart valve prototype*

To determine the hemodynamics of the heart valve prototype, TEHVs were placed in a left-heart flow loop, previously detailed [275]. The simulator consists of four main components: flow, pressure, data acquisition, and flow visualization. Pressure and flow data at 1000 Hz over 100 simulated cardiac cycles with 3 technical repeats. Two cardiac outputs, 2.5 and 5 L/min, were evaluated using a water-glycerin mixture (36% glycerin), which recapitulates the kinematic viscosity of blood. Using previous methods [275, 276],

the following parameters were computed: the effective orifice area, mean and max transvalvular pressure gradient, regurgitation volume, leakage volume. The time to open and close for the valve during one cardiac cycle was also determined through a slow-motion video at 240 frames per second using an iPhone Xs. A total of 4 valves were tested under aortic valve flow and pressure conditions.

6.3.3 *Statistical Analysis*

All quantitative data were expressed as the mean ± standard deviation (SD). Statistical analysis was performed using Prism 8 (Graphpad) and all experiments were tested for normality using the Shapiro-Wilk test. For statistical analysis of hemodynamic data, a one-way ANOVA with post hoc Tukey-Kamer test was used to compare the hemodynamic measurements (mean/max TVPG, EOA, leakage volume, etc.) between the TEHVs. For all experiments, unless otherwise stated, sample size n = 4 or greater and technical replicates were used. Statistical significance was considered at a value of $p < 0.05$.

6.4 Results

6.4.1 *TEHV prototype design*

To demonstrate feasibility of using PCL as the load-bearing layer of the multilayered leaflet scaffold, a valve stent composed of three posts was first designed to have an inner diameter of 17 mm and a 19 mm outer diameter as shown in Figure 25a. In order to test in the flow loop, an additional outer ring (Figure 25b) was added to the valve stent for proper placement. The PCL leaflet was 3D printed with circumferential strand

orientation as shown in Figure 25c. Next, the leaflet was successfully wrapped around the valve stent using cyanoacrylate. The placement of the leaflet was measured to have an excess length of 2 mm above the valve post. In Figure 25 (d,e) the mounted PCL leaflet can be observed in an open and closed state. This approach enabled consistency between valve prototypes and an average of 30-40 minutes assembling time.

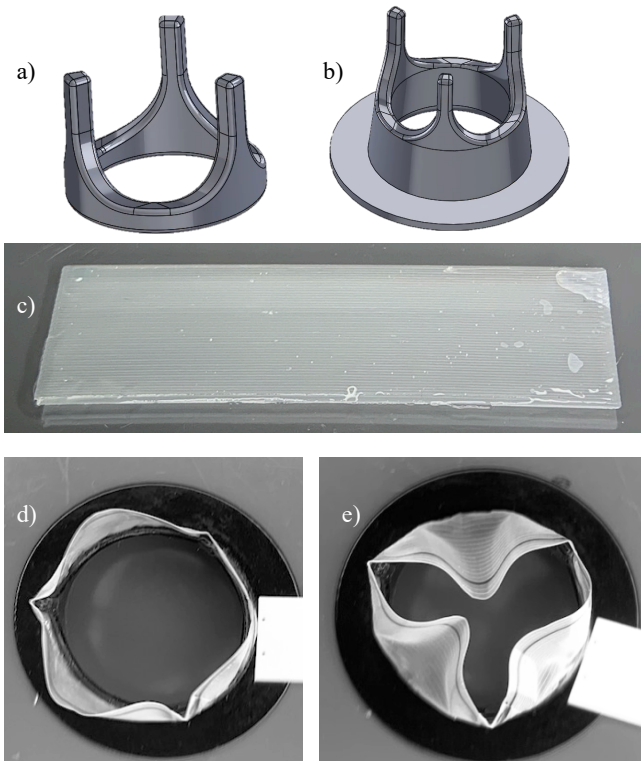

Figure 25. TEHV prototype components. A) Valve stent of 17 mm ID and 19 OD was designed using SolidWorks. B) An additional outer diameter at the bottom of the valve stent was added to enable placement and fixation to the pulsatile flow loop. C) Image of the PCL valve leaflet with circumferential strand orientation. D, E) Completely assembled TEHV, where the leaflet was fixated to the valve stent via cyanoacrylate.

6.4.2 *TEHV hemodynamic profile*

The hemodynamic profile of the TEHV was characterized using a pulsatile flow loop capable of mimicking physiological flow rates. First, the opening and closing of the valve was observed using slow-motion video. The TEHV experienced rapid valve opening at less than 0.1 seconds followed by 0.2 seconds of ejection time. Rapid valve closing occurred at 0.4 seconds. These three phases were continuously observed throughout the 100 cardiac cycles. A side-view and cross-sectional view of the valve opening, and closing can be observed in Figure 26. Valves were inspected after hemodynamic testing and no visible deformation or damage was observed. Next, the hemodynamic profile of the TEHVs was characterized through four parameters: effective orifice area (EOA), changes in volume, mean transvalvular pressure gradient (TVPG), and maximum transvalvular pressure gradient (max. TVPG). In Figure 27, the EOA at 2.5 L/min cardiac output was 1.2 cm^2, and at 5L/min the EOA was 1.4 cm^2. At 5L/min cardiac output, the TEHV was within the EOA range for the St. Jude mechanical valve and MitroFlow valve, which were 1.5 and 1.2 cm^2, respectively [277, 278]. As for the changes in volume, minimal regurgitation was detected for both cardiac outputs. The closing volume of the valve was 3.2 and 3.4 mL for the 2.5 L/min and 5L/min. Leakage volume was minimal for both cardiac volumes, with the maximum volume reaching 2.8 mL. Another metric utilized to assess the hemodynamic profile of the TEHV is the mean TVPG, which was 10.4 mm Hg at a 5L/min cardiac output, and this was even lower at 2.9 mm Hg for the 2.5L/min cardiac output. Again, the TEHV has comparable mean TVPG to the St. Jude and Mitroflow valves, which were reported to be 10.9 to 11.4 mm Hg, respectively [277, 278]. The max TVPG at 2.5L/min was 23.5 mm

Hg and at 5L/min cardiac output, the max TVPG peaked at 37 mm Hg. These values are higher than the commercially valves, which had average max TVPG of 20.2 mm Hg.

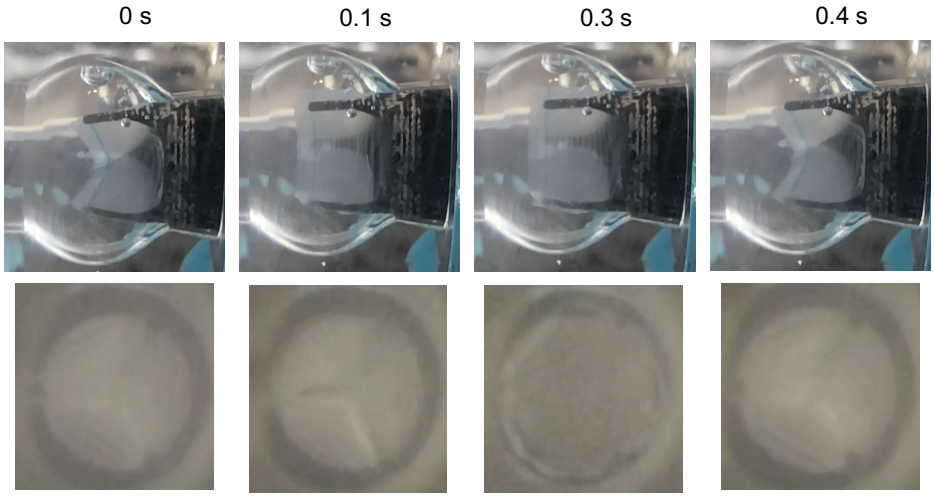

Figure 26. TEHV opening and closure during a cardiac cycle. A TEHV of 19 mm OD and 17 mm ID with a 40-um thick leaflet scaffold was tested under aortic valve condition of 70 beats per minute with 5L/min output for 100 cycles. Through the transparent polycarbonate test chamber, a slow-motion video of 240 frames per second was captured. The TEHV opened and closed at 0.4 seconds.

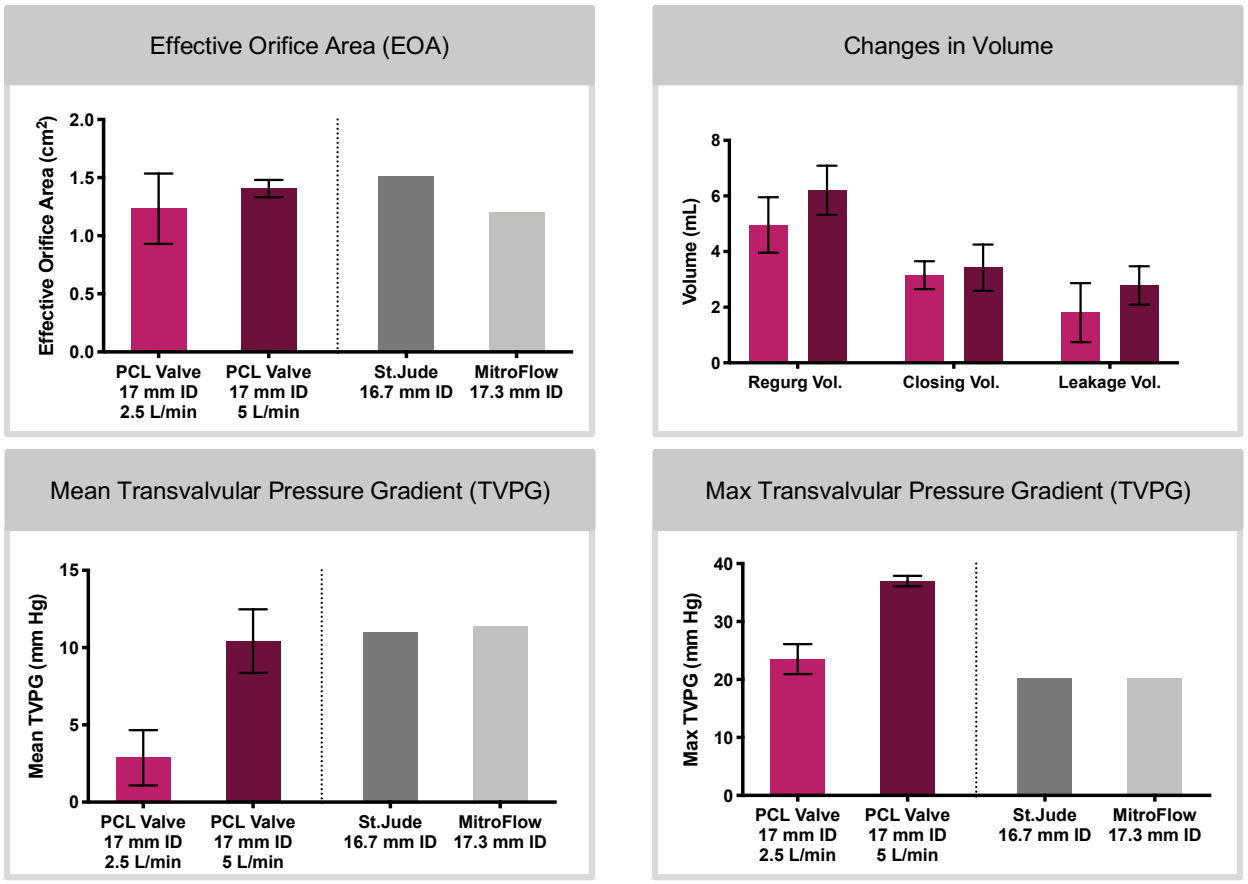

Figure 27. Evaluation of valve performance under pulsatile flow conditions. Effective orifice area of the TEHV was 1.5 cm^2 at 2.5 and 5 L/min and demonstrated comparable EOA to St. Jude Reagent valve and MitroFlow valve [279]. The mean transvalvular pressure gradient (TVPG) of the PCL valve also had comparable values to commercially available valves. At both the cardiac outputs of 2.5 and 5 L/min, there was minimal regurgitation, closing, and leakage volume. N = 4.

6.5 Discussion

While developing a multilayered leaflet capable of repairing and remodeling is important, it is just as essential to test whether this leaflet is capable of withstanding aortic valve flow and pressure conditions. In aim 3, the feasibility of using the PCL as the fibrosa layer of the manufactured heart valve leaflet described in CHAPTER 5 is evaluated under physiological aortic flow and pressure conditions.

Previous groups have developed TEHVs that function under pulmonic valve conditions [39, 147, 280]; however, to this date only one TEHV has been capable of withstanding aortic conditions, which is an off-the-shelf decellularized TEHV [270]. Thus, the objective was to evaluate whether our rational-design for the multilayered leaflet has the capacity to mechanically function under aortic physiological flow conditions. In this aim, only the PCL layer was tested under flow conditions. Future studies will include the multilayered leaflet with the cell-laden hydrogel layer. Before testing, the PCL scaffold was assembled onto a valve stent with reproducibility. The TEHVs tested under aortic valve conditions demonstrated EOAs comparable to the St. Jude mechanical valve and MitroFlow valve of similar size under 5L/min cardiac output [277, 278]. Furthermore, there were minimal changes to the regurgitation, closing, and leakage volumes suggesting the TEHVs were opening and closing properly. The mean transvalvular pressure gradient was also similar to the St. Jude mechanical valve and MitroFlow valves. The only difference was the maximum transvalvular pressure gradient, which was much higher than commercially available valves. This could be due to a number of factors such as obstruction during hemodynamic testing, the valve stent material, as well as the valve leaflet itself. The underlying reason for a max transvalvular pressure gradient will be further investigated by

conducting PIV hemodynamic studies. Interestingly, this higher max TVPG could be due to the properties of a polymer leaflet. In a previous study, a polymeric valves composed of a combination styrene block copolymers with a 21 mm inner diameter exhibited a max TVPG of 30 and 43 mm Hg when testing two different blends of the block polymers [281]. This could suggest heart valve composed of polymers have a different hemodynamic profile compared to biological or mechanical valves.

Thus, it would be valuable to have a control valve to compare to the TEHV developed in this study. Perhaps, it may not be reasonable to compare our TEHV to a mechanical valve such as the St. Jude because these valves are very different in their design and materials. Alternatively, a control could be a valve composed of the same valve stent with a pericardium leaflet, or alternatively a similar commercially available valve, which can be either a biological heart valve such as the MitroFlow valve or a polymeric heart valve such as Poli-valve [281].

While these are initial tests, the TEHV composed of just the PCL layer demonstrates promising results and future studies will involve the multilayered leaflet. Once the feasibility of the multilayered leaflet is assessed under hemodynamic conditions, the next step is to evaluate the performance of this valve long-term in a bioreactor and eventually in an *in vivo* model at the pulmonary and aortic position.

6.6 Conclusion

Most TEHVs have been developed for the pulmonary position as TEHVs capable of withstanding aortic valve conditions are required to be more durable. In this aim, the PCL component of the multilayered leaflet was assembled into a valve stent to evaluate whether

this layer of the TEHV, which is designed to be the load-bearing layer, can withstand aortic valve flow and pressure conditions. The hemodynamic studies demonstrate the TEHV has similar EOA and mean transvalvular pressure gradient to commercially available valves. While TEHV is promising, future studies are necessary to evaluate the multilayered leaflet under aortic valve conditions, fatigue properties, and overall remodeling potential in a bioreactor.

CHAPTER 7 CONCLUSION AND FUTURE DIRECTIONS

Heart valve disease is an increasing clinical burden associated with high morbidity and mortality [14-16]. Congenital heart defects contribute to the prevalence of heart valve disease and account for 1 to 2% of births [227]. Meanwhile, rheumatic fever is the main cause for heart valve disease in developing countries [8, 9]. With limited biological diagnostics or drugs to prevent heart valve disease, pediatric patients can have the following interventions: valve repair, replacement, or the Ross procedure. Most patients are treated with a mechanical or a biological valve replacement when valve repair or surgical interventions fail. While prosthetic valves can last up to 10 years, there is risk of calcification, thrombogenicity, and leaflet tearing [10]. For pediatric patients, commercially available implants are limited by size and most importantly they fail to grow. Without the regenerative capacity, children may require several surgical interventions, which introduces another level of risk for thromboembolism and operative mortality [31, 282]. An ideal heart valve for children would be available in various sizes, non-immunogenic, exhibit durable hemodynamics, and have the potential to couple with somatic growth. To address and minimize the numerous risks with current heart valves, this study aimed to develop tissue engineered heart valves (TEHVs) by combining three components, 1) autologous cells, 2) regenerative biomaterials, and 3) 3D bioprinting to generate a heart valve scaffold capable of promoting and enabling mechanical function in the aortic valve position, growth, and biological integration.

This thesis project is a first step toward replacement valve therapy for children, where technology and stem cell advancements have been applied to generating a tissue engineered

heart valve. In Aim 1, developing a suitable cell source for tissue engineering is a critical component for the success and durability of TEHVs. In this aim, we addressed this problem by differentiating iMSCs from iPSCs and then further maturing these cells into VIC-like cells by introducing them into a 3D culture designed to mimic the properties of the valve leaflets. First, a modified differentiation protocol was utilized to differentiate iPSCs into iMSCs using a feeder-free approach. Next, iMSCs were encapsulated into PEGDA hydrogels to study the effects of a 3D culture in the maturation of iMSCs into VIC-like cells. Encapsulated iMSCs demonstrated a transition from an activated VIC-like phenotype to a more quiescent state. In addition, collagen deposition was identified in cell-laden PEGDA hydrogels, corresponding to the potential use of iMSCs as a cell source for TEHVs. As such, these experiments highlight the importance of a 3D culture environment to influence cell phenotype and function as well as contribute a potential new option for seeding TEHVs. As for future studies, iMSCs would need to be studied long-term to understand their regenerative and remodeling potential, such as the production of proteoglycans, elastin, and matrix metalloproteinases. The use of PEGDA is to demonstrate, that as a simplified model, iMSCs can progress towards a VIC-like phenotype. However, further work is necessary to study these cells, long-term, as a potential cell source for heart valve tissue engineering, especially in more physiologically relevant conditions.

In Aim 2, we demonstrated a multilayered heart valve leaflet composed of 3D printed PCL and a hydrogel layer can recapitulate structural features of the native leaflets. Both materials had physiologically relevant mechanical properties, slow degradation, and maintained a healthy VIC-like phenotype. Furthermore, the multilayered leaflet under

pulsatile shear stress conditions resulted in collagen type I production suggesting the leaflet is capable of ECM production over time. While our results are promising, future studies are necessary to evaluate the long-term remodeling of multilayered leaflet through the cell-laden iMSCs. It is important to study whether there is evidence of leaflet retraction over the remodeling phase, as this has commonly been an issue with other TEHVs [254]. In addition, future studies will need to investigate the addition of VECs to the outer surfaces of the scaffold as VECs are responsible for rendering the leaflet non-thrombogenic. As mentioned before, nitric oxide (NO) production of VECs is considered to be protective and maintains VICs in a quiescent phenotype [92]. Apart from this, VECs also regulate the immune and inflammatory responses by preventing coagulation through release of tissue factor and thrombin inhibitors, and preventing platelet activation by releasing nitric oxide, prostacyclin, and exonucleotidases [283].

In Aim 3, the objective was to evaluate the feasibility of using the PCL as the fibrosa layer of the manufactured heart valve leaflet, described in CHAPTER 5 , under physiological aortic flow and pressure conditions. Most TEHVs have been developed for the pulmonary position as TEHVs capable of withstanding aortic valve conditions need to be more durable. In this aim, the PCL component of the multilayered leaflet was assembled onto a valve stent to evaluate whether this layer of the TEHV, which is designed to be the load-bearing layer, can withstand aortic valve flow and pressure conditions. The hemodynamic studies demonstrate the TEHV has similar EOA and mean transvalvular pressure gradient to commercially available valves. While these findings are promising, future studies are necessary to evaluate the multilayered leaflet, which includes the GelMA/PEGDA hydrogel layer, under aortic valve conditions. The TEHVs' fatigue

properties as well as the overall remodeling potential will also need to be evaluated using a bioreactor. The overall goal is to develop a TEHV for pre-clinical testing and to do so our TEHV must first be tested and validated under simulated aortic valve conditions using a pulsatile flow loop. Then, long-term performance will be evaluated through an *in vivo* sheep model, where valve integration and remodeling with the host will be studied along with the hemodynamic profile of the valve. Another consideration for assessing the TEHV under *in vivo* conditions is the position in which to test the TEHV. While the objective of this study was to develop a TEHV for the aortic valve, it may be worthwhile investigating the remodeling of the TEHV under pulmonic conditions, which will be an environment more conducive to ECM regeneration and remodeling given the less harsh mechanical forces. While, the aortic valve position will evaluate the durability and overall mechanical function under flow conditions.

The culmination of this work will forge new paths toward patient-specific therapies for pediatric heart valve patients. The application of stem cells, especially iPSCs, presents a new source for seeding TEHVs, enabling the field to have a scalable and more accessible cell source. While exciting, this cell source will need to be extensively characterized to ensure safety and efficacy. Nonetheless, this is an advancement important for addressing the cell source. Meanwhile, the utilization of 3D bioprinting to design more representative scaffolds, such as the circumferential orientation of the collagen fibers, allows for more complexity to be introduced into the geometry and composition of the scaffolds. 3D printing enables scaffolds to be more representative of its biological host. The approaches and strategy used in this thesis have all made a positive impact towards generating a tissue engineered heart valve for pediatric patients. The identification of 3D printing the PCL

scaffold using orientation that enables this material to function under physiological hemodynamics is believed to be the most promising results from this work. Using this material as the foundation for the valve leaflet, this presents the potential to develop a TEHV quickly by implementing other strategies such as the *in-situ* tissue engineering and also the ability to make modifications to this layer to achieve physiologically relevant mechanical properties. While the use of other approaches can have broader impact, the ultimate goal is to use a patient-specific method to ensure better outcomes for pediatric patients by eliminating the need for valve refitting surgeries through its regenerative capacity.

APPENDIX.

APPENDIX A. Additional Methods

Table 4 List of Antibodies and Stains.

Antibody	Supplier	Catalog #	Host
CD90 BUV395	BD Biosciences	563804	Mouse
CD44 v450	Tonbio	75-0441	Rat
CD45 PE	Tonbio	50-0459	Mouse
CD71 APC	Santa Cruz Biotechnology	sc9099	Rabbit
αSMA	ABCAM	ab32575	Mouse
Vimentin	Santa Cruz Biotechnology		Rabbit
Alexa Fluor® 488	Life Technologies		Anti- Rabbit
Alexa Fluor® 488	Life Technologies		Anti- Mouse

Stain	Supplier	Catalog #
DAPI	Invitrogen	D1306
Rhodamine-Phalloidin	Invitrogen	R415
Fluorescein-5-Maleimide	Sigma	38132

APPENDIX B. Aim 1 Methods and Supplemental Results

A.1 **Methods:**

i. Derivation of integration-free human iPSCs

Procedures for collection and processing of human dermal fibroblasts for derivation of iPSCs were approved by the Institutional Review Board of Emory University and Children's Healthcare of Atlanta. To generate integration-free iPSC lines, human fibroblasts were derived from a skin biopsy of a healthy child as described previously [284]. The fibroblasts maintained in growth phase at passage 4 were harvested and washed once in PBS. $5x10^5$ cells were re-suspended in Amaxa nucleofection solution V (Lonza) and Yamanaka episomal plasmids [285]: pCXLE-hOct3/4-shp53-F (Addgene number 27077), pCXLE-hSK (Addgene number 27078), and pCXLE-hUL (Addgene number 27080) were used for reprogramming. Episomal plasmids (1 μg each) were added to the cell suspension and the cells were transfected using program U-023 on a Nucleofector device II. Immediately following transfection, cells were re-suspended in fibroblast medium containing 10 μM ROCK inhibitor (Stemgent) and transferred to a 10 cm tissue culture dish coated with 0.5% gelatin, and medium was changed daily. At day 7 post transfection, 1 x 10^5 viable cells were seeded into one well of a 6-well plate containing mouse embryonic fibroblast (MEF) feeders. The next day, fibroblast medium was changed to MEF conditioned medium (MEF-CM) supplemented with 8 ng/ml bFGF. At day 21 post transfection, cells were live stained with TRA-1-60 to pick iPSC colonies. The TRA-1-60 positive colonies were picked and transferred to the feeder cells. Colonies picked were

maintained on feeders for 7 days and subsequently adapted to feeder-free cultures on Matrigel in MEF-CM [244].

ii. Hydrogel Functionalization

Hydrogel functionalization was performed by conjugating slow-degrading (GGGLGPAGGK) (LGPA) peptide (Cayman Chemical, MI) to acrylate-PEG-succinimidyl valeric acid (ACR-PEG-SVA; Laysan Bio, Inc., AL) in 50 mM sodium bicarbonate buffer solution at pH 8.5 (Sigma). LGPA peptide was incorporated into the PEG mesh network to enable MMP-sensitive degradation [253]. ACR-PEG-SVA was combined with LGPA at a 1:2.2 molar ratio (ACRY-PEG-SVA: LGPA) and reacted overnight at room temperature under constant agitation. PEG-LGPA-PEG was then dialyzed with MWCO membrane 3400 against 4 L of ultrapure water for 3 days with 4-5 water changes per day. Samples were then lyophilized into a dry powder. Conjugation was confirmed using MALDI-TOF.

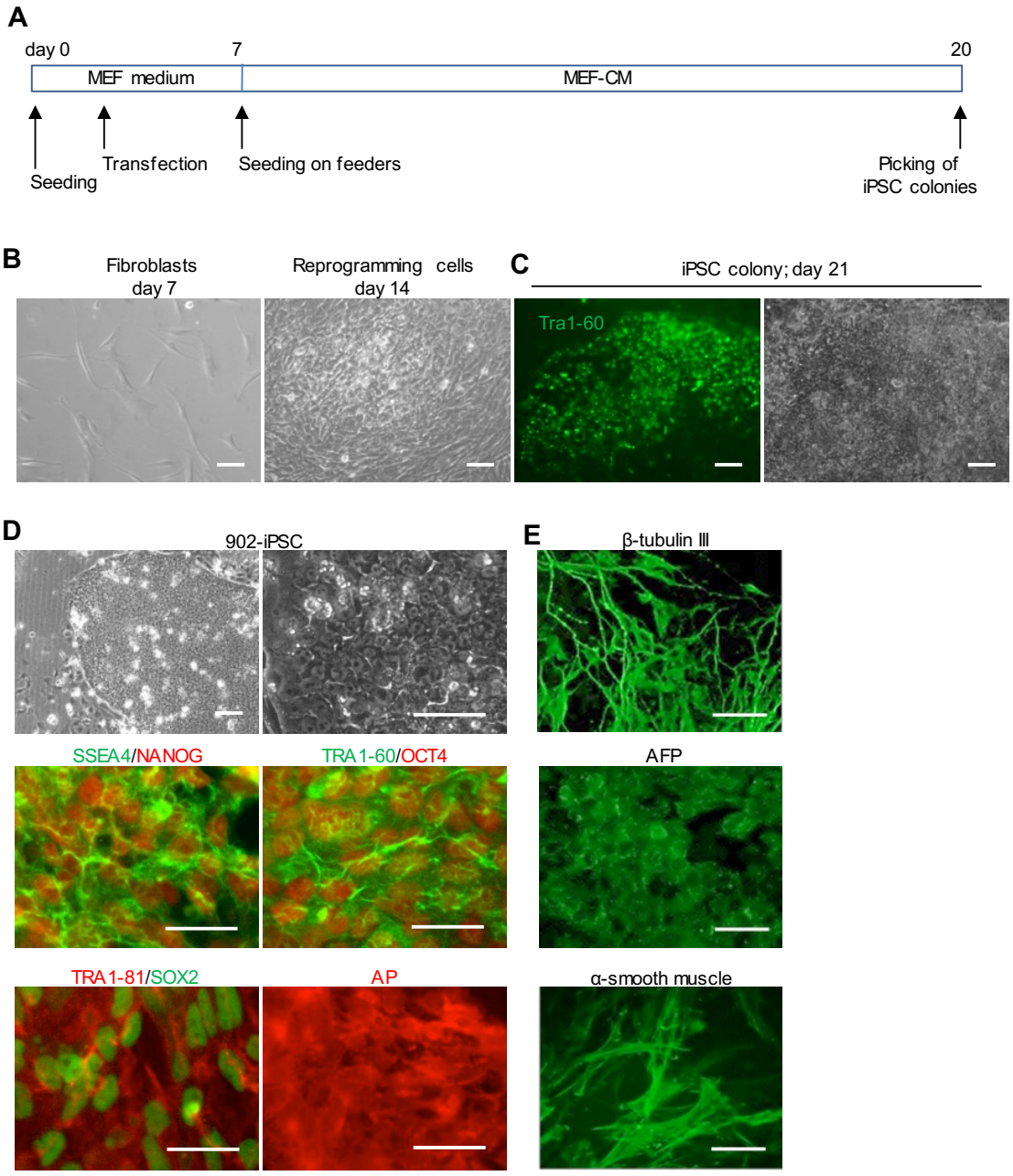

Figure 28. Derivation and characterization of human iPSCs. (A) Procedure of derivation of iPSCs. (B) Cell morphology showing fibroblast after day 7 and emergence of iPSC colony day 14 after nucleofection. (C) Live staining of stem cell marker TRA1-60 and phase-contract images of corresponding iPSC colony at day 21. (D) Characterization of iPSCs adapted to feeder-free cultures by immunocytochemical analysis of TRA1-81, TRA1-60, SSEA-4, OCT4, NANOG, and SOX2. Alkaline phosphatase (AP) was detected after the

cells were incubated with AP substrate solution. (E) Detection of β-tubulin III, α-fetal protein (AFP) and α-smooth muscle actin (SMA) in EB outgrowth. Scale bar = 100 μm.

A.2 **Results:**

iii. Derivation and characterization of human iPSCs

To generate integration-free iPSC lines, human fibroblasts were transfected with episomal plasmids expressing 6 reprogramming factors and then replated on gelatin-coated plates immediately following transfection [1]. At day 7 post transfection, morphology of cells remained fibroblast-like (Figure 28A). These cells were then maintained in a culture condition to support stem cell proliferation [1]. We observed that colonies started appearing 7 days after the cells were onto mouse embryonic fibroblast feeders (Figure 28B). At day 21 post transfection, TRA1-60-positive colonies with typical pluripotent stem cell morphology were detected following live staining (Figure 28C). Further, individual iPSCs colonies were manually picked and maintained on feeders for 7 days and subsequently adapted to feeder-free cultures. The 902-iPSC line had typical undifferentiated cell morphology and expressed surface markers of human pluripotent stem cells, SSEA-4, TRA1-60, and TRA1-81 (Figure 28D). These surface marker-positive cells were also positive for transcription factors of stem cells, NANOG, OCT4, and SOX2. In addition, these cells showed positive alkaline phosphatase (AP) activities, another indicator of pluripotent stem cells (Figure 28D). Next, we evaluated differentiation potential of the iPSC line through the formation of embryoid bodies (EB) [1]. The EB outgrowth contained cell types of all three germ layers as detected by the expression of β-tubulin III (ectoderm), α-smooth muscle actin (mesoderm), and α-fetal protein (endoderm) (Figure 28E).

iv. Conjugation of RGDS and LGPA to PEG

The NMR and MALDI-TOF data confirm the conjugation of RGDS to acrylate-PEG-SVA. In the NMR spectra, three distinct RGDS peaks are observed at 4.5, 4.0, and 3.10 ppm (Figure 29). In addition, a shift in mass can be detected once RGDS is conjugated to PEG (Figure 30). The expected mass after conjugation is 3600 Da (acrylate-PEG-SVA) plus 433 Da (RGDS) minus 115 Da (N-Hydroxysuccinimide; NHS leaving group), which results in an average mass of 3900 Da for PEG-RGDS. The mass of the conjugated PEG-RGDS was measured at 3956 Da. Although the mass of acrylate-PEG-SVA is supposed to be an average of 3400 Da, there can be batch-to-batch mass variations. The acrylate-PEG-SVA used here was detected to average at 3600 Da. Furthermore, MALDI-TOF was also used to verify conjugation of acrylate-PEG-SVA and LGPA (a slow-degrading peptide). In Figure 31, there are two peaks at 4250 Da and 8337 Da. The first peak corresponds to PEG conjugated to one LGPA peptide and the second peak is the result of PEG-LGPA-PEG conjugation.

v. iMSC phenotype comparison to VICs and HDFs after 28 days of encapsulation

The phenotype of iMSCs post-encapsulation at 28 days was compared to VICs and HDFs, maintained in same hydrogel conditions. The amount of fluorescence for each marker was quantified and normalized to get the percent area of fluorescence. Based on these results, iMSCs express similar levels of αSMA, vimentin, and periostin compared to VICs. However, collagen levels were significantly higher than both VICs and HDFs, and significantly lower in calponin expression when compared to VICs (Figure 32).

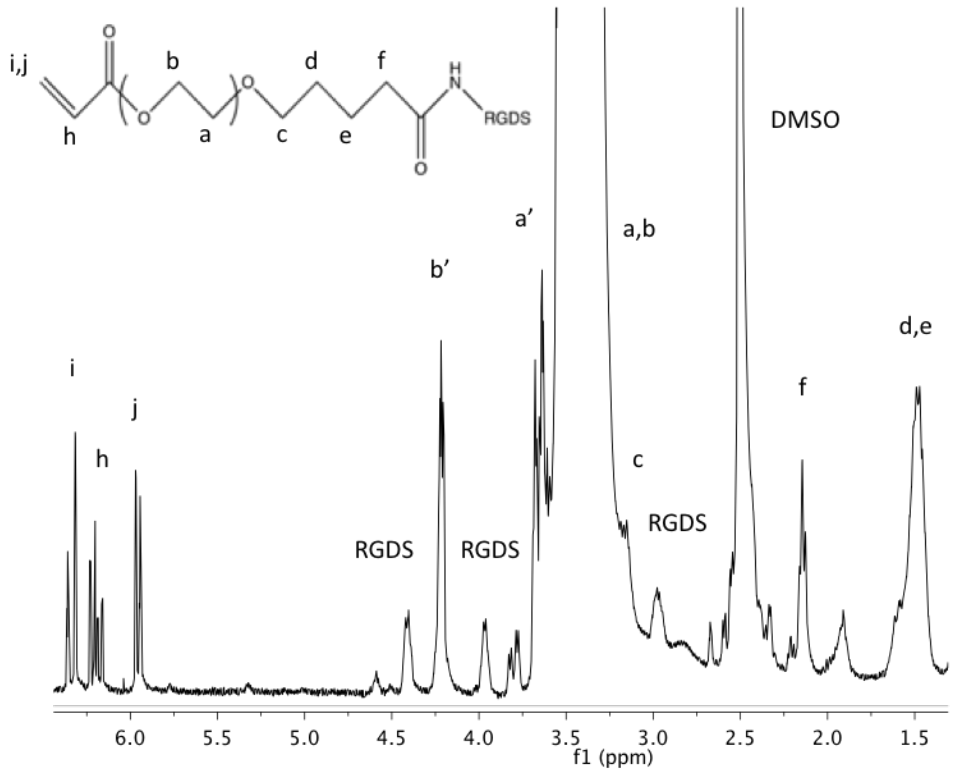

Figure 29. ^{1}H NMR spectra of acrylate-PEG-RGDS. PEG-RGDS was dissolved in DMSO for ^{1}H NMR characterization. Successful conjugation was confirmed by distinct RGDS peaks at 4.5, 4.0, and 3.10 ppm.

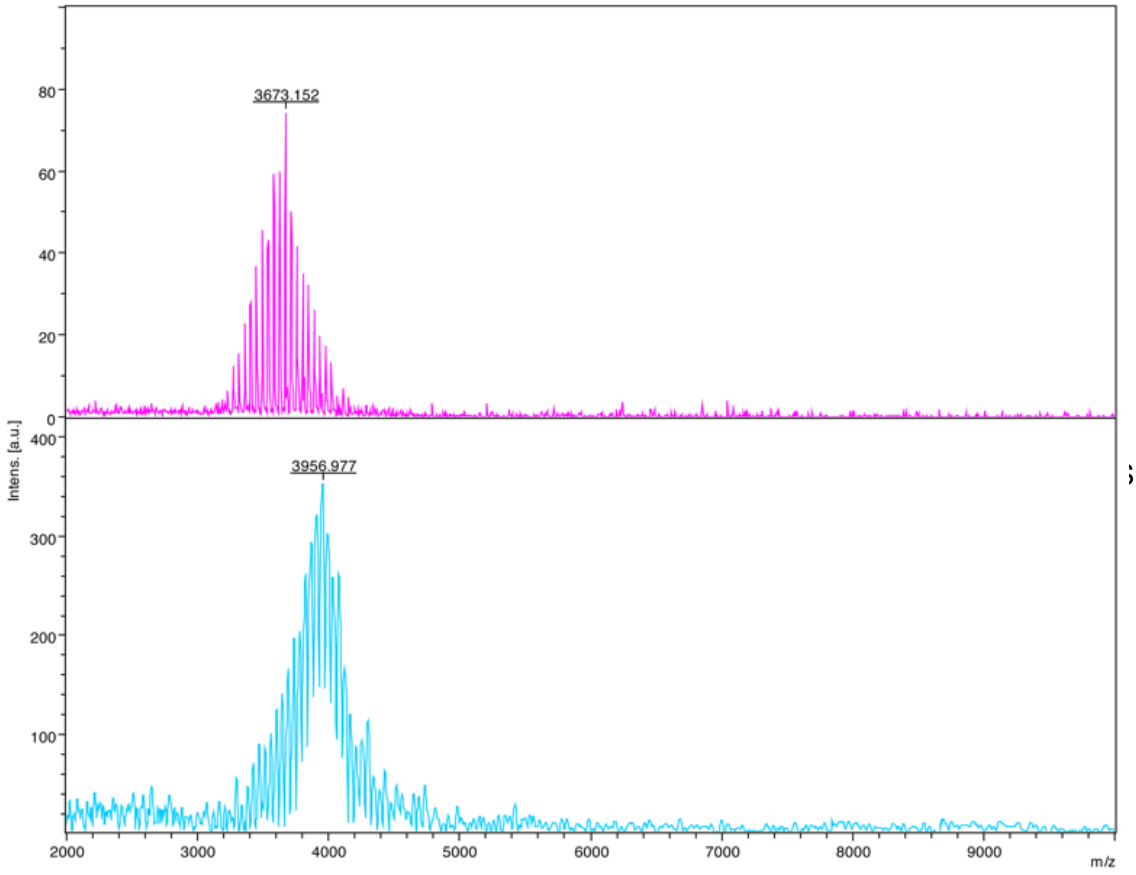

Figure 30. MALDI-TOF spectra of acrylate-PEG-RGDS. PEG-RGDS was dissolved into water and mixed at a 1:1 ratio with matrix a-cyano-4-hydroxycinnamic acid. A linear negative mode data acquisition mode was used with a mass range of 2,000 to 10,000. A shift in the spectra is detected after RGDS conjugation.

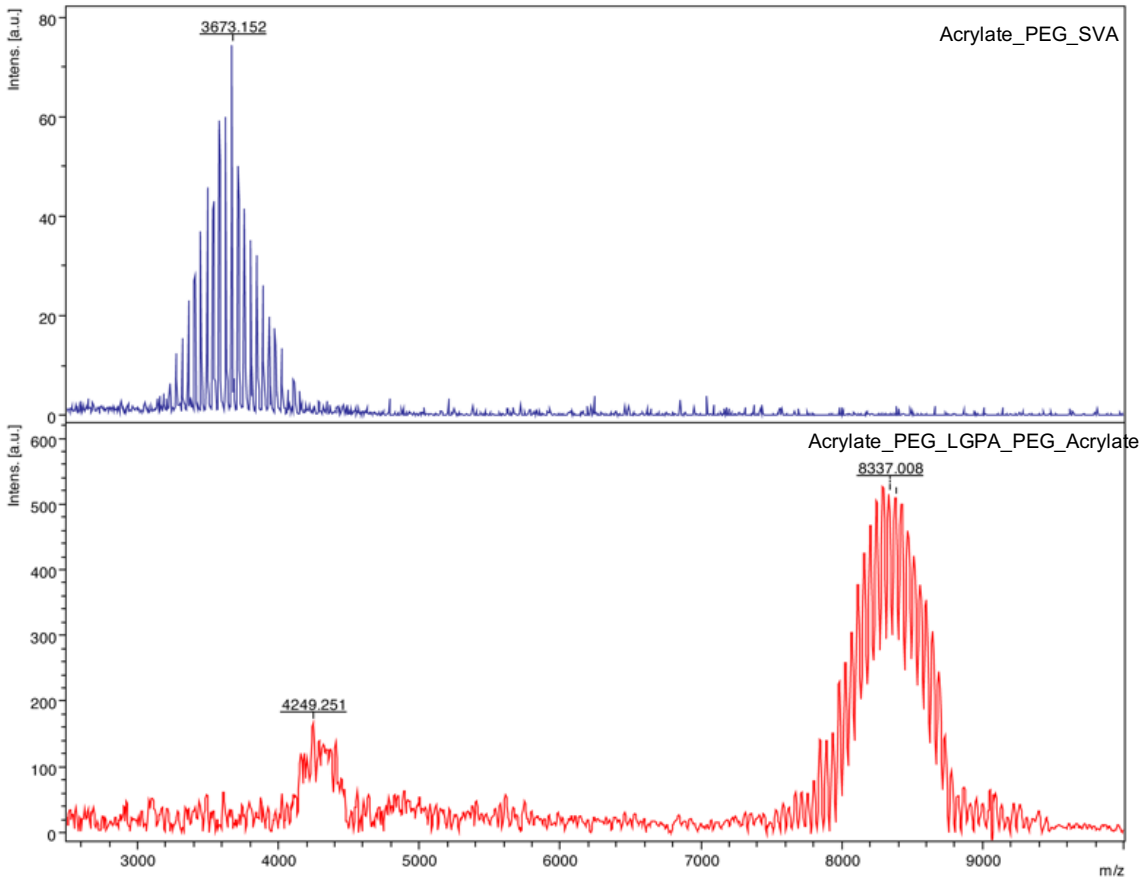

Figure 31. MALDI-TOF spectra of acrylate-PEG-LGPA-PEG-acrylate. PEG-LGPA-PEG was dissolved into water and mixed at a 1:1 ratio with matrix a-cyano-4-hydroxycinnamic acid. A linear negative mode data acquisition mode was used with a mass range of 2,000 to 10,000. There are two peaks present, one at 4200 and the other at 8300 Daltons. This corresponds to PEG-LGPA and PEG-LGPA-PEG polymer.

vi. iMSC phenotype characterization in degradable PEGDA hydrogels.

All three cell types, iMSCs, VICs, and HDFs, were encapsulated in 5% PEG-LGPA-PEG hydrogels with 5 mM RGDS. This hydrogel has a slow-degrading peptide sequence (LGPA), which is degraded by cells through MMP-secretion [253]. In Figure 33, there is a maintained level of αSMA expression in iMSC encapsulated hydrogels. While, VICs and

HDFs undergo demonstrated a decrease in αSMA expression. VICs have higher levels of vimentin expression at day 28, while no expression of vimentin was detected in hydrogels with iMSCs and HDFs. Interestingly, large cell aggregates were observed only in the iMSC group after 14 days. In Figure 34, both controls, VICs and HDFs, had observed collagen secretion after 28 days of encapsulation. However, iMSCs had minimal staining for collagen type I and, again, formed large cell aggregates. Furthermore, iMSCs maintained periostin expression throughout all time points similar to VICs and had minimal expression of calponin. Meanwhile, HDFs experienced a decrease in periostin expression as shown in Figure 35.

vii. Mechanical properties of degradable PEG hydrogels.

Compression testing demonstrated the average modulus of degradable PEG hydrogels at 1-minute white-light exposure to be 8 kPa. While, when cells were encapsulated into degradable PEG hydrogels, the modulus increased significantly to 11.8 kPa, and after 28 days of encapsulation, there was a significant decrease in the average modulus to 5.2 kPa. It is worthwhile mentioning that the modulus after 28 days of encapsulation was significantly higher than non-degrading PEGDA hydrogels (Figure 36B). Cells could potentially remodel the degradable ECM more readily compared to non-degrading PEGDA hydrogels. Thus, resulting in a higher modulus.

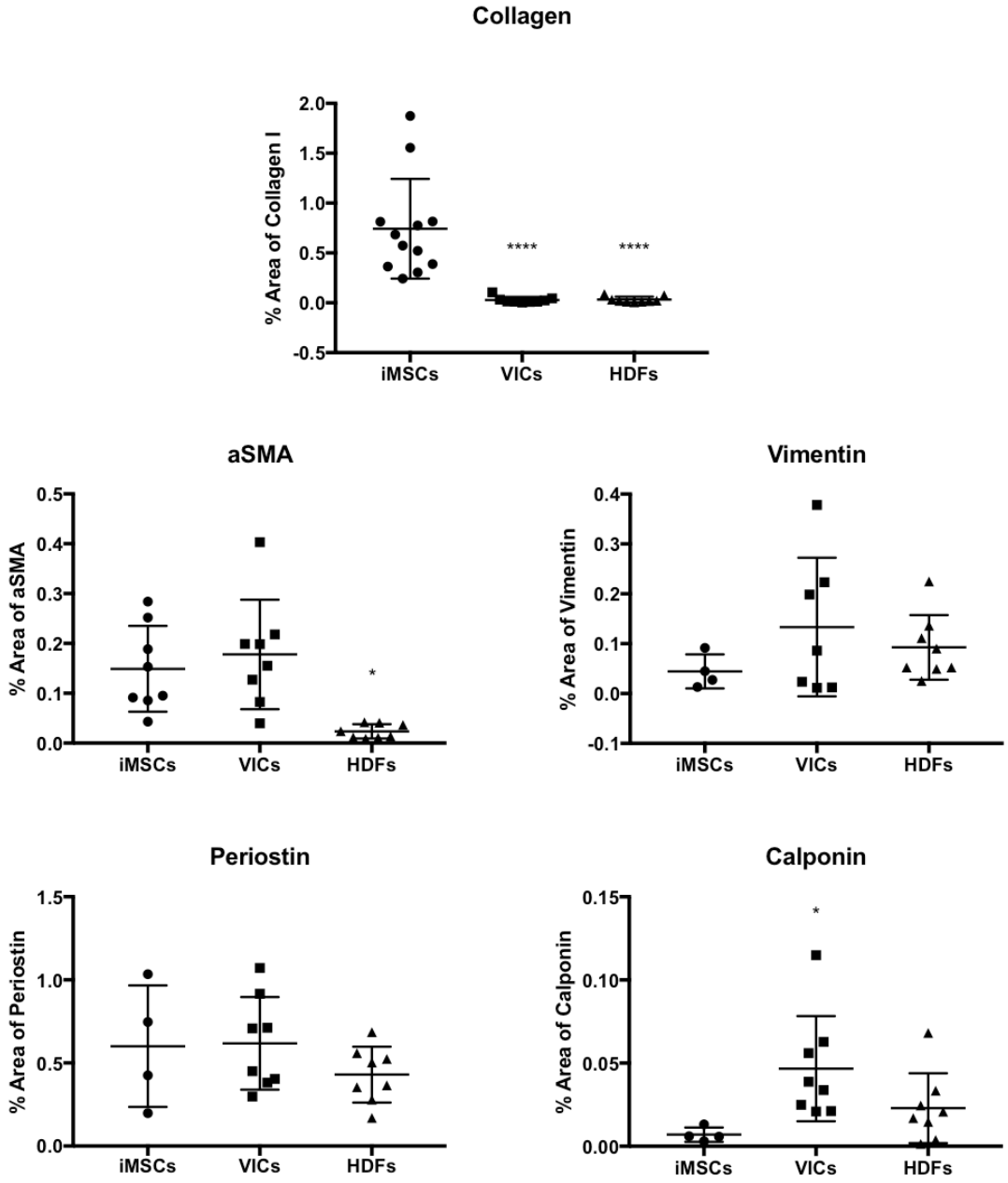

Figure 32. iMSC phenotype comparison to VICs and HDFs after 28 days of encapsulation. The amount of collagen, αSMA, vimentin, periostin, and calponin was quantified using fluorescent images. The expression of each marker was compared between cell types after 28 days of encapsulation in non-degrading PEGDA hydrogels. Significance was

determined comparing to iMSCs using One-way ANOVA with post-hoc Tukey-Kramer test. *p<0.05; ***p<0.001. N = 4-8.

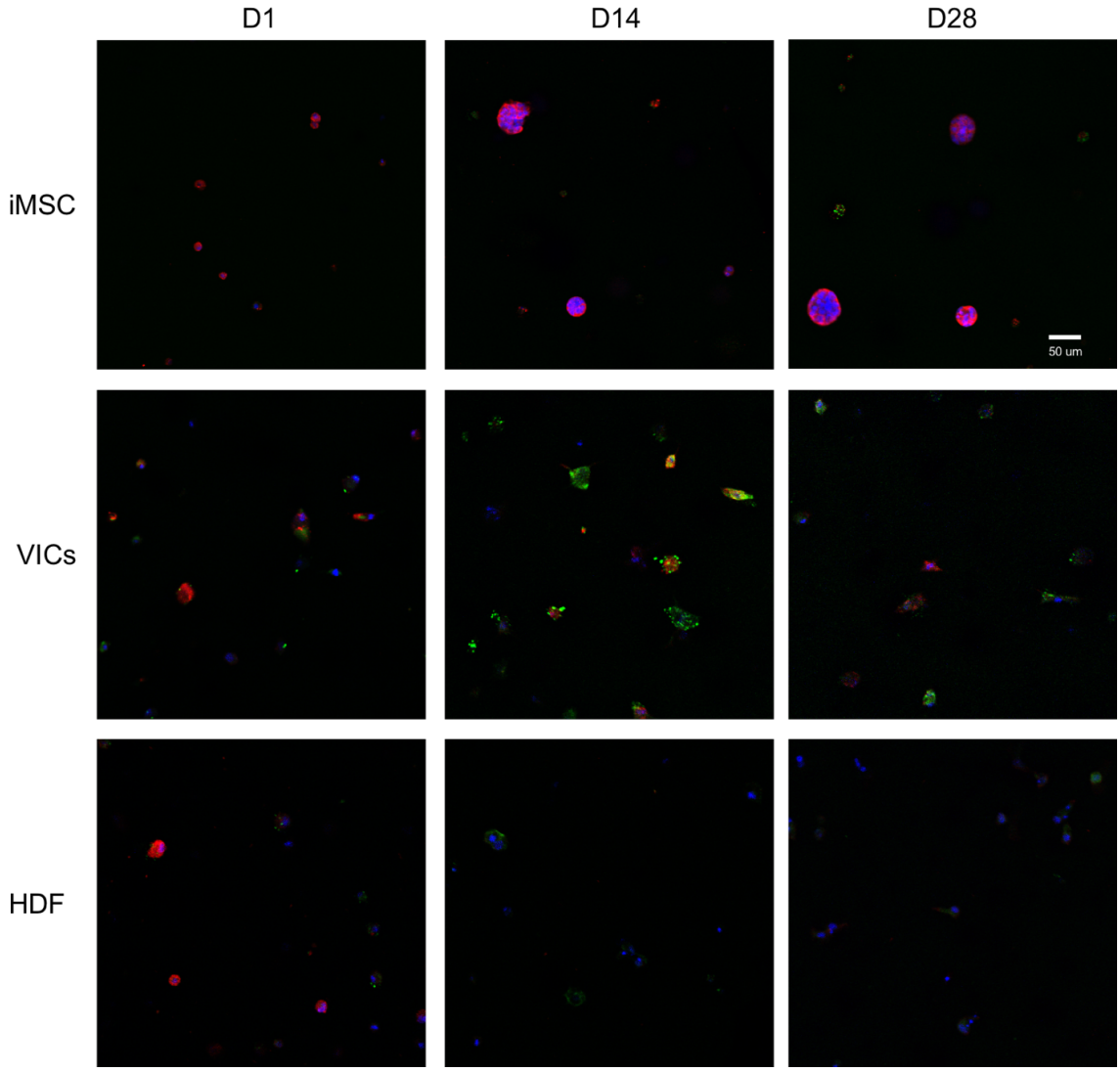

Figure 33. Alpha-smooth muscle and vimentin expression in cell-laden degradable PEGDA hydrogels. iMSCs, VICs, and HDFs were encapsulated into 5% w/v PEG-LGPA-PEG hydrogels with 5 mM RGDS for 1, 14, and 28 days. αSMA. There is a maintained level of αSMA expression can be observed with iMSCs. Meanwhile, VICs and HDFs undergo a decrease in αSMA expression. VICs have higher levels of vimentin expression

at day 28, while no expression of vimentin is observed for HDFs. DAPI=Blue; Vimentin= Green; αSMA = Red. Scale bar 50 μm. N = 3.

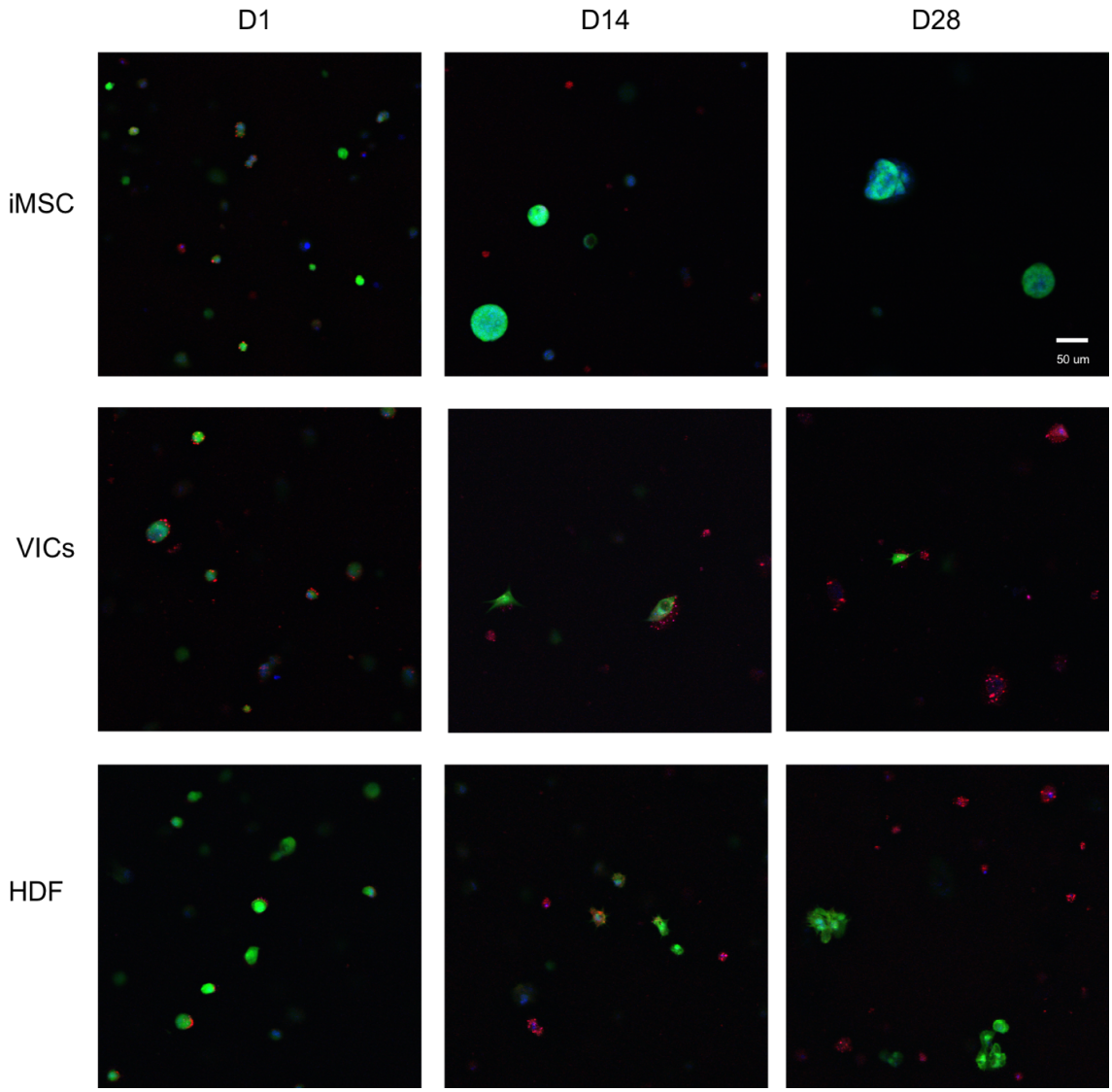

Figure 34. Collagen expression in cell-laden degradable PEGDA hydrogels. iMSCs, VICs, and HDFs were encapsulated into 5% w/v PEG-LGPA-PEG hydrogels with 5 mM RGDS for 1, 14, and 28 days. Both controls, VICs and HDFs, had observed collagen secretion

after 28 days of encapsulation. However, iMSCs had minimal staining for collagen type I. DAPI = Blue. Cell membrane = Green. Collagen type I= Red. Scale bar 50 μm. N = 3.

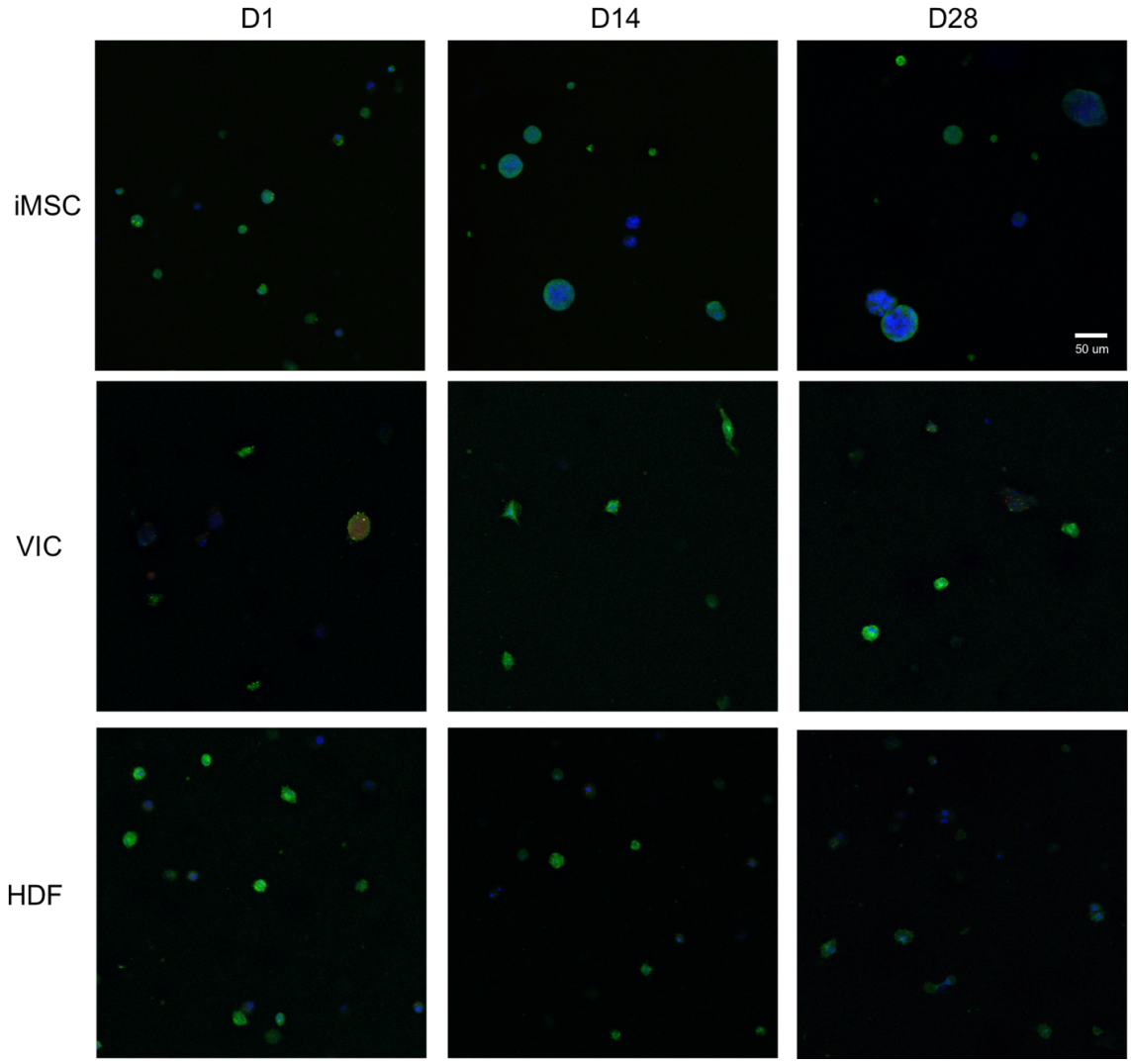

Figure 35. Periostin and calponin expression in cell-laden degradable PEGDA hydrogels. iMSCs, VICs, and HDFs were encapsulated into 5% w/v PEG-LGPA-PEG hydrogels with 5 mM RGDS for 1,14, and 28 days. iMSCs maintained periostin expression throughout all time points similar to VICs and had minimal expression of calponin. Meanwhile, HDFs

experienced a decrease in periostin expression. DAPI=Blue; Periostin= Green; Calponin = Red. Scale bar 50 μm. N = 3.

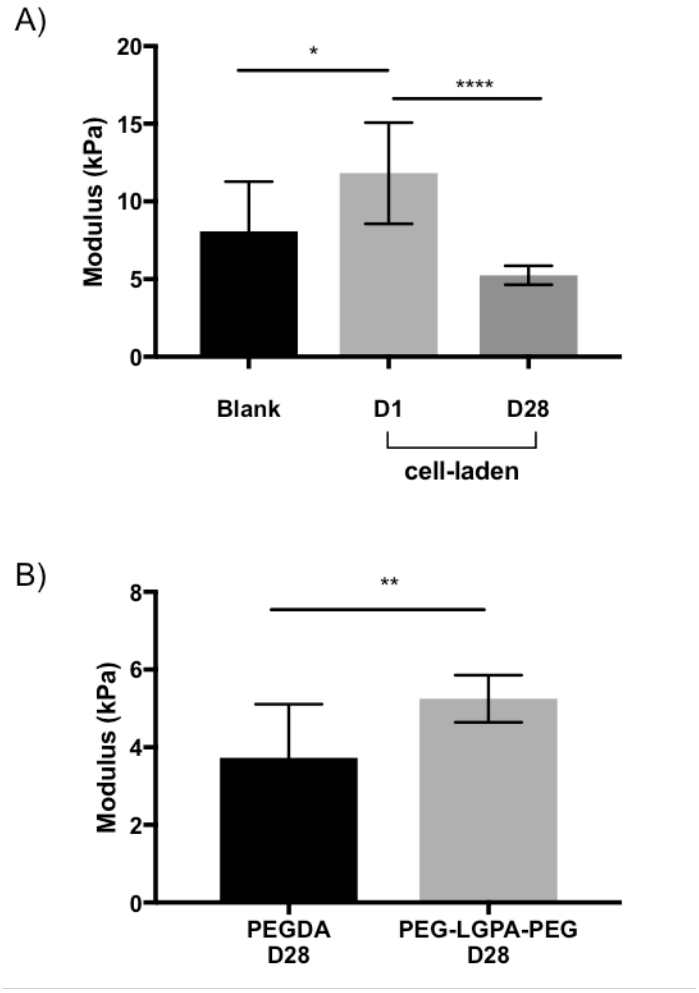

Figure 36. Mechanical properties of degradable PEG hydrogels. A) Compression testing was used to determine the bulk modulus of 5% v/w PEG-LGPA-PEG hydrogels with 5mM RGDS, crosslinked with white-light for 1-minute. The elastic modulus in PEGDA only hydrogels was an average of 8 kPa. While cell-laden PEGDA hydrogels had a modulus of 11.8 kPa, which decreased to 5.2 kPa after 28 days. B) A comparison of moduli after 28

days of encapsulation between non-degradable PEGDA and degradable PEG hydrogels. *p<0.05; ** p<0.01; ****p<0.0001 t-test; N = 8-10.

APPENDIX C. Aim 2 Methods and Supplemental Results

A.3 **Results:**

viii. Degradation of PCL scaffolds over 8 months

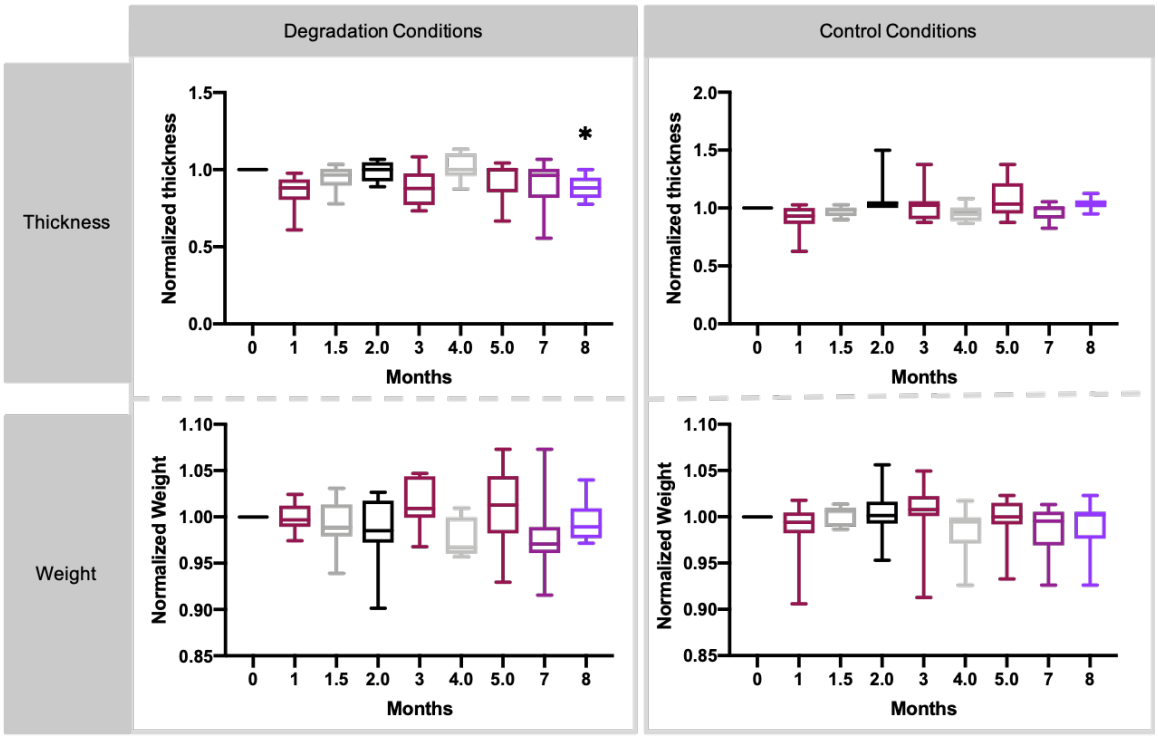

Figure 37. PCL Degradation. Scaffolds were characterized through changes in thickness and weight over an 8-month period. The thickness and weight were measured and normalized to day 0. Kruskal-Wallis test, * p < 0.05.

ix. Rheological properties of GelMA/PEGDA Bioink

The rheological properties of GelMA/PEGDa bioink was evaluated over 28 days. In Figure 38, the storage and loss modulus for blank and cell-laden hydrogel was evaluated. There was no statistical difference among the time points.

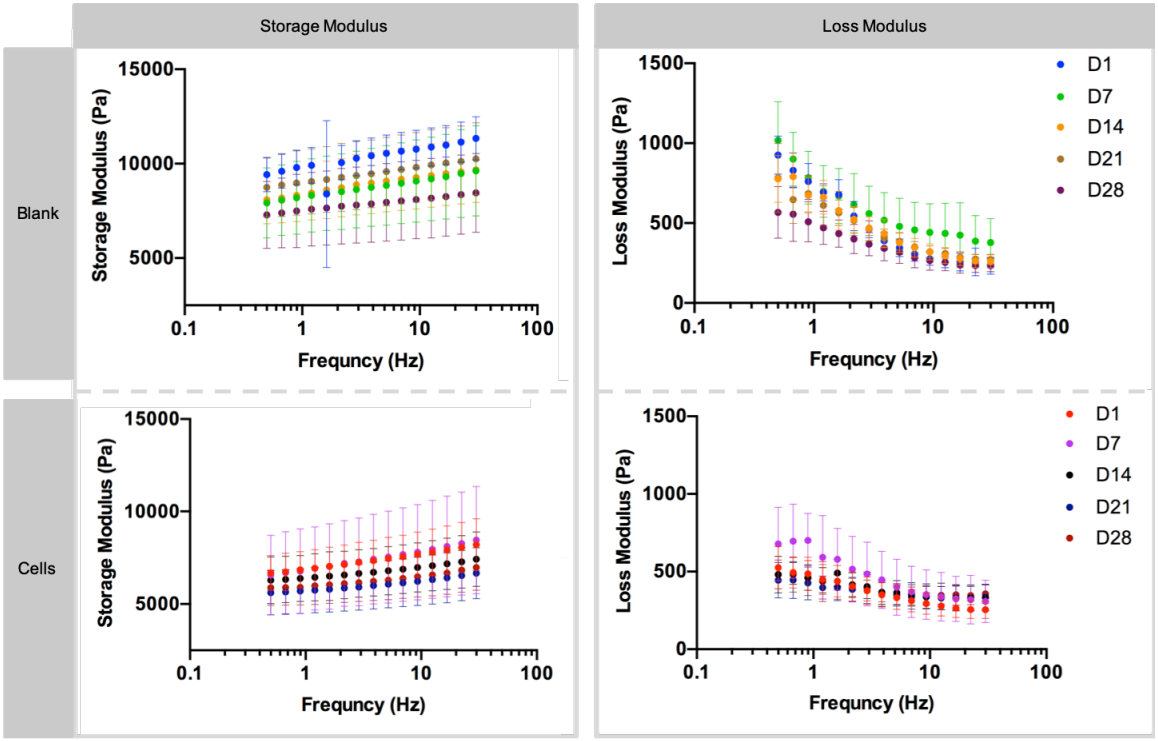

Figure 38. Rheological characterization. Frequency sweeps of storage moduli and loss moduli of blank GelMA + PEGDA hydrogels and GelMA + PEGDA hydrogels with encapsulated cells over 28 days measured by rheology. Two-way ANOVA, ** $p < 0.001$, **** $p < 0.0001$.

REFERENCES

[1] M. Back, T.C. Gasser, J.B. Michel, G. Caligiuri, Biomechanical factors in the biology of aortic wall and aortic valve diseases, Cardiovascular research 99(2) (2013) 232-41.

[2] V.L. Gott, D.E. Alejo, D.E. Cameron, Mechanical heart valves: 50 years of evolution, The Annals of thoracic surgery 76(6) (2003) S2230-9.

[3] J. Wohrle, B. Gonska, C. Rodewald, J. Seeger, D. Scharnbeck, W. Rottbauer, Transfemoral Aortic Valve Implantation with the New Edwards Sapien 3 Valve for Treatment of Severe Aortic Stenosis-Impact of Valve Size in a Single Center Experience, PloS one 11(3) (2016) e0151247.

[4] R. Henaine, F. Roubertie, M. Vergnat, J. Ninet, Valve replacement in children: a challenge for a whole life, Arch Cardiovasc Dis 105(10) (2012) 517-28.

[5] C. Detter, T. Fischlein, C. Feldmeier, G. Nollert, B. Reichart, Aortic valvotomy for congenital valvular aortic stenosis: a 37-year experience, The Annals of thoracic surgery 71(5) (2001) 1564-71.

[6] M. Samanek, Congenital heart malformations: prevalence, severity, survival, and quality of life, Cardiology in the young 10(3) (2000) 179-85.

[7] J.J. Takkenberg, N.M. Rajamannan, R. Rosenhek, A.S. Kumar, J.R. Carapetis, M.H. Yacoub, D. Society for Heart Valve, The need for a global perspective on heart valve disease epidemiology. The SHVD working group on epidemiology of heart valve disease founding statement, The Journal of heart valve disease 17(1) (2008) 135-9.

[8] E. Marijon, M. Mirabel, D.S. Celermajer, X. Jouven, Rheumatic heart disease, Lancet 379(9819) (2012) 953-64.

[9] M. Writing Group, D. Mozaffarian, E.J. Benjamin, A.S. Go, D.K. Arnett, M.J. Blaha, M. Cushman, S.R. Das, S. de Ferranti, J.P. Despres, H.J. Fullerton, V.J. Howard, M.D. Huffman, C.R. Isasi, M.C. Jimenez, S.E. Judd, B.M. Kissela, J.H. Lichtman, L.D. Lisabeth, S. Liu, R.H. Mackey, D.J. Magid, D.K. McGuire, E.R. Mohler, 3rd, C.S. Moy, P. Muntner, M.E. Mussolino, K. Nasir, R.W. Neumar, G. Nichol, L. Palaniappan, D.K. Pandey, M.J. Reeves, C.J. Rodriguez, W. Rosamond, P.D. Sorlie, J. Stein, A. Towfighi, T.N. Turan, S.S. Virani, D. Woo, R.W. Yeh, M.B. Turner, C. American Heart Association Statistics, S. Stroke Statistics, Executive Summary: Heart Disease and Stroke Statistics--2016 Update: A Report From the American Heart Association, Circulation 133(4) (2016) 447-54.

[10] M.S. Sacks, F.J. Schoen, J.E. Mayer, Bioengineering challenges for heart valve tissue engineering, Annual review of biomedical engineering 11 (2009) 289-313.

[11] A.L.Y. Nachlas, S. Li, R. Jha, M. Singh, C. Xu, M.E. Davis, Human iPSC-derived mesenchymal stem cells encapsulated in PEGDA hydrogels mature into valve interstitial-like cells, Acta biomaterialia 71 (2018) 235-246.

[12] A.L.Y. Nachlas, S. Li, M.E. Davis, Developing a Clinically Relevant Tissue Engineered Heart Valve-A Review of Current Approaches, Advanced healthcare materials 6(24) (2017).

[13] V.L. Roger, A.S. Go, D.M. Lloyd-Jones, E.J. Benjamin, J.D. Berry, W.B. Borden, D.M. Bravata, S. Dai, E.S. Ford, C.S. Fox, H.J. Fullerton, C. Gillespie, S.M. Hailpern, J.A. Heit, V.J. Howard, B.M. Kissela, S.J. Kittner, D.T. Lackland, J.H. Lichtman, L.D. Lisabeth, D.M. Makuc, G.M. Marcus, A. Marelli, D.B. Matchar, C.S. Moy, D. Mozaffarian, M.E. Mussolino, G. Nichol, N.P. Paynter, E.Z. Soliman, P.D. Sorlie, N. Sotoodehnia, T.N. Turan, S.S. Virani, N.D. Wong, D. Woo, M.B. Turner, C. American Heart Association Statistics, S. Stroke Statistics, Executive summary: heart disease and stroke statistics--2012 update: a report from the American Heart Association, Circulation 125(1) (2012) 188-97.

[14] S. Jana, A. Lerman, Bioprinting a cardiac valve, Biotechnol Adv 33(8) (2015) 1503-21.

[15] M. Writing Group, D. Mozaffarian, E.J. Benjamin, A.S. Go, D.K. Arnett, M.J. Blaha, M. Cushman, S.R. Das, S. de Ferranti, J.P. Despres, H.J. Fullerton, V.J. Howard, M.D. Huffman, C.R. Isasi, M.C. Jimenez, S.E. Judd, B.M. Kissela, J.H. Lichtman, L.D. Lisabeth, S. Liu, R.H. Mackey, D.J. Magid, D.K. McGuire, E.R. Mohler, 3rd, C.S. Moy, P. Muntner, M.E. Mussolino, K. Nasir, R.W. Neumar, G. Nichol, L. Palaniappan, D.K. Pandey, M.J. Reeves, C.J. Rodriguez, W. Rosamond, P.D. Sorlie, J. Stein, A. Towfighi, T.N. Turan, S.S. Virani, D. Woo, R.W. Yeh, M.B. Turner, C. American Heart Association Statistics, S. Stroke Statistics, Heart Disease and Stroke Statistics-2016 Update: A Report From the American Heart Association, Circulation 133(4) (2016) e38-360.

[16] E.J. Benjamin, M.J. Blaha, S.E. Chiuve, M. Cushman, S.R. Das, R. Deo, S.D. de Ferranti, J. Floyd, M. Fornage, C. Gillespie, C.R. Isasi, M.C. Jimenez, L.C. Jordan, S.E. Judd, D. Lackland, J.H. Lichtman, L. Lisabeth, S. Liu, C.T. Longenecker, R.H. Mackey, K. Matsushita, D. Mozaffarian, M.E. Mussolino, K. Nasir, R.W. Neumar, L. Palaniappan, D.K. Pandey, R.R. Thiagarajan, M.J. Reeves, M. Ritchey, C.J. Rodriguez, G.A. Roth, W.D. Rosamond, C. Sasson, A. Towfighi, C.W. Tsao, M.B. Turner, S.S. Virani, J.H. Voeks, J.Z. Willey, J.T. Wilkins, J.H. Wu, H.M. Alger, S.S. Wong, P. Muntner, C. American Heart Association Statistics, S. Stroke Statistics, Heart Disease and Stroke Statistics-2017 Update: A Report From the American Heart Association, Circulation 135(10) (2017) e146-e603.

[17] J.I. Hoffman, S. Kaplan, The incidence of congenital heart disease, Journal of the American College of Cardiology 39(12) (2002) 1890-900.

[18] B. Iung, A. Vahanian, Epidemiology of valvular heart disease in the adult, Nature reviews. Cardiology 8(3) (2011) 162-72.

[19] A.H. Chester, I. El-Hamamsy, J.T. Butcher, N. Latif, S. Bertazzo, M.H. Yacoub, The living aortic valve: From molecules to function, Global cardiology science & practice 2014(1) (2014) 52-77.

[20] A. Vahanian, O. Alfieri, F. Andreotti, M.J. Antunes, G. Baron-Esquivias, H. Baumgartner, M.A. Borger, T.P. Carrel, M. De Bonis, A. Evangelista, V. Falk, B. Iung, P. Lancellotti, L. Pierard, S. Price, H.J. Schafers, G. Schuler, J. Stepinska, K. Swedberg, J. Takkenberg, U.O. Von Oppell, S. Windecker, J.L. Zamorano, M. Zembala, C. Joint Task Force on the Management of Valvular Heart Disease of the European Society of, S. the European Association for Cardio-Thoracic, [Guidelines on the management of valvular heart disease (version 2012). The Joint Task Force on the Management of Valvular Heart Disease of the European Society of Cardiology (ESC) and the European Association for Cardio-Thoracic Surgery (EACTS)], G Ital Cardiol (Rome) 14(3) (2013) 167-214.

[21] T. Karamlou, K. Jang, W.G. Williams, C.A. Caldarone, G. Van Arsdell, J.G. Coles, B.W. McCrindle, Outcomes and associated risk factors for aortic valve replacement in 160 children: a competing-risks analysis, Circulation 112(22) (2005) 3462-9.

[22] E.L. Chaikof, The Development of Prosthetic Heart Valves—Lessons in Form and Function, N Engl J Med 357(14) (2007) 1368-1371.

[23] S.H. Rahimtoola, Choice of prosthetic heart valve in adults an update, Journal of the American College of Cardiology 55(22) (2010) 2413-26.

[24] H. Oxenham, P. Bloomfield, D.J. Wheatley, R.J. Lee, J. Cunningham, R.J. Prescott, H.C. Miller, Twenty year comparison of a Bjork-Shiley mechanical heart valve with porcine bioprostheses, Heart 89(7) (2003) 715-721.

[25] K. Hammermeister, G.K. Sethi, W.G. Henderson, F.L. Grover, C. Oprian, S.H. Rahimtoola, Outcomes 15 years after valve replacement with a mechanical versus a bioprosthetic valve: Final report of the Veterans Affairs randomized trial, Journal of the American College of Cardiology 36(4) (2000) 1152-1158.

[26] S.J. Head, M. Celik, A.P. Kappetein, Mechanical versus bioprosthetic aortic valve replacement, Eur Heart J (2017).

[27] K.E. Hammermeister, G.K. Sethi, W.G. Henderson, C. Oprian, T. Kim, S. Rahimtoola, A comparison of outcomes in men 11 years after heart-valve replacement with a mechanical valve or bioprosthesis. Veterans Affairs Cooperative Study on Valvular Heart Disease, N Engl J Med 328(18) (1993) 1289-96.

[28] D. Kiss, S. Anwaruddin, Recent clinical trials in valvular heart disease, Curr Opin Cardiol 32(4) (2017) 343-347.

[29] P. Bloomfield, Choice of heart valve prosthesis, Heart 87(6) (2002) 583-89.

[30] J. Chambers, Prosthetic heart valves, Int J Clin Pract 68(10) (2014) 1227-1230.

[31] B. Alsoufi, Aortic valve replacement in children: Options and outcomes, J Saudi Heart Assoc 26(1) (2014) 33-41.

[32] G. Hoffmann, G. Lutter, J. Cremer, Durability of bioprosthetic cardiac valves, Dtsch Arztebl Int 105(8) (2008) 143-8.

[33] X. Zhang, B. Xu, D.S. Puperi, A.L. Yonezawa, Y. Wu, H. Tseng, M.L. Cuchiara, J.L. West, K.J. Grande-Allen, Integrating valve-inspired design features into poly(ethylene glycol) hydrogel scaffolds for heart valve tissue engineering, Acta biomaterialia 14 (2015) 11-21.

[34] G. American College of Cardiology/American Heart Association Task Force on Practice, A. Society of Cardiovascular, A. Society for Cardiovascular, Interventions, S. Society of Thoracic, R.O. Bonow, B.A. Carabello, C. Kanu, A.C. de Leon, Jr., D.P. Faxon, M.D. Freed, W.H. Gaasch, B.W. Lytle, R.A. Nishimura, P.T. O'Gara, R.A. O'Rourke, C.M. Otto, P.M. Shah, J.S. Shanewise, S.C. Smith, Jr., A.K. Jacobs, C.D. Adams, J.L. Anderson, E.M. Antman, D.P. Faxon, V. Fuster, J.L. Halperin, L.F. Hiratzka, S.A. Hunt, B.W. Lytle, R. Nishimura, R.L. Page, B. Riegel, ACC/AHA 2006 guidelines for the management of patients with valvular heart disease: a report of the American College of Cardiology/American Heart Association Task Force on Practice Guidelines (writing committee to revise the 1998 Guidelines for the Management of Patients With Valvular Heart Disease): developed in collaboration with the Society of Cardiovascular Anesthesiologists: endorsed by the Society for Cardiovascular Angiography and Interventions and the Society of Thoracic Surgeons, Circulation 114(5) (2006) e84-231.

[35] P. Kiefer, F. Gruenwald, J. Kempfert, H. Aupperle, J. Seeburger, F.W. Mohr, T. Walther, Crimping May Affect the Durability of Transcatheter Valves: An Experimental Analysis, Annals of Thoracic Surgery 92(1) (2011) 155-160.

[36] M.W. Chu, M.A. Borger, F.W. Mohr, T. Walther, Transcatheter heart-valve replacement: update, CMAJ 182(8) (2010) 791-5.

[37] B.R. Lindman, K.P. Alexander, P.T. O'Gara, J. Afilalo, Futility, benefit, and transcatheter aortic valve replacement, JACC Cardiovasc Interv 7(7) (2014) 707-16.

[38] C. Petit, Pediatric Transcatheter Valve Replacement, Circulation 131(22) (2015) 1943-1945.

[39] A. Driessen-Mol, M.Y. Emmert, P.E. Dijkman, L. Frese, B. Sanders, B. Weber, N. Cesarovic, M. Sidler, J. Leenders, R. Jenni, J. Grunenfelder, V. Falk, F.P. Baaijens, S.P. Hoerstrup, Transcatheter implantation of homologous "off-the-shelf" tissue-engineered heart valves with self-repair capacity: long-term functionality and rapid in vivo remodeling in sheep, Journal of the American College of Cardiology 63(13) (2014) 1320-9.

[40] M. Simonato, J. Webb, R. Kornowski, A. Vahanian, C. Frerker, H. Nissen, S. Bleiziffer, A. Duncan, J. Rodes-Cabau, G.F. Attizzani, E. Horlick, A. Latib, R. Bekeredjian, M. Barbanti, T. Lefevre, A. Cerillo, J.M. Hernandez, G. Bruschi, K. Spargias, A. Iadanza, S. Brecker, J.H. Palma, A. Finkelstein, M. Abdel-Wahab, P. Lemos, A.S.

Petronio, D. Champagnac, J.M. Sinning, S. Salizzoni, M. Napodano, C. Fiorina, A. Marzocchi, M. Leon, D. Dvir, Transcatheter Replacement of Failed Bioprosthetic Valves: Large Multicenter Assessment of the Effect of Implantation Depth on Hemodynamics After Aortic Valve-in-Valve, Circ Cardiovasc Interv 9(6) (2016).

[41] D.Y. Cheung, B. Duan, J.T. Butcher, Current progress in tissue engineering of heart valves: multiscale problems, multiscale solutions, Expert Opin Biol Ther 15(8) (2015) 1155-72.

[42] S. Arjunon, S. Rathan, H. Jo, A.P. Yoganathan, Aortic valve: mechanical environment and mechanobiology, Annals of biomedical engineering 41(7) (2013) 1331-46.

[43] I. Vesely, Heart valve tissue engineering, Circulation research 97(8) (2005) 743-55.

[44] S. Jana, R.T. Tranquillo, A. Lerman, Cells for tissue engineering of cardiac valves, Journal of tissue engineering and regenerative medicine 10(10) (2016) 804-824.

[45] A.H. Chester, J.D. Kershaw, P. Sarathchandra, M.H. Yacoub, Localisation and function of nerves in the aortic root, Journal of molecular and cellular cardiology 44(6) (2008) 1045-52.

[46] L.M. Eisenberg, R.R. Markwald, Molecular Regulation of Atrioventricular Valvuloseptal Morphogenesis, Circulation research 77(1) (1995) 1-6.

[47] M. Puceat, Embryological origin of the endocardium and derived valve progenitor cells: from developmental biology to stem cell-based valve repair, Biochim Biophys Acta 1833(4) (2013) 917-22.

[48] A.C. Liu, V.R. Joag, A.I. Gotlieb, The emerging role of valve interstitial cell phenotypes in regulating heart valve pathobiology, The American journal of pathology 171(5) (2007) 1407-18.

[49] T.C. Flanagan, A. Pandit, Living artificial heart valve alternatives: a review, Eur Cell Mater 6 (2003) 28-45; discussion 45.

[50] S.W. Rabkin, P. Lodhia, M.W. Luong, P38 MAP Kinase in Valve Interstitial Cells is Activated by Angiotensin II or Nitric Oxide/Peroxynitrite, but Reduced by Toll-Like Receptor-2 Stimulation, Journal of Heart Valve Disease 18(6) (2009) 653-661.

[51] S. Smith, P.M. Taylor, A.H. Chester, S.P. Allen, S.A. Dreger, M. Eastwood, M.H. Yacoub, Force generation of different human cardiac valve interstitial cells: relevance to individual valve function and tissue engineering, The Journal of heart valve disease 16(4) (2007) 440-6.

[52] Y.T. Konttinen, P. Nykanen, D. Nordstrom, H. Saari, J. Sandelin, S. Santavirta, T. Kouri, DNA synthesis in prolyl 4-hydroxylase positive fibroblasts in situ in synovial tissue. An autoradiography-immunoperoxidase double labeling study, J Rheumatol 16(3) (1989) 339-45.

[53] R.H. Messier, B.L. Bass, H.M. Aly, J.L. Jones, P.W. Domkowski, R.B. Wallace, R.A. Hopkins, Dual Structural and Functional Phenotypes of the Porcine Aortic-Valve Interstitial Population - Characteristics of the Leaflet Myofibroblast, J Surg Res 57(1) (1994) 1-21.

[54] A. Roy, N.J. Brand, M.H. Yacoub, Molecular characterization of interstitial cells isolated from human heart valves, Journal of Heart Valve Disease 9(3) (2000) 459-464.

[55] V. Garcia-Martinez, J.M. Hurle, Cell shape and cytoskeletal organization of the endothelial cells of the semilunar heart valves in the developing chick, Anat Embryol (Berl) 174(1) (1986) 83-9.

[56] D.L. Mulholland, A.I. Gotlieb, Cell biology of valvular interstitial cells, Can J Cardiol 12(3) (1996) 231-236.

[57] F. Lupu, M. Simionescu, Organization of the intercellular junctions in the endothelium of cardiac valves, J Submicrosc Cytol 17(2) (1985) 119-32.

[58] D.A. Filip, A. Radu, M. Simionescu, Interstitial cells of the heart valves possess characteristics similar to smooth muscle cells, Circulation research 59(3) (1986) 310-20.

[59] J.T. Butcher, R.M. Nerem, Valvular endothelial cells and the mechanoregulation of valvular pathology, Philosophical transactions of the Royal Society of London. Series B, Biological sciences 362(1484) (2007) 1445-57.

[60] P. Batten, A.M. McCormack, M.L. Rose, M.H. Yacoub, Valve interstitial cells induce donor-specific T-cell anergy, J Thorac Cardiov Sur 122(1) (2001) 129-135.

[61] B.E. Sumpio, J.T. Riley, A. Dardik, Cells in focus: endothelial cell, The international journal of biochemistry & cell biology 34(12) (2002) 1508-12.

[62] A.M. Segura, R.E. Luna, K. Horiba, W.G. Stetler-Stevenson, H.A. McAllister, J.T. Willerson, V.J. Ferrans, Immunohistochemistry of matrix metalloproteinases and their inhibitors in thoracic aortic aneurysms and aortic valves of patients with Marfan's syndrome, Circulation 98(19) (1998) Ii331-Ii337.

[63] E. Rabkin, M. Aikawa, J.R. Stone, Y. Fukumoto, P. Libby, F.J. Schoen, Activated interstitial myofibroblasts express catabolic enzymes and mediate matrix remodeling in myxomatous heart valves, Circulation 104(21) (2001) 2525-2532.

[64] R.C. Elkins, P.E. Dawson, S. Goldstein, S.P. Walsh, K.S. Black, Decellularized human valve allografts, Annals of Thoracic Surgery 71(5) (2001) S428-S432.

[65] M.F. O'Brien, S. Goldstein, S. Walsh, K.S. Black, R. Elkins, D. Clarke, The SynerGraft valve: a new acellular (nonglutaraldehyde-fixed) tissue heart valve for autologous recellularization first experimental studies before clinical implantation, Semin Thorac Cardiovasc Surg 11(4 Suppl 1) (1999) 194-200.

[66] E.R. Mohler, M.K. Chawla, A.W. Chang, N. Vyavahare, R.J. Levy, L. Graham, F.H. Gannon, Identification and characterization of calcifying valve cells from human and canine aortic valves, Journal of Heart Valve Disease 8(3) (1999) 254-260.

[67] F. Chalajour, H. Treede, A. Ebrahimnejad, H. Lauke, H. Reichenspurner, S. Ergun, Angiogenic activation of valvular endothelial cells in aortic valve stenosis, Experimental cell research 298(2) (2004) 455-64.

[68] A.C.W. Zannettino, C.A. Holding, P. Diamond, G.J. Atkins, P. Kostakis, A. Farrugia, J. Gamble, L.B. To, D.M. Findlay, D.R. Haynes, Osteoprotegerin (OPG) is localized to the Weibel-Palade bodies of human vascular endothelial cells and is physically associated with von Willebrand factor, Journal of cellular physiology 204(2) (2005) 714-723.

[69] L. Osman, M.H. Yacoub, N. Latif, M. Amrani, A.H. Chester, Role of human valve interstitial cells in valve calcification and their response to atorvastatin, Circulation 114 (2006) I547-I552.

[70] J.H. Chen, C.Y. Yip, E.D. Sone, C.A. Simmons, Identification and characterization of aortic valve mesenchymal progenitor cells with robust osteogenic calcification potential, The American journal of pathology 174(3) (2009) 1109-19.

[71] P.M. Taylor, S.P. Allen, M.H. Yacoub, Phenotypic and functional characterization of interstitial cells from human heart valves, pericardium and skin, The Journal of heart valve disease 9(1) (2000) 150-8.

[72] A.H. Chester, P.M. Taylor, Molecular and functional characteristics of heart-valve interstitial cells, Philosophical transactions of the Royal Society of London. Series B, Biological sciences 362(1484) (2007) 1437-43.

[73] G.A. Walker, K.S. Masters, D.N. Shah, K.S. Anseth, L.A. Leinwand, Valvular myofibroblast activation by transforming growth factor-beta: implications for pathological extracellular matrix remodeling in heart valve disease, Circulation research 95(3) (2004) 253-60.

[74] S.T. Gould, K.S. Anseth, Role of cell-matrix interactions on VIC phenotype and tissue deposition in 3D PEG hydrogels, Journal of tissue engineering and regenerative medicine (2013).

[75] W.D. Merryman, H.Y. Huang, F.J. Schoen, M.S. Sacks, The effects of cellular contraction on aortic valve leaflet flexural stiffness, Journal of biomechanics 39(1) (2006) 88-96.

[76] C.H. Ku, P.H. Johnson, P. Batten, P. Sarathchandra, R.C. Chambers, P.M. Taylor, M.H. Yacoub, A.H. Chester, Collagen synthesis by mesenchymal stem cells and aortic valve interstitial cells in response to mechanical stretch, Cardiovascular research 71(3) (2006) 548-56.

[77] K. Balachandran, P. Sucosky, H. Jo, A.P. Yoganathan, Elevated cyclic stretch alters matrix remodeling in aortic valve cusps: implications for degenerative aortic valve disease, Am J Physiol-Heart C 296(3) (2009) H756-H764.

[78] N. Latif, P. Sarathchandra, P.S. Thomas, J. Antoniw, P. Batten, A.H. Chester, P.M. Taylor, M.H. Yacoub, Characterization of structural and signaling molecules by human valve interstitial cells and comparison to human mesenchymal stem cells, The Journal of heart valve disease 16(1) (2007) 56-66.

[79] S.T. Gould, E.E. Matherly, J.N. Smith, D.D. Heistad, K.S. Anseth, The role of valvular endothelial cell paracrine signaling and matrix elasticity on valvular interstitial cell activation, Biomaterials 35(11) (2014) 3596-606.

[80] C.M. Kirschner, D.L. Alge, S.T. Gould, K.S. Anseth, Clickable, photodegradable hydrogels to dynamically modulate valvular interstitial cell phenotype, Advanced healthcare materials 3(5) (2014) 649-57.

[81] W.D. Merryman, I. Youn, H.D. Lukoff, P.M. Krueger, F. Guilak, R.A. Hopkins, M.S. Sacks, Correlation between heart valve interstitial cell stiffness and transvalvular pressure: implications for collagen biosynthesis, Am J Physiol-Heart C 290(1) (2006) H224-H231.

[82] S.G. Moesgaard, L.H. Olsen, B. Aasted, B.M. Viuff, L.G. Pedersen, H.D. Pedersen, A.P. Harrison, Direct measurements of nitric oxide release in relation to expression of endothelial nitric oxide synthase in isolated porcine mitral valves, J Vet Med A 54(3) (2007) 156-160.

[83] L. Siney, M.J. Lewis, Nitric oxide release from porcine mitral valves, Cardiovascular research 27(9) (1993) 1657-61.

[84] L.R. Balaoing, A.D. Post, A.Y. Lin, H. Tseng, J.L. Moake, K.J. Grande-Allen, Laminin Peptide-Immobilized Hydrogels Modulate Valve Endothelial Cell Hemostatic Regulation, PloS one 10(6) (2015) e0130749.

[85] J.T. Butcher, G.J. Mahler, L.A. Hockaday, Aortic valve disease and treatment: the need for naturally engineered solutions, Adv Drug Deliv Rev 63(4-5) (2011) 242-68.

[86] B. Imberti, D. Seliktar, R.M. Nerem, A. Remuzzi, The response of endothelial cells to fluid shear stress using a co-culture model of the arterial wall, Endothelium : journal of endothelial cell research 9(1) (2002) 11-23.

[87] J.T. Butcher, A.M. Penrod, A.J. Garcia, R.M. Nerem, Unique morphology and focal adhesion development of valvular endothelial cells in static and fluid flow environments, Arteriosclerosis, thrombosis, and vascular biology 24(8) (2004) 1429-34.

[88] J.D. Deck, Endothelial-Cell Orientation on Aortic-Valve Leaflets, Cardiovascular research 20(10) (1986) 760-767.

[89] R.S. Farivar, L.H. Cohn, E.G. Soltesz, T. Mihaljevic, J.D. Rawn, J.G. Byrne, Transcriptional profiling and growth kinetics of endothelium reveals differences between cells derived from porcine aorta versus aortic valve, Eur J Cardio-Thorac 24(4) (2003) 527-534.

[90] S.V. Lopez-Quintero, R. Amaya, M. Pahakis, J.M. Tarbell, The endothelial glycocalyx mediates shear-induced changes in hydraulic conductivity, Am J Physiol Heart Circ Physiol 296(5) (2009) H1451-6.

[91] P.F. Davies, Multiple signaling pathways in flow-mediated endothelial mechanotransduction: PYK-ing the right location, Arteriosclerosis, thrombosis, and vascular biology 22(11) (2002) 1755-7.

[92] K. Bosse, C.P. Hans, N. Zhao, S.N. Koenig, N. Huang, A. Guggilam, S. LaHaye, G. Tao, P.A. Lucchesi, J. Lincoln, B. Lilly, V. Garg, Endothelial nitric oxide signaling regulates Notch1 in aortic valve disease, Journal of molecular and cellular cardiology 60 (2013) 27-35.

[93] J. Richards, I. El-Hamamsy, S. Chen, Z. Sarang, P. Sarathchandra, M.H. Yacoub, A.H. Chester, J.T. Butcher, Side-specific endothelial-dependent regulation of aortic valve calcification: interplay of hemodynamics and nitric oxide signaling, The American journal of pathology 182(5) (2013) 1922-31.

[94] S. Ramaswamy, D. Gottlieb, G.C. Engelmayr, Jr., E. Aikawa, D.E. Schmidt, D.M. Gaitan-Leon, V.L. Sales, J.E. Mayer, Jr., M.S. Sacks, The role of organ level conditioning on the promotion of engineered heart valve tissue development in-vitro using mesenchymal stem cells, Biomaterials 31(6) (2010) 1114-25.

[95] B. Weber, M.Y. Emmert, L. Behr, R. Schoenauer, C. Brokopp, C. Drogemuller, P. Modregger, M. Stampanoni, D. Vats, M. Rudin, W. Burzle, M. Farine, E. Mazza, T. Frauenfelder, A.C. Zannettino, G. Zund, O. Kretschmar, V. Falk, S.P. Hoerstrup, Prenatally engineered autologous amniotic fluid stem cell-based heart valves in the fetal circulation, Biomaterials 33(16) (2012) 4031-43.

[96] G. Aleksieva, T. Hollweck, N. Thierfelder, U. Haas, F. Koenig, C. Fano, M. Dauner, E. Wintermantel, B. Reichart, C. Schmitz, B. Akra, Use of a special bioreactor for the cultivation of a new flexible polyurethane scaffold for aortic valve tissue engineering, Biomed Eng Online 11 (2012) 92.

[97] T.E. Perry, S. Kaushal, F.W.H. Sutherland, K.J. Guleserian, J. Bischoff, M. Sacks, J.E. Mayer, Bone marrow as a cell source for tissue engineering heart valves, Annals of Thoracic Surgery 75(3) (2003) 761-767.

[98] L.A. Hockaday, K.H. Kang, N.W. Colangelo, P.Y. Cheung, B. Duan, E. Malone, J. Wu, L.N. Girardi, L.J. Bonassar, H. Lipson, C.C. Chu, J.T. Butcher, Rapid 3D printing of anatomically accurate and mechanically heterogeneous aortic valve hydrogel scaffolds, Biofabrication 4(3) (2012) 035005.

[99] A.M.T. Quinlan, K.L. Billiar, Investigating the role of substrate stiffness in the persistence of valvular interstitial cell activation, Journal of Biomedical Materials Research Part A 100a(9) (2012) 2474-2482.

[100] J.L. Cuy, B.L. Beckstead, C.D. Brown, A.S. Hoffman, C.M. Giachelli, Adhesive protein interactions with chitosan: Consequences for valve endothelial cell growth on tissue-engineering materials, Journal of Biomedical Materials Research Part A 67a(2) (2003) 538-547.

[101] P.D. Nair, J. Cuy, C.M. Giachelli, B.D. Ratner, V. Vogel, R.M. Nerem, Biodegradable amino acid-hydrogel porous scaffold for the tissue engineering of the heart valve, P Ann Int Ieee Embs (2002) 856-857.

[102] V.L. Sales, B.A. Mettler, G.C. Engelmayr, E. Aikawa, J. Bischoff, D.P. Martin, A. Exarhopoulos, M.A. Moses, F.J. Schoen, M.S. Sacks, J.E. Mayer, Endothelial Progenitor Cells as a Sole Source for Ex Vivo Seeding of Tissue-Engineered Heart Valves, Tissue Eng Pt A 16(1) (2010) 257-267.

[103] S.P. Hoerstrup, R. Sodian, S. Daebritz, J. Wang, E.A. Bacha, D.P. Martin, A.M. Moran, K.J. Guleserian, J.S. Sperling, S. Kaushal, J.P. Vacanti, F.J. Schoen, J.E. Mayer, Functional living trileaflet heart valves grown in vitro, Circulation 102(19) (2000) 44-49.

[104] F. Juthier, A. Vincentelli, J. Gaudric, D. Corseaux, O. Fouquet, C. Calet, T. Le Tourneau, V. Soenen, C. Zawadzki, O. Fabre, S. Susen, A. Prat, B. Jude, Decellularized heart valve as a scaffold for in vivo recellularization: Deleterious effects of granulocyte colony-stimulating factor, J Thorac Cardiov Sur 131(4) (2006) 843-852.

[105] F.D.A. da Costa, A.C.B.A. Costa, R. Prestes, A.C. Domanski, E.M. Balbi, A.D.A. Ferreira, S.V. Lopes, The Early and Midterm Function of Decellularized Aortic Valve Allografts, Annals of Thoracic Surgery 90(6) (2010) 1854-1861.

[106] B. Duan, L.A. Hockaday, K.H. Kang, J.T. Butcher, 3D bioprinting of heterogeneous aortic valve conduits with alginate/gelatin hydrogels, Journal of biomedical materials research. Part A 101(5) (2013) 1255-64.

[107] C.E. Sarraf, A.B. Harris, A.D. McCulloch, M. Eastwood, Cell proliferation rates in an artificial tissue-engineered environment, Cell Proliferat 38(4) (2005) 215-221.

[108] S.P. Hoerstrup, A. Kadner, S. Melnitchouk, A. Trojan, K. Eid, J. Tracy, R. Sodian, J.F. Visjager, S.A. Kolb, J. Grunenfelder, G. Zund, M.I. Turina, Tissue engineering of functional trileaflet heart valves from human marrow stromal cells, Circulation 106(13) (2002) I143-I150.

[109] F.W. Sutherland, T.E. Perry, Y. Yu, M.C. Sherwood, E. Rabkin, Y. Masuda, G.A. Garcia, D.L. McLellan, G.C. Engelmayr, Jr., M.S. Sacks, F.J. Schoen, J.E. Mayer, Jr., From stem cells to viable autologous semilunar heart valve, Circulation 111(21) (2005) 2783-91.

[110] F. Colazzo, P. Sarathchandra, R.T. Smolenski, A.H. Chester, Y.T. Tseng, J.T. Czernuszka, M.H. Yacoub, P.M. Taylor, Extracellular matrix production by adipose-derived stem cells: implications for heart valve tissue engineering, Biomaterials 32(1) (2011) 119-27.

[111] F. Colazzo, A.H. Chester, P.M. Taylor, M.H. Yacoub, Induction of Mesenchymal to Endothelial Transformation of Adipose-Derived Stem Cells, Journal of Heart Valve Disease 19(6) (2010) 736-744.

[112] D. Schmidt, A. Mol, B. Odermatt, S. Neuenschwander, C. Breymann, M. Gossi, M. Genoni, G. Zund, S.P. Hoerstrup, Engineering of biologically active living heart valve leaflets using human umbilical cord-derived progenitor cells, Tissue engineering 12(11) (2006) 3223-3232.

[113] R. Sodian, P. Schaefermeier, S. Abegg-Zips, W.M. Kuebler, M. Shakibaei, S. Daebritz, J. Ziegelmueller, C. Schmitz, B. Reichart, Use of Human Umbilical Cord Blood-Derived Progenitor Cells for Tissue-Engineered Heart Valves, Annals of Thoracic Surgery 89(3) (2010) 819-828.

[114] D. Schmidt, J. Achermann, B. Odermatt, C. Breymann, A. Mol, M. Genoni, G. Zund, S.P. Hoerstrup, Prenatally fabricated autologous human living heart valves based on amniotic fluid-derived progenitor cells as single cell source, Circulation 116(11) (2007) I64-I70.

[115] D. Schmidt, A. Mol, C. Breymann, J. Achermann, B. Odermatt, M. Gossi, S. Neuenschwander, R. Pretre, M. Genoni, G. Zund, S.P. Hoerstrup, Living autologous heart valves engineered from human prenatally harvested progenitors, Circulation 114 (2006) I125-I131.

[116] D. Schmidt, J. Achermann, B. Odermatt, M. Genoni, G. Zund, S.P. Hoerstrup, Cryopreserved amniotic fluid-derived cells: a lifelong autologous fetal stem cell source for heart valve tissue engineering, The Journal of heart valve disease 17(4) (2008) 446-55; discussion 455.

[117] D. Schmidt, P.E. Dijkman, A. Driessen-Mol, R. Stenger, C. Mariani, A. Puolakka, M. Rissanen, T. Deichmann, B. Odermatt, B. Weber, M.Y. Emmert, G. Zund, F.P. Baaijens, S.P. Hoerstrup, Minimally-invasive implantation of living tissue engineered heart valves: a comprehensive approach from autologous vascular cells to stem cells, Journal of the American College of Cardiology 56(6) (2010) 510-20.

[118] N. Masoumi, N. Annabi, A. Assmann, B.L. Larson, J. Hjortnaes, N. Alemdar, M. Kharaziha, K.B. Manning, J.E. Mayer, Jr., A. Khademhosseini, Tri-layered elastomeric scaffolds for engineering heart valve leaflets, Biomaterials 35(27) (2014) 7774-85.

[119] K. Takahashi, S. Yamanaka, Induction of pluripotent stem cells from mouse embryonic and adult fibroblast cultures by defined factors, Cell 126(4) (2006) 663-76.

[120] K. Balachandran, P. Sucosky, A.P. Yoganathan, Hemodynamics and mechanobiology of aortic valve inflammation and calcification, International journal of inflammation 2011 (2011) 263870.

[121] I. Vesely, The role of elastin in aortic valve mechanics, Journal of biomechanics 31(2) (1998) 115-23.

[122] I. Vesely, R. Noseworthy, Micromechanics of the fibrosa and the ventricularis in aortic valve leaflets, Journal of biomechanics 25(1) (1992) 101-13.

[123] G.W. Christie, Anatomy of aortic heart valve leaflets: the influence of glutaraldehyde fixation on function, European journal of cardio-thoracic surgery : official journal of the European Association for Cardio-thoracic Surgery 6 Suppl 1 (1992) S25-32; discussion S33.

[124] Y.F. Missirlis, C.D. Armeniades, Stress analysis of the aortic valve during diastole: important parameters, Journal of biomechanics 9(7) (1976) 477-80.

[125] S. Hinderer, J. Seifert, M. Votteler, N. Shen, J. Rheinlaender, T.E. Schaffer, K. Schenke-Layland, Engineering of a bio-functionalized hybrid off-the-shelf heart valve, Biomaterials 35(7) (2014) 2130-9.

[126] R.M. Buchanan, M.S. Sacks, Interlayer micromechanics of the aortic heart valve leaflet, Biomech Model Mechanobiol 13(4) (2014) 813-26.

[127] B. Duan, L.A. Hockaday, E. Kapetanovic, K.H. Kang, J.T. Butcher, Stiffness and adhesivity control aortic valve interstitial cell behavior within hyaluronic acid based hydrogels, Acta biomaterialia 9(8) (2013) 7640-50.

[128] B. Duan, Z. Yin, L. Hockaday Kang, R.L. Magin, J.T. Butcher, Active tissue stiffness modulation controls valve interstitial cell phenotype and osteogenic potential in 3D culture, Acta biomaterialia 36 (2016) 42-54.

[129] J. Sohier, I. Carubelli, P. Sarathchandra, N. Latif, A.H. Chester, M.H. Yacoub, The potential of anisotropic matrices as substrate for heart valve engineering, Biomaterials 35(6) (2014) 1833-44.

[130] H. Tseng, D.S. Puperi, E.J. Kim, S. Ayoub, J.V. Shah, M.L. Cuchiara, J.L. West, K.J. Grande-Allen, Anisotropic poly(ethylene glycol)/polycaprolactone hydrogel-fiber composites for heart valve tissue engineering, Tissue engineering. Part A 20(19-20) (2014) 2634-45.

[131] H. Tseng, M.L. Cuchiara, C.A. Durst, M.P. Cuchiara, C.J. Lin, J.L. West, K.J. Grande-Allen, Fabrication and mechanical evaluation of anatomically-inspired quasilaminate hydrogel structures with layer-specific formulations, Annals of biomedical engineering 41(2) (2013) 398-407.

[132] B. Duan, E. Kapetanovic, L.A. Hockaday, J.T. Butcher, Three-dimensional printed trileaflet valve conduits using biological hydrogels and human valve interstitial cells, Acta biomaterialia 10(5) (2014) 1836-46.

[133] M.S. Sacks, W. David Merryman, D.E. Schmidt, On the biomechanics of heart valve function, Journal of biomechanics 42(12) (2009) 1804-24.

[134] C. Otto, Clinical practice. Evaluation and management of chronic mitral regurgitation., N Engl J Med 345(10) (2001) 740-6.

[135] C.H. Yap, N. Saikrishnan, A.P. Yoganathan, Experimental measurement of dynamic fluid shear stress on the ventricular surface of the aortic valve leaflet, Biomech Model Mechanobiol 11(1-2) (2012) 231-44.

[136] C.H. Yap, N. Saikrishnan, G. Tamilselvan, A.P. Yoganathan, Experimental measurement of dynamic fluid shear stress on the aortic surface of the aortic valve leaflet, Biomech Model Mechanobiol 11(1-2) (2012) 171-82.

[137] C.I. Fisher, J. Chen, W.D. Merryman, Calcific nodule morphogenesis by heart valve interstitial cells is strain dependent, Biomechanics and Modeling in Mechanobiology 12(1) (2012) 5-17.

[138] R.B. Hinton, K.E. Yutzey, Heart valve structure and function in development and disease, Annu Rev Physiol 73 (2011) 29-46.

[139] Y.F. Missirlis, M. Chong, Aortic valve mechanics--Part I: material properties of natural porcine aortic valves, J Bioeng 2(3-4) (1978) 287-300.

[140] R. Brewer, R. Mentzer, J. Deck, R. Ritter, J. Trefil, S. Nolan, An in vivo study of dimensional changes of the aortic valve leaflets during the cardiac cycle, J Thorac Cardiovasc Surg 74(4) (1977) 645-650.

[141] M. Thubrikar, S. Nolan, L. Bosher, J. Deck, THe cyclic changes and structure of the base of the aortic valve, Am Heart J 99(2) (1980) 217-224.

[142] G.C. Engelmayr, D.K. Hildebrand, F.W.H. Sutherland, J.E. Mayer, M.S. Sacks, A novel bioreactor for the dynamic flexural stimulation of tissue engineered heart valve biomaterials, Biomaterials 24(14) (2003) 2523-2532.

[143] N.J. Driessen, A. Mol, C.V. Bouten, F.P. Baaijens, Modeling the mechanics of tissue-engineered human heart valve leaflets, J Biomech 40(2) (2007) 325-34.

[144] S.H. Alavi, M. Soriano Baliarda, N. Bonessio, L. Valdevit, A. Kheradvar, A Tri-Leaflet Nitinol Mesh Scaffold for Engineering Heart Valves, Ann Biomed Eng 45(2) (2017) 413-426.

[145] R. Sodian, S.P. Hoerstrup, J. Sperling, D. Martin, S. Daebritz, J.E. Mayer, J. Vacanti, Evaluation of biodegradable, three-dimensional matrices for tissue engineering of heart valves, ASAIO J 46 (2000b) 107-110.

[146] S.P. Hoerstrup, R. Sodian, S. Daebritz, J. Wang, E. Bacha, D. Martin, A. Moran, K. Guleserian, J. Sperling, S. Kaushal, J. Vacanti, F.J. Schoen, J.E. Mayer, Functional living trileaflet heart valves grown in vitro, Circulation 102 (2000) 44-49.

[147] J. Kluin, H. Talacua, A.I. Smits, M.Y. Emmert, M.C. Brugmans, E.S. Fioretta, P.E. Dijkman, S.H. Sontjens, R. Duijvelshoff, S. Dekker, M.W. Janssen-van den Broek, V. Lintas, A. Vink, S.P. Hoerstrup, H.M. Janssen, P.Y. Dankers, F.P. Baaijens, C.V. Bouten, In situ heart valve tissue engineering using a bioresorbable elastomeric implant - From material design to 12 months follow-up in sheep, Biomaterials 125 (2017) 101-117.

[148] S.P. Hoerstrup, R. Sodian, J. Sperling, J. Vacanti, J.E. Mayer, New pulsatile bioreactor for in vitro formation of tissue engineered heart valves, Tissue Engineering 6(1) (2000) 75-79.

[149] S. Jockenhoevel, G. Zund, S.P. Hoerstrup, A. Schnell, M. Turina, Cardiovascular Tissue Engineering: A New Laminar Flow Chamber for In VItro Improvement of Mechanical Tissue Properties, ASAIO J 48(1) (2002) 8-11.

[150] A. Mol, N.J. Driessen, M.C. Rutten, S.P. Hoerstrup, C.V. Bouten, F.P. Baaijens, Tissue engineering of human heart valve leaflets: a novel bioreactor for a strain-based conditioning approach, Ann Biomed Eng 33(12) (2005) 1778-88.

[151] G.C. Engelmayr, Jr., L. Soletti, S.C. Vigmostad, S.G. Budilarto, W.J. Federspiel, K.B. Chandran, D.A. Vorp, M.S. Sacks, A novel flex-stretch-flow bioreactor for the study of engineered heart valve tissue mechanobiology, Ann Biomed Eng 36(5) (2008) 700-12.

[152] S. Ramaswamy, S.M. Boronyak, T. Le, A. Holmes, F. Sotiropoulos, M.S. Sacks, A novel bioreactor for mechanobiological studies of engineered heart valve tissue formation under pulmonary arterial physiological flow conditions, J Biomech Eng 136(12) (2014) 121009.

[153] G.L. Converse, E.E. Buse, K.R. Neill, C.R. McFall, H.N. Lewis, M.C. VeDepo, R.W. Quinn, R.A. Hopkins, Design and efficacy of a single-use bioreactor for heart valve tissue engineering, J Biomed Mater Res B Appl Biomater 105(2) (2017) 249-259.

[154] S.T. Rashid, H.J. Salacinski, G. Hamilton, A.M. Seifalian, The use of animal models in developing the discipline of cardiovascular tissue engineering: a review, Biomaterials 25(9) (2004) 1627-1637.

[155] M. Taramasso, M.Y. Emmert, D. Reser, A. Guidotti, N. Cesarovic, M. Campagnol, A. Addis, F. Nietlispach, S.P. Hoerstrup, F. Maisano, Pre-clinical In Vitro and In Vivo Models for Heart Valve Therapies, J Cardiovasc Transl Res 8(5) (2015) 319-27.

[156] K. Mendelson, F.J. Schoen, Heart valve tissue engineering: concepts, approaches, progress, and challenges, Annals of biomedical engineering 34(12) (2006) 1799-819.

[157] S.L. Goodman, Sheep, pig and human platelet-material interactions with model cardiovascular biomaterials, Journal of Biomedical Materials Research 45(3) (1999) 240-250.

[158] M.Y. Emmert, B. Weber, P. Wolint, L. Behr, S. Sammut, T. Frauenfelder, L. Frese, J. Scherman, C.E. Brokopp, C. Templin, J. Grunenfelder, G. Zund, V. Falk, S.P. Hoerstrup, Stem cell-based transcatheter aortic valve implantation: first experiences in a pre-clinical model, JACC Cardiovasc Interv 5(8) (2012) 874-83.

[159] M. Gallo, H. Poser, T. Bottio, A. Bonetti, P. Franci, F. Naso, E. Buratto, F. Zanella, G. Perona, C. Dal Lin, R. Bianco, M. Spina, R. Busetto, M. Marchini, F. Ortolani, L. Iop, G. Gerosa, The Vietnamese pig as a translational animal model to evaluate tissue engineered heart valves: promising early experience, Int J Artif Organs 40(4) (2017) 142-149.

[160] D. Miranda-Nieves, E.L. Chaikof, Collagen and Elastin Biomaterials for the Fabrication of Engineered Living Tissues, ACS Biomaterials Science & Engineering 3(5) (2017) 694-711.

[161] N. Bhardwaj, S.C. Kundu, Electrospinning: a fascinating fiber fabrication technique, Biotechnol Adv 28(3) (2010) 325-47.

[162] S.V. Murphy, A. Atala, 3D bioprinting of tissues and organs, Nature biotechnology 32(8) (2014) 773-85.

[163] Y. Huang, X.F. Zhang, G. Gao, T. Yonezawa, X. Cui, 3D bioprinting and the current applications in tissue engineering, Biotechnol J (2017).

[164] J.F. Mano, G.A. Silva, H.S. Azevedo, P.B. Malafaya, R.A. Sousa, S.S. Silva, L.F. Boesel, J.M. Oliveira, T.C. Santos, A.P. Marques, N.M. Neves, R.L. Reis, Natural origin biodegradable systems in tissue engineering and regenerative medicine: present status and some moving trends, J R Soc Interface 4(17) (2007) 999-1030.

[165] B. Widner, R. Behr, S. Von Dollen, M. Tang, T. Heu, A. Sloma, D. Sternberg, P.L. Deangelis, P.H. Weigel, S. Brown, Hyaluronic acid production in Bacillus subtilis, Appl Environ Microbiol 71(7) (2005) 3747-52.

[166] F.J. O'Brien, Biomaterials & scaffolds for tissue engineering, Materials Today 14(3) (2011) 88-95.

[167] M.C. Gómez-Guillén, B. Giménez, M.E. López-Caballero, M.P. Montero, Functional and bioactive properties of collagen and gelatin from alternative sources: A review, Food Hydrocolloids 25(8) (2011) 1813-1827.

[168] G. Veit, B. Kobbe, D.R. Keene, M. Paulsson, M. Koch, R. Wagener, Collagen XXVIII, a novel von Willebrand factor A domain-containing protein with many imperfections in the collagenous domain, J Biol Chem 281(6) (2006) 3494-504.

[169] J.A. Ramshaw, Y.Y. Peng, V. Glattauer, J.A. Werkmeister, Collagens as biomaterials, J Mater Sci Mater Med 20 Suppl 1 (2009) S3-8.

[170] R.A. Berg, D.J. Prockop, The thermal transition of a non-hydroxylated form of collagen. Evidence for a role for hydroxyproline in stabilizing the triple-helix of collagen, Biochemical and biophysical research communications 52(1) (1973) 115-20.

[171] G.D. Prestwich, S. Atzet, Chapter I.2.7 - Engineered Natural Materials A2 - Ratner, Buddy D, in: A.S. Hoffman, F.J. Schoen, J.E. Lemons (Eds.), Biomaterials Science (Third Edition), Academic Press2013, pp. 195-209.

[172] C. Yang, P.J. Hillas, J.A. Baez, M. Nokelainen, J. Balan, J. Tang, R. Spiro, J.W. Polarek, The application of recombinant human collagen in tissue engineering, BioDrugs 18(2) (2004) 103-19.

[173] J.L. Zhu, L.J. Kaufman, Collagen I Self-Assembly: Revealing the Developing Structures that Generate Turbidity, Biophys J 106(8) (2014) 1822-1831.

[174] D.L. Christiansen, E.K. Huang, F.H. Silver, Assembly of type I collagen: fusion of fibril subunits and the influence of fibril diameter on mechanical properties, Matrix Biology 19(5) (2000) 409-420.

[175] B.A. Roeder, K. Kokini, J.E. Sturgis, J.P. Robinson, S.L. Voytik-Harbin, Tensile mechanical properties of three-dimensional type I collagen extracellular matrices with varied microstructure, J Biomech Eng-T Asme 124(2) (2002) 214-222.

[176] N. Annabi, J.W. Nichol, X. Zhong, C. Ji, S. Koshy, A. Khademhosseini, F. Dehghani, Controlling the porosity and microarchitecture of hydrogels for tissue engineering, Tissue engineering. Part B, Reviews 16(4) (2010) 371-83.

[177] C.Y. Yip, J.H. Chen, R. Zhao, C.A. Simmons, Calcification by valve interstitial cells is regulated by the stiffness of the extracellular matrix, Arteriosclerosis, thrombosis, and vascular biology 29(6) (2009) 936-42.

[178] P.M. Taylor, E. Sachlos, S.A. Dreger, A.H. Chester, J.T. Czernuszka, M.H. Yacoub, Interaction of human valve interstitial cells with collagen matrices manufactured using rapid prototyping, Biomaterials 27(13) (2006) 2733-2737.

[179] P. Ayala, J. Caves, E. Dai, L. Siraj, L. Liu, O. Chaudhuri, C.A. Haller, D.J. Mooney, E.L. Chaikof, Engineered composite fascia for stem cell therapy in tissue repair applications, Acta biomaterialia 26 (2015) 1-12.

[180] O.F. Khan, D.N. Voice, B.M. Leung, M.V. Sefton, A novel high-speed production process to create modular components for the bottom-up assembly of large-scale tissue-engineered constructs, Advanced healthcare materials 4(1) (2015) 113-20.

[181] K. Nuutila, M. Peura, S. Suomela, M. Hukkanen, A. Siltanen, A. Harjula, J. Vuola, E. Kankuri, Recombinant human collagen III gel for transplantation of autologous skin cells in porcine full-thickness wounds, Journal of tissue engineering and regenerative medicine 9(12) (2015) 1386-93.

[182] T.C. Flanagan, B. Wilkins, A. Black, S. Jockenhoevel, T.J. Smith, A.S. Pandit, A collagen-glycosaminoglycan co-culture model for heart valve tissue engineering applications, Biomaterials 27(10) (2006) 2233-46.

[183] R.A. Gould, K. Chin, T.P. Santisakultarm, A. Dropkin, J.M. Richards, C.B. Schaffer, J.T. Butcher, Cyclic strain anisotropy regulates valvular interstitial cell phenotype and tissue remodeling in three-dimensional culture, Acta biomaterialia 8(5) (2012) 1710-9.

[184] J.A. Matthews, G.E. Wnek, D.G. Simpson, G.L. Bowlin, Electrospinning of collagen nanofibers, Biomacromolecules 3(2) (2002) 232-8.

[185] Y. Liu, Y. Xu, Z. Wang, D. Wen, W. Zhang, S. Schmull, H. Li, Y. Chen, S. Xue, Electrospun nanofibrous sheets of collagen/elastin/polycaprolactone improve cardiac repair after myocardial infarction, Am J Transl Res 8(4) (2016) 1678-94.

[186] C. Huang, R. Chen, Q. Ke, Y. Morsi, K. Zhang, X. Mo, Electrospun collagen-chitosan-TPU nanofibrous scaffolds for tissue engineered tubular grafts, Colloids Surf B Biointerfaces 82(2) (2011) 307-15.

[187] J. Baek, S. Sovani, W. Choi, S. Jin, S.P. Grogan, D.D. D'Lima, Meniscal Tissue Engineering Using Aligned Collagen Fibrous Scaffolds: Comparison of Different Human Cell Sources, Tissue engineering. Part A (2017).

[188] M. Nakamura, S. Iwanaga, C. Henmi, K. Arai, Y. Nishiyama, Biomatrices and biomaterials for future developments of bioprinting and biofabrication, Biofabrication 2(1) (2010) 014110.

[189] M. Hospodiuk, M. Dey, D. Sosnoski, I.T. Ozbolat, The bioink: A comprehensive review on bioprintable materials, Biotechnol Adv 35(2) (2017) 217-239.

[190] L. Koch, A. Deiwick, S. Schlie, S. Michael, M. Gruene, V. Coger, D. Zychlinski, A. Schambach, K. Reimers, P.M. Vogt, B. Chichkov, Skin tissue generation by laser cell printing, Biotechnology and bioengineering 109(7) (2012) 1855-63.

[191] S. Rhee, J.L. Puetzer, B.N. Mason, C.A. Reinhart-King, L.J. Bonassar, 3D Bioprinting of Spatially Heterogeneous Collagen Constructs for Cartilage Tissue Engineering, ACS Biomaterials Science & Engineering 2(10) (2016) 1800-1805.

[192] C.M. Smith, A.L. Stone, R.L. Parkhill, R.L. Stewart, M.W. Simpkins, A.M. Kachurin, W.L. Warren, S.K. Williams, Three-dimensional bioassembly tool for generating viable tissue-engineered constructs, Tissue engineering 10(9-10) (2004) 1566-76.

[193] C.M. Homenick, G. de Silveira, H. Sheardown, A. Adronov, Pluronics as crosslinking agents for collagen: novel amphiphilic hydrogels, Polymer International 60(3) (2011) 458-465.

[194] C.D. Buckley, D. Pilling, N.V. Henriquez, G. Parsonage, K. Threlfall, D. Scheel-Toellner, D.L. Simmons, A.N. Akbar, J.M. Lord, M. Salmon, RGD peptides induce apoptosis by direct caspase-3 activation, Nature 397(6719) (1999) 534-9.

[195] E. Ruoslahti, RGD and other recognition sequences for integrins, Annu Rev Cell Dev Biol 12 (1996) 697-715.

[196] S.A. Dreger, P. Thomas, E. Sachlos, A.H. Chester, J.T. Czernuszka, P.M. Taylor, M.H. Yacoub, Potential for synthesis and degradation of extracellular matrix proteins by valve interstitial cells seeded onto collagen scaffolds, Tissue engineering 12(9) (2006) 2533-40.

[197] M.E. Tedder, J. Liao, B. Weed, C. Stabler, H. Zhang, A. Simionescu, D.T. Simionescu, Stabilized collagen scaffolds for heart valve tissue engineering, Tissue engineering. Part A 15(6) (2009) 1257-68.

[198] R.W. Farndale, J.J. Sixma, M.J. Barnes, P.G. de Groot, The role of collagen in thrombosis and hemostasis, J Thromb Haemost 2(4) (2004) 561-73.

[199] X. Zhang, B. Xu, D.S. Puperi, Y. Wu, J.L. West, K.J. Grande-Allen, Application of hydrogels in heart valve tissue engineering, J Long Term Eff Med Implants 25(1-2) (2015) 105-34.

[200] A.I. Van Den Bulcke, B. Bogdanov, N. De Rooze, E.H. Schacht, M. Cornelissen, H. Berghmans, Structural and rheological properties of methacrylamide modified gelatin hydrogels, Biomacromolecules 1(1) (2000) 31-8.

[201] X.D. Li, L. Jin, G. Balian, C.T. Laurencin, D.G. Anderson, Demineralized bone matrix gelatin as scaffold for osteochondral tissue engineering, Biomaterials 27(11) (2006) 2426-2433.

[202] D. Loessner, C. Meinert, E. Kaemmerer, L.C. Martine, K. Yue, P.A. Levett, T.J. Klein, F.P.W. Melchels, A. Khademhosseini, D.W. Hutmacher, Functionalization, preparation and use of cell-laden gelatin methacryloyl-based hydrogels as modular tissue culture platforms, Nat Protoc 11(4) (2016) 727-746.

[203] J.B. Rose, S. Pacelli, A.J. El Haj, H.S. Dua, A. Hopkinson, L.J. White, F.R.A.J. Rose, Gelatin-Based Materials in Ocular Tissue Engineering, Materials 7(4) (2014) 3106-3135.

[204] J.A. Benton, B.D. Fairbanks, K.S. Anseth, Characterization of valvular interstitial cell function in three dimensional matrix metalloproteinase degradable PEG hydrogels, Biomaterials 30(34) (2009) 6593-603.

[205] J. Zhu, Bioactive modification of poly(ethylene glycol) hydrogels for tissue engineering, Biomaterials 31(17) (2010) 4639-56.

[206] X. Zhang, B. Xu, D.S. Puperi, Y. Wu, J.L. West, K.J. Grande-Allen, Hydrogel Review, Journal of Long-Term Effects of Medical Implants 25(0) (2015) 105-134.

[207] S. Lee, X. Tong, F. Yang, Effects of the poly(ethylene glycol) hydrogel crosslinking mechanism on protein release, Biomater Sci 4(3) (2016) 405-11.

[208] N.A. Peppas, A.S. Hoffman, Hydrogels, Biomaterials Science2013, pp. 166-179.

[209] H. Wang, M.W. Tibbitt, S.J. Langer, L.A. Leinwand, K.S. Anseth, Hydrogels preserve native phenotypes of valvular fibroblasts through an elasticity-regulated PI3K/AKT pathway, Proc Natl Acad Sci U S A 110(48) (2013) 19336-41.

[210] L.H. Kang, P.A. Armstrong, L.J. Lee, B. Duan, K.H. Kang, J.T. Butcher, Optimizing Photo-Encapsulation Viability of Heart Valve Cell Types in 3D Printable Composite Hydrogels, Ann Biomed Eng (2016).

[211] Y. Wu, D.S. Puperi, K.J. Grande-Allen, J.L. West, Ascorbic acid promotes extracellular matrix deposition while preserving valve interstitial cell quiescence within 3D hydrogel scaffolds, Journal of tissue engineering and regenerative medicine (2015).

[212] C.A. Durst, M.P. Cuchiara, E.G. Mansfield, J.L. West, K.J. Grande-Allen, Flexural characterization of cell encapsulated PEGDA hydrogels with applications for tissue engineered heart valves, Acta biomaterialia 7(6) (2011) 2467-76.

[213] T. Jin, I. Stanciulescu, Numerical investigation of the influence of pattern topology on the mechanical behavior of PEGDA hydrogels, Acta biomaterialia 49 (2017) 247-259.

[214] S. Jana, B.J. Tefft, D.B. Spoon, R.D. Simari, Scaffolds for tissue engineering of cardiac valves, Acta biomaterialia 10(7) (2014) 2877-93.

[215] M. Treiser, S. Abramson, R. Langer, J. Kohn, Degradable and Resorbable Biomaterials, Biomaterials Science2013, pp. 179-195.

[216] B.D. Ulery, L.S. Nair, C.T. Laurencin, Biomedical Applications of Biodegradable Polymers, J Polym Sci B Polym Phys 49(12) (2011) 832-864.

[217] M. Lieshout, G. Peters, M. Rutten, F. Baaijens, A Knitted, Fibrin-Covered Polycaprolactone Scaffold for Tissue Engineering of the Aortic Valve, Tissue Engineering 12 (2006) 481-487.

[218] M.M. Brugmans, A. Driessen-Mol, M.P. Rubbens, M.A. Cox, F.P. Baaijens, Poly-epsilon-caprolactone scaffold and reduced in vitro cell culture: beneficial effect on compaction and improved valvular tissue formation, J Tissue Eng Regen Med 9(12) (2015) E289-301.

[219] M.M. Brugmans, R.S. Soekhradj-Soechit, D. van Geemen, M. Cox, C.V. Bouten, F.P. Baaijens, A. Driessen-Mol, Superior Tissue Evolution in Slow-Degrading Scaffolds for Valvular Tissue Engineering, Tissue engineering. Part A 22(1-2) (2016) 123-32.

[220] M. Schleicher, H.P. Wendel, O. Fritze, U.A. Stock, In vivo tissue engineering of heart valves: evolution of a novel concept, Regen Med 4(4) (2009) 613-9.

[221] S. Kishimoto, Y. Takewa, Y. Nakayama, K. Date, H. Sumikura, T. Moriwaki, M. Nishimura, E. Tatsumi, Sutureless aortic valve replacement using a novel autologous tissue heart valve with stent (stent biovalve): proof of concept, J Artif Organs 18(2) (2015) 185-90.

[222] P.E. Dijkman, A. Driessen-Mol, L. Frese, S.P. Hoerstrup, F.P. Baaijens, Decellularized homologous tissue-engineered heart valves as off-the-shelf alternatives to xeno- and homografts, Biomaterials 33(18) (2012) 4545-54.

[223] B. Weber, P.E. Dijkman, J. Scherman, B. Sanders, M.Y. Emmert, J. Grunenfelder, R. Verbeek, M. Bracher, M. Black, T. Franz, J. Kortsmit, P. Modregger, S. Peter, M. Stampanoni, J. Robert, D. Kehl, M. van Doeselaar, M. Schweiger, C.E. Brokopp, T. Walchli, V. Falk, P. Zilla, A. Driessen-Mol, F.P. Baaijens, S.P. Hoerstrup, Off-the-shelf human decellularized tissue-engineered heart valves in a non-human primate model, Biomaterials 34(30) (2013) 7269-80.

[224] S. Jahnavi, U. Saravanan, N. Arthi, G.S. Bhuvaneshwar, T.V. Kumary, S. Rajan, R.S. Verma, Biological and mechanical evaluation of a Bio-Hybrid scaffold for autologous valve tissue engineering, Materials science & engineering. C, Materials for biological applications 73 (2017) 59-71.

[225] A.K. Capulli, M.Y. Emmert, F.S. Pasqualini, D. Kehl, E. Caliskan, J.U. Lind, S.P. Sheehy, S.J. Park, S. Ahn, B. Weber, J.A. Goss, S.P. Hoerstrup, K.K. Parker, JetValve: Rapid manufacturing of biohybrid scaffolds for biomimetic heart valve replacement, Biomaterials 133 (2017) 229-241.

[226] B. Duan, State-of-the-Art Review of 3D Bioprinting for Cardiovascular Tissue Engineering, Annals of biomedical engineering 45(1) (2017) 195-209.

[227] J. Hoffman, The global burden of congenital heart disease, Cardiovascular journal of Africa 24(4) (2013) 141-5.

[228] S.H. Rahimtoola, Choice of prosthetic heart valve for adult patients, Journal of the American College of Cardiology 41(6) (2003) 893-904.

[229] F.J. Schoen, Future directions in tissue heart valves: impact of recent insights from biology and pathology, The Journal of heart valve disease 8(4) (1999) 350-8.

[230] W. Huang, D.Z. Xiao, Y.G. Wang, Z.X. Shan, X.Y. Liu, Q.X. Lin, M. Yang, J. Zhuang, Y.X. Li, X.Y. Yu, Fn14 Promotes Differentiation of Human Mesenchymal Stem Cells into Heart Valvular Interstitial Cells by Phenotypic Characterization, Journal of cellular physiology 229(5) (2014) 580-587.

[231] N. Masoumi, B.L. Larson, N. Annabi, M. Kharaziha, B. Zamanian, K.S. Shapero, A.T. Cubberley, G. Camci-Unal, K.B. Manning, J.E. Mayer, Jr., A. Khademhosseini, Electrospun PGS:PCL microfibers align human valvular interstitial cells and provide tunable scaffold anisotropy, Advanced healthcare materials 3(6) (2014) 929-39.

[232] D. Schmidt, P.E. Dijkman, A. Driessen-Mol, R. Stenger, C. Mariani, A. Puolakka, M. Rissanen, T. Deichmann, B. Odermatt, B. Weber, M.Y. Emmert, G. Zund, F.P.T. Baaijens, S.P. Hoerstrup, Minimally-Invasive Implantation of Living Tissue Engineered Heart Valves A Comprehensive Approach From Autologous Vascular Cells to Stem Cells, Journal of the American College of Cardiology 56(6) (2010) 510-520.

[233] T. Shinoka, P.X. Ma, D. Shum-Tim, C.K. Breuer, R.A. Cusick, G. Zund, R. Langer, J.P. Vacanti, J.E. Mayer, Jr., Tissue-engineered heart valves. Autologous valve leaflet replacement study in a lamb model, Circulation 94(9 Suppl) (1996) II164-8.

[234] R.A. Rippel, H. Ghanbari, A.M. Seifalian, Tissue-engineered heart valve: future of cardiac surgery, World J Surg 36(7) (2012) 1581-91.

[235] J. Copier, M. Bodman-Smith, A. Dalgleish, Current status and future applications of cellular therapies for cancer, Immunotherapy 3(4) (2011) 507-16.

[236] Y. Jung, G. Bauer, J.A. Nolta, Concise review: Induced pluripotent stem cell-derived mesenchymal stem cells: progress toward safe clinical products, Stem cells 30(1) (2012) 42-7.

[237] O. Katsara, L.G. Mahaira, E.G. Iliopoulou, A. Moustaki, A. Antsaklis, D. Loutradis, K. Stefanidis, C.N. Baxevanis, M. Papamichail, S.A. Perez, Effects of donor age, gender, and in vitro cellular aging on the phenotypic, functional, and molecular characteristics of mouse bone marrow-derived mesenchymal stem cells, Stem Cells Dev 20(9) (2011) 1549-61.

[238] Q. Lian, Y. Zhang, J. Zhang, H.K. Zhang, X. Wu, Y. Zhang, F.F. Lam, S. Kang, J.C. Xia, W.H. Lai, K.W. Au, Y.Y. Chow, C.W. Siu, C.N. Lee, H.F. Tse, Functional mesenchymal stem cells derived from human induced pluripotent stem cells attenuate limb ischemia in mice, Circulation 121(9) (2010) 1113-23.

[239] V. Sabapathy, S. Kumar, hiPSC-derived iMSCs: NextGen MSCs as an advanced therapeutically active cell resource for regenerative medicine, Journal of Cellular and Molecular Medicine 20(8) (2016) 1571-1588.

[240] K.T. Nguyen, J.L. West, Photopolymerizable hydrogels for tissue engineering applications, Biomaterials 23(22) (2002) 4307-14.

[241] K.M. Mabry, R.L. Lawrence, K.S. Anseth, Dynamic stiffening of poly(ethylene glycol)-based hydrogels to direct valvular interstitial cell phenotype in a three-dimensional environment, Biomaterials 49 (2015) 47-56.

[242] C. Xu, J. Jiang, V. Sottile, J. McWhir, J. Lebkowski, M.K. Carpenter, Immortalized fibroblast-like cells derived from human embryonic stem cells support undifferentiated cell growth, Stem cells 22(6) (2004) 972-80.

[243] S. Ali, M.L. Cuchiara, J.L. West, Micropatterning of poly(ethylene glycol) diacrylate hydrogels, Methods Cell Biol 121 (2014) 105-19.

[244] C. Xu, M.S. Inokuma, J. Denham, K. Golds, P. Kundu, J.D. Gold, M.K. Carpenter, Feeder-free growth of undifferentiated human embryonic stem cells, Nature biotechnology 19(10) (2001) 971-4.

[245] Y.Y. Zhou, F. Zeng, Integration-free methods for generating induced pluripotent stem cells, Genomics Proteomics Bioinformatics 11(5) (2013) 284-7.

[246] R. Kang, Y. Zhou, S. Tan, G. Zhou, L. Aagaard, L. Xie, C. Bunger, L. Bolund, Y. Luo, Mesenchymal stem cells derived from human induced pluripotent stem cells retain adequate osteogenicity and chondrogenicity but less adipogenicity, Stem Cell Res Ther 6 (2015) 144.

[247] K. Okita, T. Ichisaka, S. Yamanaka, Generation of germline-competent induced pluripotent stem cells, Nature 448(7151) (2007) 313-7.

[248] V.K. Bajpai, P. Mistriotis, Y.H. Loh, G.Q. Daley, S.T. Andreadis, Functional vascular smooth muscle cells derived from human induced pluripotent stem cells via mesenchymal stem cell intermediates, Cardiovascular research 96(3) (2012) 391-400.

[249] B. Weber, M.Y. Emmert, S.P. Hoerstrup, Stem cells for heart valve regeneration, Swiss medical weekly 142 (2012) w13622.

[250] A. Hasan, K. Ragaert, W. Swieszkowski, S. Selimovic, A. Paul, G. Camci-Unal, M.R. Mofrad, A. Khademhosseini, Biomechanical properties of native and tissue engineered heart valve constructs, Journal of biomechanics 47(9) (2014) 1949-63.

[251] A. Balguid, M.P. Rubbens, A. Mol, R.A. Bank, A.J. Bogers, J.P. van Kats, B.A. de Mol, F.P. Baaijens, C.V. Bouten, The role of collagen cross-links in biomechanical behavior of human aortic heart valve leaflets--relevance for tissue engineering, Tissue engineering 13(7) (2007) 1501-11.

[252] S.J. Bryant, C.R. Nuttelman, K.S. Anseth, Cytocompatibility of UV and visible light photoinitiating systems on cultured NIH/3T3 fibroblasts in vitro, J Biomater Sci Polym Ed 11(5) (2000) 439-57.

[253] F. Yang, C.G. Williams, D.A. Wang, H. Lee, P.N. Manson, J. Elisseeff, The effect of incorporating RGD adhesive peptide in polyethylene glycol diacrylate hydrogel on osteogenesis of bone marrow stromal cells, Biomaterials 26(30) (2005) 5991-8.

[254] D.S. Puperi, A. Kishan, Z.E. Punske, Y. Wu, E. Cosgriff-Hernandez, J.L. West, K.J. Grande-Allen, Electrospun Polyurethane and Hydrogel Composite Scaffolds as Biomechanical Mimics for Aortic Valve Tissue Engineering, Acs Biomaterials Science & Engineering 2(9) (2016) 1546-1558.

[255] P. Snider, K.N. Standley, J. Wang, M. Azhar, T. Doetschman, S.J. Conway, Origin of cardiac fibroblasts and the role of periostin, Circulation research 105(10) (2009) 934-47.

[256] M.I. Harhun, C.L. Huggins, K. Ratnasingham, D. Raje, R.F. Moss, K. Szewczyk, G. Vasilikostas, I.A. Greenwood, T.K. Khong, A. Wan, M. Reddy, Resident phenotypically modulated vascular smooth muscle cells in healthy human arteries, J Cell Mol Med 16(11) (2012) 2802-12.

[257] P.M. Taylor, P. Batten, N.J. Brand, P.S. Thomas, M.H. Yacoub, The cardiac valve interstitial cell, The international journal of biochemistry & cell biology 35(2) (2003) 113-8.

[258] A. Pokutta-Paskaleva, F. Sulejmani, M. DelRocini, W. Sun, Comparative mechanical, morphological, and microstructural characterization of porcine mitral and tricuspid leaflets and chordae tendineae, Acta biomaterialia 85 (2019) 241-252.

[259] Y. Zhu, C. Gao, J. Shen, Surface modification of polycaprolactone with poly(methacrylic acid) and gelatin covalent immobilization for promoting its cytocompatibility, Biomaterials 23(24) (2002) 4889-95.

[260] S. Bhutani, A.L.Y. Nachlas, M.E. Brown, T. Pete, C.T. Johnson, A.J. Garcia, M.E. Davis, Evaluation of Hydrogels Presenting Extracellular Matrix-Derived Adhesion Peptides and Encapsulating Cardiac Progenitor Cells for Cardiac Repair, ACS Biomater Sci Eng 4(1) (2018) 200-210.

[261] P. Sucosky, M. Padala, A. Elhammali, K. Balachandran, H. Jo, A.P. Yoganathan, Design of an ex vivo culture system to investigate the effects of shear stress on cardiovascular tissue, Journal of biomechanical engineering 130(3) (2008) 035001.

[262] K. Cao, P. Sucosky, Computational comparison of regional stress and deformation characteristics in tricuspid and bicuspid aortic valve leaflets, International journal for numerical methods in biomedical engineering 33(3) (2017).

[263] C. Martin, W. Sun, Biomechanical characterization of aortic valve tissue in humans and common animal models, Journal of biomedical materials research. Part A 100(6) (2012) 1591-9.

[264] H. Sun, L. Mei, C. Song, X. Cui, P. Wang, The in vivo degradation, absorption and excretion of PCL-based implant, Biomaterials 27(9) (2006) 1735-40.

[265] K. Webb, V. Hlady, P.A. Tresco, Relative importance of surface wettability and charged functional groups on NIH 3T3 fibroblast attachment, spreading, and cytoskeletal organization, Journal of biomedical materials research 41(3) (1998) 422-30.

[266] P.J. Yang, M.E. Levenston, J.S. Temenoff, Modulation of mesenchymal stem cell shape in enzyme-sensitive hydrogels is decoupled from upregulation of fibroblast markers under cyclic tension, Tissue engineering. Part A 18(21-22) (2012) 2365-75.

[267] B. Mosadegh, G. Xiong, S. Dunham, J.K. Min, Current progress in 3D printing for cardiovascular tissue engineering, Biomed Mater 10(3) (2015) 034002.

[268] P.E. Dijkman, A. Driessen-Mol, L.M. de Heer, J. Kluin, L.A. van Herwerden, B. Odermatt, F.P. Baaijens, S.P. Hoerstrup, Trans-apical versus surgical implantation of autologous ovine tissue-engineered heart valves, The Journal of heart valve disease 21(5) (2012) 670-8.

[269] J. Reimer, Z. Syedain, B. Haynie, M. Lahti, J. Berry, R. Tranquillo, Implantation of a Tissue-Engineered Tubular Heart Valve in Growing Lambs, Annals of biomedical engineering 45(2) (2017) 439-451.

[270] Z. Syedain, J. Reimer, J. Schmidt, M. Lahti, J. Berry, R. Bianco, R.T. Tranquillo, 6-month aortic valve implantation of an off-the-shelf tissue-engineered valve in sheep, Biomaterials 73 (2015) 175-84.

[271] T.C. Flanagan, J.S. Sachweh, J. Frese, H. Schnoring, N. Gronloh, S. Koch, R.H. Tolba, T. Schmitz-Rode, S. Jockenhoevel, In vivo remodeling and structural characterization of fibrin-based tissue-engineered heart valves in the adult sheep model, Tissue engineering. Part A 15(10) (2009) 2965-76.

[272] B. Schmitt, H. Spriestersbach, O.H.I. D, T. Radtke, M. Bartosch, H. Peters, M. Sigler, L. Frese, P.E. Dijkman, F.P. Baaijens, S.P. Hoerstrup, F. Berger, Percutaneous pulmonary valve replacement using completely tissue-engineered off-the-shelf heart valves: six-month in vivo functionality and matrix remodelling in sheep, EuroIntervention 12(1) (2016) 62-70.

[273] M.Y. Emmert, B.A. Schmitt, S. Loerakker, B. Sanders, H. Spriestersbach, E.S. Fioretta, L. Bruder, K. Brakmann, S.E. Motta, V. Lintas, P.E. Dijkman, L. Frese, F. Berger, F.P.T. Baaijens, S.P. Hoerstrup, Computational modeling guides tissue-engineered heart valve design for long-term in vivo performance in a translational sheep model, Sci Transl Med 10(440) (2018).

[274] M. Thubrikar, The aortic valve, CRC Press, Boca Raton, Fla., 1990.

[275] C.H. Yap, H.S. Kim, K. Balachandran, M. Weiler, R. Haj-Ali, A.P. Yoganathan, Dynamic deformation characteristics of porcine aortic valve leaflet under normal and hypertensive conditions, Am J Physiol Heart Circ Physiol 298(2) (2010) H395-405.

[276] H.L. Leo, L.P. Dasi, J. Carberry, H.A. Simon, A.P. Yoganathan, Fluid dynamic assessment of three polymeric heart valves using particle image velocimetry, Annals of biomedical engineering 34(6) (2006) 936-52.

[277] I. Sorin Group USA, Clinical Investigation Of The Mitroflow Aortic Pericardial Heart Valve, National Institute of Health - ClinicalTrials.gov, 2008, 2008.

[278] A. Sezai, Y. Kasamaki, K. Abe, M. Hata, H. Sekino, K. Shimura, K. Minami, Assessment of the St. Jude Medical Regent prosthetic valve by continuous-wave Doppler and dobutamine stress echocardiography, The Annals of thoracic surgery 89(1) (2010) 87-92.

[279] A.P. Yoganathan, Travis, B.R., Fluid Dynamics of Prosthetic Valves, in: C. Otto (Ed.), The Practice of Clinical Echocardiography, Elsevier, Washington, 2016.

[280] D. Gottlieb, T. Kunal, S. Emani, E. Aikawa, D.W. Brown, A.J. Powell, A. Nedder, G.C. Engelmayr, J.M. Melero-Martin, M.S. Sacks, J.E. Mayer, In vivo monitoring of function of autologous engineered pulmonary valve, J Thorac Cardiov Sur 139(3) (2010) 723-731.

[281] F. De Gaetano, M. Serrani, P. Bagnoli, J. Brubert, J. Stasiak, G.D. Moggridge, M.L. Costantino, Fluid dynamic characterization of a polymeric heart valve prototype (Poli-Valve) tested under continuous and pulsatile flow conditions, Int J Artif Organs 38(11) (2015) 600-6.

[282] J.K. Kirklin, D. Smith, W. Novick, D.C. Naftel, J.W. Kirklin, A.D. Pacifico, N.C. Nanda, F.R. Helmcke, R.C. Bourge, Long-term function of cryopreserved aortic homografts. A ten-year study, J Thorac Cardiovasc Surg 106(1) (1993) 154-65; discussion 165-6.

[283] V.W. van Hinsbergh, Endothelium--role in regulation of coagulation and inflammation, Semin Immunopathol 34(1) (2012) 93-106.

[284] D.C. Nguyen, T.A. Hookway, Q. Wu, R. Jha, M.K. Preininger, X. Chen, C.A. Easley, P. Spearman, S.R. Deshpande, K. Maher, M.B. Wagner, T.C. McDevitt, C. Xu, Microscale generation of cardiospheres promotes robust enrichment of cardiomyocytes derived from human pluripotent stem cells, Stem Cell Reports 3(2) (2014) 260-8.

[285] K. Okita, Y. Matsumura, Y. Sato, A. Okada, A. Morizane, S. Okamoto, H. Hong, M. Nakagawa, K. Tanabe, K. Tezuka, T. Shibata, T. Kunisada, M. Takahashi, J. Takahashi, H. Saji, S. Yamanaka, A more efficient method to generate integration-free human iPS cells, Nature methods 8(5) (2011) 409-12.

[i] [12] A.L.Y. Nachlas, S. Li, M.E. Davis, Developing a Clinically Relevant Tissue Engineered Heart Valve-A Review of Current Approaches, Advanced healthcare materials 6(24) (2017).

[ii] [11] A.L.Y. Nachlas, S. Li, R. Jha, M. Singh, C. Xu, M.E. Davis, Human iPSC-derived mesenchymal stem cells encapsulated in PEGDA hydrogels mature into valve interstitial-like cells, Acta biomaterialia 71 (2018) 235-246.